NOTICE

The quality of this microform is heavily dependent upon the quality of the original thesis submitted for microfilming. Every effort has been made to ensure the highest quality of reproduction possible.

If pages are missing, contact the university which granted the degree.

Some pages may have indistinct print especially if the original pages were typed with a poor typewriter ribbon or if the university sent us an inferior photocopy.

Reproduction in full or in part of this microform is governed by the Canadian Copyright Act, R.S.C. 1970, c. C-30, and subsequent amendments.

AVIS

La qualité de cette microforme dépend grandement de la qualité de la thèse soumise au microfilmage. Nous avons tout fait pour assurer une qualité supérieure de reproduction.

S'il manque des pages, veuillez communiquer avec l'université qui a conféré le grade.

La qualité d'impression de certaines pages peut laisser à désirer, surtout si les pages originales ont été dactylographiées à l'aide d'un ruban usé ou si l'université nous a fait parvenir une photocopie de qualité inférieure.

La reproduction, même partielle, de cette microforme est soumise à la Loi canadienne sur le droit d'auteur, SRC 1970, c. C-30, et ses amendements subséquents.

Canada

UNIVERSITY OF ALBERTA

PERFORMANCE OF 64-QAM SIGNALS IN A HYBRID AM-VSB/QAM OPTICAL FIBER TRANSMISSION SYSTEM

BY

KINH MINH PHAM

A thesis submitted to the Faculty of Graduate Studies and Research in partial fulfillment of the requirements for the degree of **Master of Science**.

DEPARTMENT OF ELECTRICAL ENGINEERING

Edmonton, Alberta

SPRING, 1994

ISBN 0-612-11337-X

Canada

UNIVERSITY OF ALBERTA

RELEASE FORM

NAME OF AUTHOR: **Kinh Minh Pham**

TITLE OF THESIS: **Performance of 64-QAM Signals in a Hybrid AM-VSB/QAM Optical Fiber Transmission System**

DEGREE: **Master of Science**

YEAR THIS DEGREE GRANTED: **Spring 1994**

#1002 8510 111 St.

Edmonton, Alberta

T6G 1H7

DATE: DEC. 17th 1993

UNIVERSITY OF ALBERTA

FACULTY OF GRADUATE STUDIES AND RESEARCH

The undersigned certify that they have read, and recommend to the Faculty of Graduate Studies and Research for acceptance, a thesis entitled **PERFORMANCE OF 64-QAM SIGNALS IN A HYBRID AM-VSB/QAM OPTICAL FIBER TRANSMISSION SYSTEM** submitted by **KINH MINH PHAM** in partial fulfillment of the requirements for the degree of **MASTER OF SCIENCE** in Electrical Engineering.

G. D. Cormack, Co-Supervisor

J. Conradi, Co-Supervisor

P. A. Goud, Internal Examiner

U. Maydell, External Examiner

Date: Dec. 10 1993

DEDICATION

To my parents,

for their love, encouragement and support.

To my brother Hoang Anh Nguyen

for guiding and guarding me throughout the time

that I was lost and confused.

In memory of my sister, Chi Thu -

Her strength, courage and gentleness were singular.

ABSTRACT

Optical transmission of digital multi-level QAM and analog AM-VSB television signals is of interest to both the telecommunication and CATV industries. This fiber-optic video signal transport scheme has the advantages of compatibility with the existing CATV network and of channel capacity sufficient to meet anticipated future requirements for compressed digital video signals.

This thesis contains a comprehensive study of the performance of a hybrid AM-VSB/QAM optical transmission system based on theoretical analysis and laboratory measurements, with particular emphasis on determining the impact of noise and nonlinear distortion on the bit error rate (BER) performance of the QAM signals.

The random nature of nonlinear distortion products within a 10 MHz bandwidth is investigated. By combining a theoretical BER analysis employing Middleton's Class A noise model and experiments, we verify the impact of non-Gaussian impulsive noise on the BER performance of a 64-QAM signal in a hybrid AM-VSB/QAM optical fiber transmission system. The specific parameters that are evaluated experimentally and theoretically are the modulation index, signal to noise ratio (SNR), and signal to nonlinear distortion ratio (SNLD). In addition, the performance degradation due to the interaction between fiber dispersion and Erbium Doped Fiber Amplifier's non-flat gain spectrum is discussed.

Finally, a channel capacity study based on the experimental measurements is presented in order to show the feasibility of simultaneous transmission of digital and analog video signals over optical fiber.

ACKNOWLEDGEMENTS

My thanks are due first to my supervisors, Dr. George Cormack and Dr. Jan Conradi, who provided me not only with an excellent research environment at TRLabs, but also an opportunity to broaden my research experience through the BNR/TRLabs Internship program. Without their technical guidance and support, this work would not have been possible. In addition, I would like to thank the members of my examining committee, Dr. George Cormack, Dr. Jan Conradi, Dr. Paul Goud, and Prof. Ursula Mayd·ll for revicwing this thesis.

I would also like to acknowledge my gratitude to the managers and members of technical staff at Bell-Northern Research; Dr. Jack Terry, Carl Anderson, Bob Thomas, Hyung Kim, and John Goodwin for providing the facilities for the experimental results reported in this thesis.

I wish to extend my special thanks to David Clegg for his assistance and advice in the design of the analog optical transmitter and receiver. I am also grateful to many of my colleagues; Dobby Lam, Dino Corazza, Eric Cauchon, and Greg May for many interesting and stimulating discussions.

I wish to acknowledge the Natural Sciences and Engineering Research Council, Telecommunications Research Laboratories, and the University of Alberta for their generous financial support without which this work would not have been possible.

Finally, I would like to thank my family for their continuing support and encouragement over the years. I will be forever indebted to my family for the sacrifices they have made in order for me to have an opportunity to grow and develop in freedom.

This work was supported by the Natural Sciences and Engineering Research Council of Canada, Bell-Northern Research, and TRLabs through the NSERC/BNR/TRLabs Industrial Research Chair in Fiber Optic Communications at the University of Alberta.

TABLE OF CONTENTS

LIST OF TABLES

LIST OF FIGURES

LIST OF ABBREVIATIONS AND ACRONYMS

AC	Alternate Current
A/D	Analog/Digital
AGC	Automatic Gain Control
AM-VSB	Vestigial Sideband Amplitude Modulation
APC/FC	Angled Physical Contact Fiber Connector
ASE	Amplified Spontaneous Noise
ATC	American Television and Communications Corporation
ATDE	Adaptive Time Domain Equalizer
B-ISDN	Broadband Integrated Services Digital Network
BER	Bit Error Rate
BNR	Bell-Northern Research
CATV	Community Antenna Television
SNLD	Signal to Nonlinear Distortion Ratio
CNR	Carrier to Noise Ratio
CODEC	Coder-Decoder
CSO	Composite Second Order
CTB	Composite Triple Beat
D/A	Digital/Analog
dB	Decibel
DC	Direct Current
DFB	Distributed Feedback
DSB-AM-SC	Double Sideband, Amplitude Suppressed Carrier
EDFA	Erbium Doped Fiber Amplifier
FEC	Forward Correction Coding

FM	Frequency Modulation
HP	Hewlett Packard
I	Inphase
IF	Intermediate Frequency
ISI	Intersymbol Interference
L-I	Light Power versus Current
LNA	Low Noise Amplifier
LO	Local Oscillator
mss	Maximum Steady State
NCTA	National Cable Television Association
NTSC	National Television Systems Committee
PAM	Pulse Amplitude Modulation
psd	power spectral density
Q	Quadrature
QAM	Quadrature Amplitude Modulation
RF	Radio Frequency
RIN	Relative Intensity Noise
SCM	Subcarrier Multiplexing
SNR	Signal to Noise Ratio
TEC	Thermoelectric Cooler
TDM	Time Division Multiplexing
TV	Television
WDM	Wavelength Division Multiplexing

LIST OF SYMBOLS

The first occurrence of each symbol is given in brackets following the definition.

$\langle\ \rangle$	refers to time average
$\{\ \}$	refers to power spectral density
Λ	impulsive index (3.40)
B	effective noise bandwidth (3.16)
d_{min}	minimum distance between two neighboring states (3.31)
ΔI	variation in current (3.4)
$\{(\Delta P(f))^2\}$	spectral density of the mean square deviation of the light output of the laser (3.19)
f	frequency of the carrier (3.5)
F	noise factor (3.16)
Γ'	mean power ratio of the Gaussian noise component to the non-Gaussian impulsive noise component (3.40)
$h_{o,k}$	coefficients in the autocorrelation function of the laser output (3.24)
I_{bias}	bias current (3.4)
$I_{eff,p}$	effective peak current (3.12)
$I_{eff,rms}$	effective rms current (3.10)
I_p	peak current (3.8)
I_{rms}	rms current (3.7)
I_{th}	threshold current (3.4)

$\langle i_{AM-VSB}^2 \rangle$	time-averaged square of AM-VSB carrier current (3.13)
$\langle i_{QAM}^2 \rangle$	time-averaged square of QAM signal current (3.15)
$\langle i_{RIN}^2 \rangle$	time-averaged square of relative intensity noise current (3.18)
$\langle i_{sh}^2 \rangle$	time-averaged square of shot noise current (3.17)
$\langle i_T^2 \rangle$	time-averaged square of thermal noise current (3.16)
k	Boltzmann's constant (3.16)
m	modulation index (3.2)
m_{rms}	rms modulation index (3.7)
$m_{eff,p}$	effective peak modulation index (3.12)
$m_{eff,rms}$	effective rms modulation index (3.10)
$m(t)$	modulating signal (3.2)
μ	total rms modulation index (3.6)
M	number of QAM signal levels
N	number of channels (3.6)
N_o	noise power (3.35)
N_{total}	total noise power (Gaussian noise plus impulsive noise) (3.40)
P_{av}	average received QAM channel signal power (3.36)
P_{QAM}	average transmitted QAM channel signal power (3.11)
P_{bias}	average transmitted optical power at the bias current level (3.1)
P_o	average received optical power (3.13)
P_e	one-directional probability of a symbol error (3.31)

P_{2-dir}	probability of a correct decision for the symbols that are subject to two-directional errors (3.30)
P_{3-dir}	probability of a correct decision for the symbols that are subject to three-directional errors (3.30)
P_{4-dir}	probability of a correct decision for the symbols that are subject to four-directional errors (3.30)
PF_M	ratio of the QAM signal peak power to the QAM signal rms power (3.36)
$P(C\|m_i)$	probability of a correct decision given that the symbol , S1, is transmitted (3.30)
$P(E_{symbol})$	average symbol error probability (3.30)
$P(E_{bit})$	average bit error probability (3.39)
$p(\theta)$	probability density function of signal amplitude (3.31)
$p_{I+G}(n)$	Gaussian noise combined with non-Gaussian impulsive noise probability distribution function (3.40)
$p_i(t)$	general M-ary QAM signal (2.1)
$p'(t)$	pulse shape (2.1)
$P(t)$	transmitted optical power waveform (3.1)
q	electronic charge (3.17)
$\Re$	responsivity (3.13)
R	input resistance (3.11)
R_{eq}	equivalent resistance of the photodiode load (3.16)
${}_{NLD}R_n(t)$	nonlinear distortion term of the autocorrelation function of the laser output (3.24)
${}_sR_n(t)$	signal term of the autocorrelation function of the laser output (3.23)
S	peak QAM signal envelope (3.36)

σ^2	variance
σ_j^2	$(j/A+\Gamma')/(1+\Gamma')$ (3.40)
T	absolute temperature (3.16)
θ	phase of the carrier (3.5)
${}_{NLD}W(f)$	nonlinear distortion power spectral density (3.27)

1. INTRODUCTION

The past few years have shown a significant increase in the development of optical fiber transmission technology and its acceptance by various industries. Some of the potential advantages that optical fiber transmission offers are high bandwidth, low loss, immunity to electromagnetic interference and crosstalk, insensitivity to temperature changes, and reduced size for multiple transmission paths. In many instances, these advantages can translate into significant system performance improvements. Therefore, it is natural that there is an intensive interest in ways to implement fiber optic technology to improve existing communication systems.

The most extensive application of fiber optics is in the telephone industry. Much of today's voice long-distance interoffice and intercity trunking signals are carried by optical fibers, providing increased transmission capacity and reliability compared to both copper based and microwave radio transmission systems. At present, as the technology of the lightwave components such as semiconductor lasers and photodiode matures and its costs are decreased, it is technically and economically justified to use optical fibers not only in long-distance transmission of telephone signals, but also for shorter distance systems connecting a central switching office to local loop distribution units. The implementation of optical fibers is now expanding to the last stretch of telephone networks as telephone operating companies are planning Fiber-in-the-Loop systems in the distribution plant and have their ultimate goal Fiber-to-the-Home systems. This system will then be a full fiber optic network and will support the envisaged broadband services [1].

Although there has been substantial growth in voice networks recently due to high demand for second and third telephone lines to the home, Community Antenna Television (CATV) networks have been growing at a faster rate than telecommunication

networks. Furthermore, currently envisaged special video services such as pay-per-view and switched on-demand video promise an even higher growth rate of video service networks, as well as increases in operating revenues. As a result, CATV is currently one of the fastest growing application areas of fiber optics. Optical fibers in a video distribution network provide improved reliability and better quality signals to customers. Furthermore, optical fibers are considered to be the most cost efficient way of increasing channel capacity for future revenue growth. More importantly, integration of video services into the already deployed voice and data fiber optic networks would provide a fully integrated broadband service to subscribers [2]. Realizing the importance of video services for future broadband networks, there has been an intensive effort in the research and development of lightwave multichannel video systems. This thesis is an integral part of this effort.

In this introduction, the evolution from a copper-based distribution system to an optical fiber multichannel system is discussed. This is followed by a brief description of the advent of digital video transmission. Finally, objectives and the organization of the thesis are presented.

1.1 Evolution From Copper-based to Optical Fiber Multichannel CATV system.

The original purpose of CATV systems was to deliver off-the-air broadcast signals in areas where TV signal reception with conventional TV antennas was inadequate. For these areas, large community antennas were set up to share the received broadcast signals among many TV sets. Typical areas needing community antenna services were rural areas far away from TV broadcast antennas and metropolitan areas subject to multi-path reflections from large buildings. In recent years, increases in the number of channels with added variety of programs attracted subscribers and resulted in a

major expansion of CATV networks even into areas which did not require the traditional community antenna services.

In order to understand how optical fiber can be used to upgrade a CATV network, it is essential to recognize the limitations of the present system. Figure 1.1 [3] illustrates schematically a typical cable TV network.

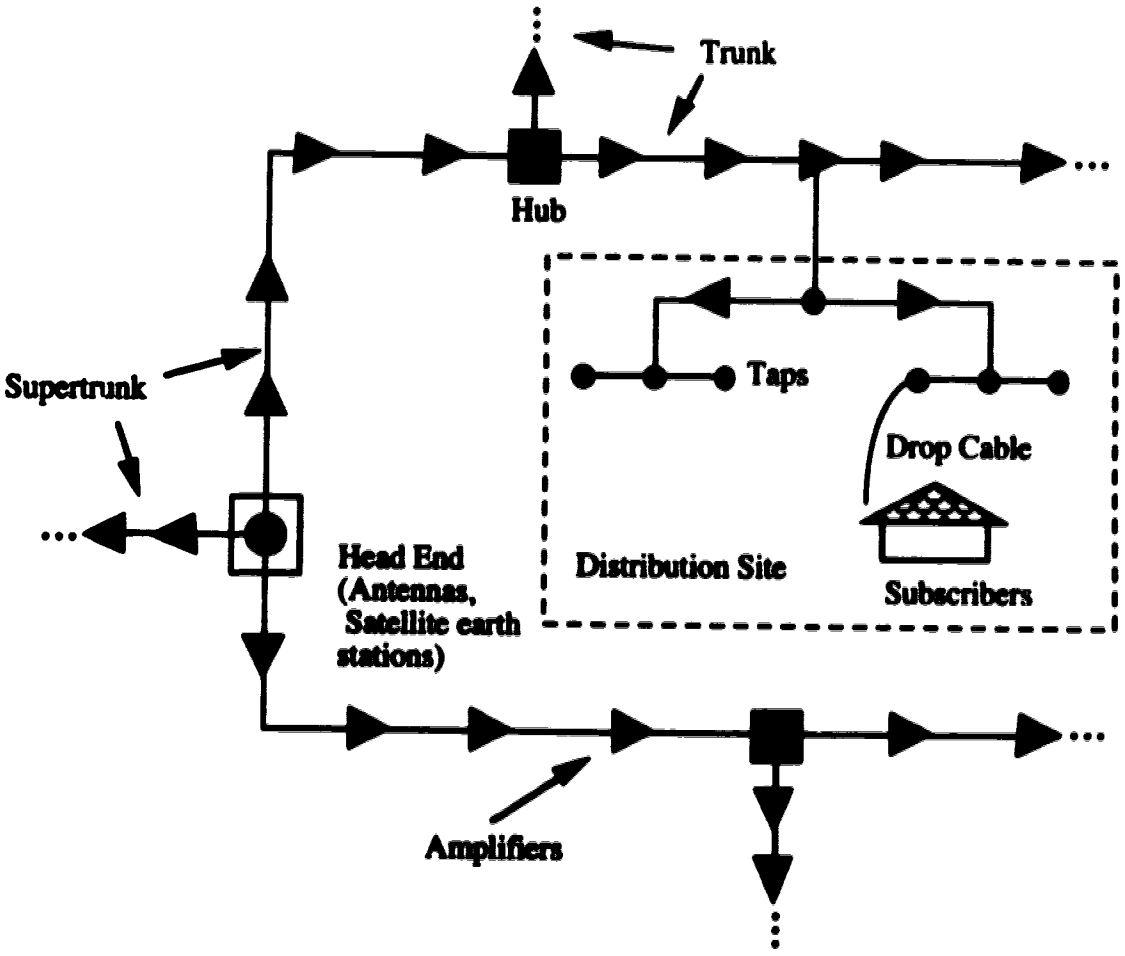

Fig. 1.1 Typical CATV distribution system

As shown in Fig. 1.1, the architecture of current CATV networks is basically a tree-and-branch type. All of the signals which are to be delivered to subscribers originate from a central head end. Typical signal sources feeding this head end are picked up with

satellite receivers, off-air antennas, and distant-feeds. At the head end, signals are amplitude modulated and filtered to a vestigial sideband format at various frequencies, combined, and then transmitted over coaxial cable to local distribution sites called hubs. The connection between the head end and hubs is referred to as supertrunking. At the hubs, CATV signals are distributed to subscribers via amplifiers and taps. Amplifiers are used to compensate for the branching and propagation loss. Taps or power splitters distribute signal power from main coaxial cables to drop cables. Drop cables are then run to subscribers' homes.

The primary cause for the system's problems and limitations is the fact that a large number of amplifiers is required to operate in series, typically one per 1000 feet [4]. Each of these amplifiers has active components and must be provided with power, thus limiting the reliability. In addition, each amplifier adds noise and intermodulation distortion to the signals passing through it. Another problem arising in this system is the limitation on transmission bandwidth caused by the high-frequency-loss characteristic of the coaxial cables. Therefore, long cascades of amplifiers give rise to systems with reliability problems and limited transmission quality [5].

Fiber optic CATV systems, on the other hand, offer a high bandwidth and low loss transmission medium which reduces the need for amplifiers, thus providing higher picture quality and improved system reliability. At present, fiber optic trunking systems are being extensively deployed in CATV networks. One of the most popular approaches to optical fiber deployment in CATV networks is the fiber backbone technique proposed by American Television and Communications Corporation (ATC) [5]. This approach is illustrated in Fig. 1.2. In this technique, fiber is used from the head end to conversion nodes, and the existing coaxial cable and amplifiers are then used from the conversion point to the feeders. This reuses the existing coaxial cable and amplifiers, but avoids the reliability and performance problems of a large number of amplifiers in cascade.

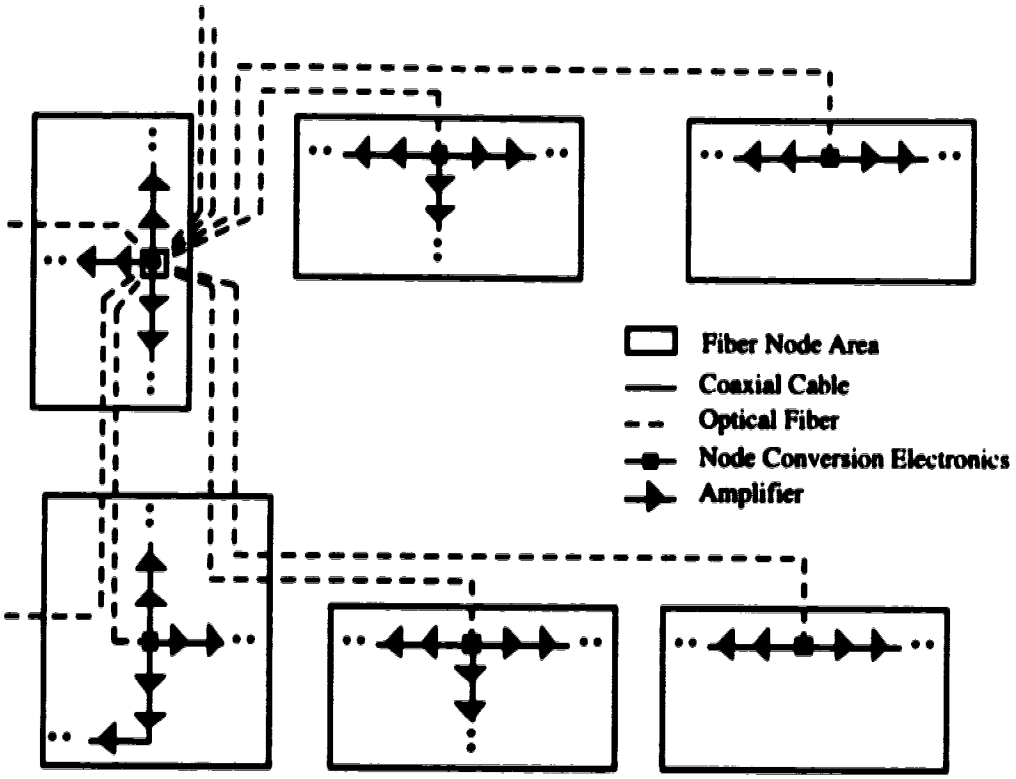

Fig. 1.2 CATV Distribution System with Fiber Backbone/Feeder

1.2 Evolution From Analog to Digital Video Transmission

In the early stages of optical fiber transmission of multichannel video signals, subcarrier multiplexing employing the analog AM-VSB modulation format was used mainly due to its low cost and compatibility with existing TV sets. The analog AM-VSB fiber optic transmission system is simple to operate, cost effective, and compatible with the current network microwave links. However, due to strict noise and distortion requirements, the total number of transmitted channels and video quality are limited to some extent.

Over the past few years, due to recent advances in digital electronics and signal processing algorithms, video signals are now being processed in the digital domain. Two of the most outstanding characteristics of digital video are robustness and flexibility.

Digitized video signals can be regenerated as often as desired without significant degradation due to noise and distortion as long as appropriate signal to noise and signal to nonlinear distortion ratios are met. Therefore, system performance is substantially independent of transmission distance. Once digitized, the signals can also be stored in digital memory and processed to enhance video quality and increase channel capacity. In addition, as the broadband integrated services digital network (B-ISDN) is developed, digital video services will be smoothly integrated into the already deployed voice and data fiber optic network.

The preceding advantages of digital video transmission are achieved at the expense of bandwidth expansion and the requirement for complex and, at present, often costly video Coder-Decoders (CODECs). At present, it is anticipated that it will take a long time for the distribution of digital video to be widespread with reasonable cost. A more practical and realizable alternative is a hybrid analog/digital fiber-optic video transport scheme employing analog AM-VSB and spectrally efficient digital QAM signals. This system is a compromise between an all-analog and an all-digital video distribution system. It has the advantage of low cost analog electronics and still has the capability of evolving in step with anticipated future requirements to transmit digital video signals.

1.3 Organization of Thesis

Although there is a growing interest in the hybrid AM-VSB/QAM optical transmission system, there are still many unresolved issues regarding system performance and, hence, the feasibility of such a system. Based on a review and assessment of the current status of hybrid AM-VSB/QAM optical transmission systems done by the author, the following major thesis research objectives were established:

(i) *To study the impact of noise and nonlinear distortion due to threshold clipping on the BER performance of 64-QAM signals based on experiments and theory.*

(ii) *To do a channel capacity study based on the feasibility of a hybrid AM-VSB/QAM optical transmission system.*

This thesis is organized in the following manner. In Chapter 2, the hybrid AM-VSB/QAM optical transmission system is described along with a discussion of system impairments, limitations, and typical performance requirements. Chapter 3 presents the theoretical analysis of BER of 64-QAM in a hybrid analog/digital optical transmission system. This analysis is based on the Middleton class A noise model which accounts for both Gaussian and non-Gaussian impulsive noise. Design and implementation of the hybrid system is described in Chapter 4. This is followed in Chapter 5 with the characterization of the optical link. Chapter 6 presents the experimental study of the impact of nonlinear distortion due to threshold clipping and noise on the BER performance of a 64-QAM signal. This chapter also discusses the effects of fiber dispersion and distortion due to the non-flat gain spectrum of Erbium Doped Fiber Amplifiers (EDFAs) on system performance. Finally, the conclusions are given in Chapter 7.

2. OPTICAL FIBER TRANSMISSION OF AM-VSB AND QAM VIDEO SIGNALS

This chapter introduces the operating characteristics of a hybrid AM-VSB/QAM optical transmission system, beginning with a description of the Subcarrier Multiplexing (SCM) technique which can be used to multiplex analog and digital signals together for transmission over optical fiber. This is followed by a discussion of the modulation formats used: Vestigial Sideband Amplitude Modulation (AM-VSB) for analog signals and Quadrature Amplitude Modulation (QAM) for digital signals. Finally, system impairments, performance parameters and requirements are discussed.

2.1 Subcarrier Multiplexing

There are many multiplexing methods for combining information signals together for transmission over an optical fiber link. The techniques are subcarrier multiplexing (SCM), time-division multiplexing (TDM), and wavelength-division multiplexing (WDM). Subcarrier multiplexing transmission over optical fibers is simple and cost effective, and thus is considered in this research project. A basic subcarrier multiplexed transmission system and a corresponding typical signal frequency spectrum are shown in Figs. 2.1 and 2.2 [5-9].

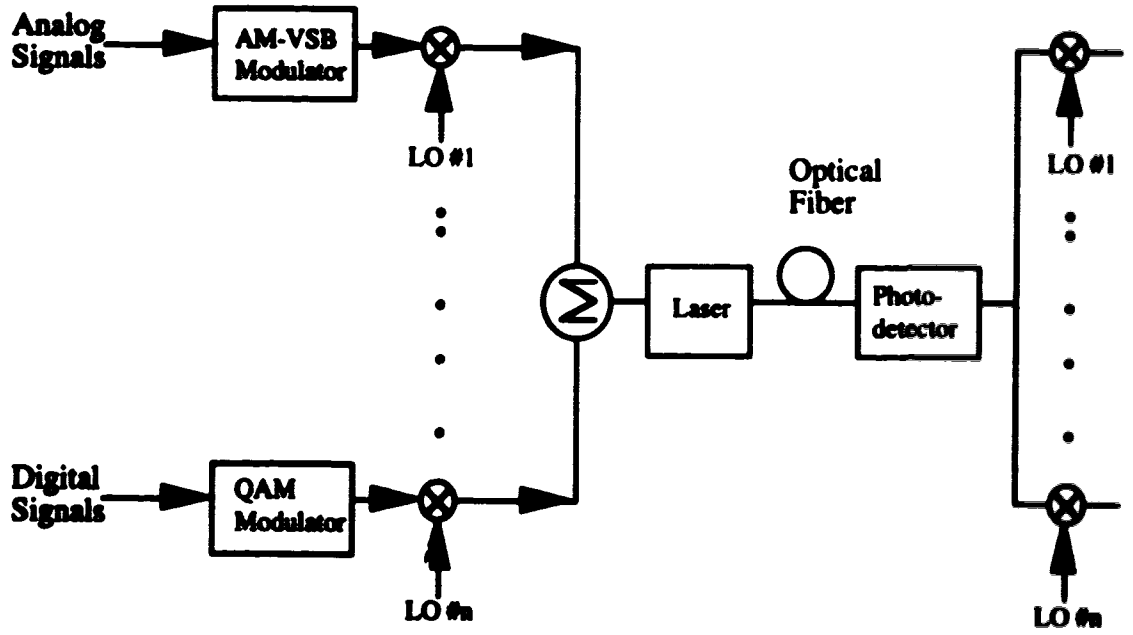

Fig. 2.1 Block diagram of a subcarrier multiplexed system

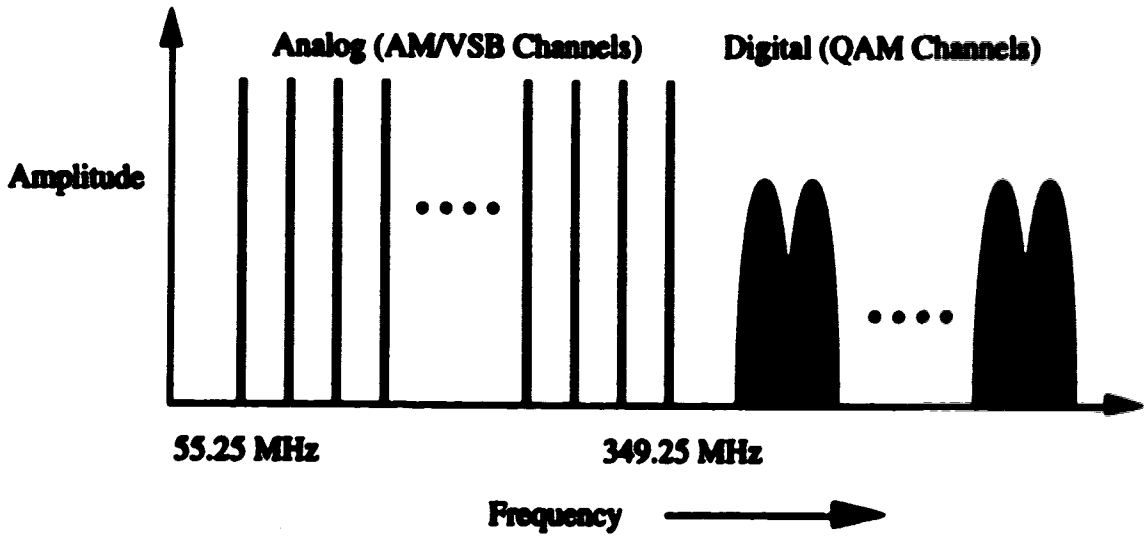

Fig. 2.2 Example frequency spectrum of subcarrier multiplexed AM-VSB carriers and QAM signals

A number of baseband analog and/or digital signals are first used to amplitude modulate a series of carriers which are then frequency division multiplexed by using local oscillators (LO's) of different frequencies. Frequency spacing between adjacent channels is set such that acceptable levels of inter-channel interference result. In general, this spacing involves a guard band between the main spectral lobes of adjacent channels. The magnitude of the spacing is determined by the type of modulation scheme and performance required.

The modulated sinusoidal carriers are then combined together into a single RF signal which modulates the intensity of a light source, typically a laser diode. The local oscillator frequencies are called subcarrier frequencies and the optical frequency is the carrier frequency. The laser is biased at an optimal point above threshold and the amplitude of the sum of the modulated sinusoidal carriers adjusted such that there is a maximum possible signal swing between turn-on threshold and saturation of the optical power versus current characteristic of the laser. The output of the laser is then coupled into the optical fiber for transmission. At the receiver, light signals are converted back to electrical signals using a photodetector. A user can then receive any one of the frequency division multiplexed channels by tuning a local oscillator and down-converting the radio frequency signals to baseband.

For analog signals, the SCM technique provides a compatible electrical interface to the North American National Television Systems Committee Amplitude Modulated Vestigial Sideband (NTSC AM-VSB) TV format. In this technique, the NTSC AM-VSB signal directly intensity modulates a laser without need for any signal conversion. In addition, because of the versatility of being able to carry a variety of signal modulation formats such as amplitude modulated (AM), frequency modulated (FM), and digital formats simultaneously, SCM systems provide a desirable carrier platform for the

implementation of broadband service networks and, therefore, is chosen, in the present work, for the optical transmission of hybrid AM-VSB/QAM signals.

2.2 Modulation Formats

Simultaneous transmission of AM-VSB and QAM signals over an optical fiber employs the subcarrier multiplexing technique. For this project, the subcarriers are modulated with analog signals using vestigial sideband amplitude modulation and digital signals using quadrature amplitude modulation.

2.2.1 Amplitude Modulation: Vestigial Sideband (AM-VSB)

Vestigial Sideband Amplitude Modulation is commonly used in television signal transmission systems because of its bandwidth efficiency and ease of implementation compared to other amplitude modulation schemes such as Double Sideband and Single Sideband Amplitude modulation. AM-VSB modulation can be achieved in two steps: amplitude modulation followed by vestigial sideband filtering. In amplitude modulation, the amplitude of a carrier is varied in proportion to a given information signal. This alters the given signal by translating its frequency components to higher frequencies. The amplitude modulated signal, carrier plus double sideband, is then passed through a vestigial sideband filter, which is a bandpass filter that attenuates most of the lower sideband. The resulting filtered signal is called a vestigial sideband signal. With AM-VSB format, most of one sideband is suppressed in such a way that the demodulation process reproduces the original signal. The characteristic of the transmitted spectrum is such that the partial suppression of the transmitted sideband is exactly compensated for by the partial transmission of the suppressed sideband, as shown in Fig. 2.3 [10].

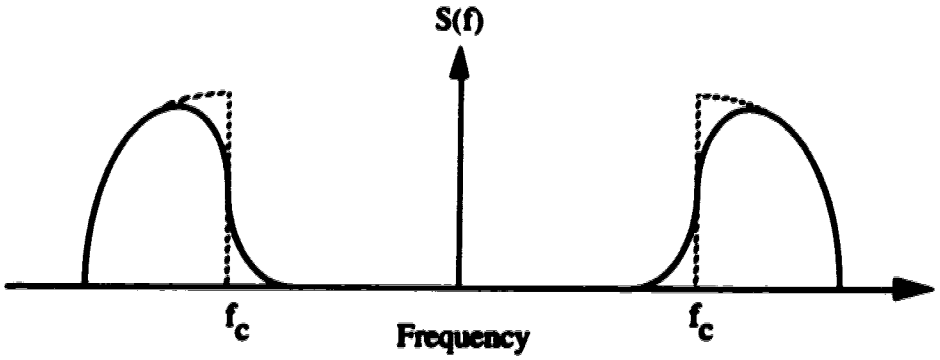

Fig. 2.3 Spectrum of an AM-VSB signal

A typical TV channel spectrum is illustrated in Fig. 2.4 [11], showing the location of major frequency components, namely the video carrier, color subcarrier, and audio carrier. As can be seen in the figure, the video carrier is located 1.25 MHz above the low frequency cut-off of the channel. For example, for Channel 2* whose spectrum is assigned between 54 MHz and 60 MHz, the video carrier is located at 55.25 MHz. Within a TV spectrum, the video carrier is the most dominant frequency component, and performance testing of the CATV signal is often carried out using the video carrier only.

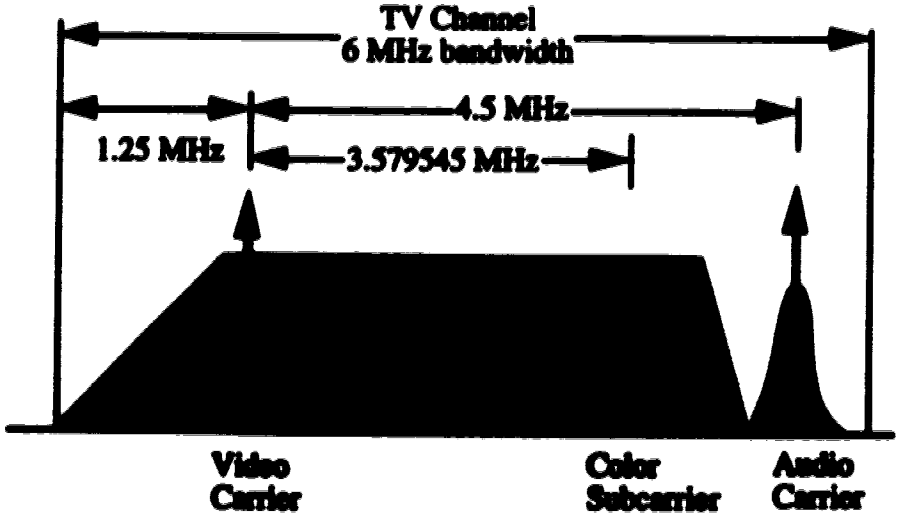

Fig. 2.4. Spectrum of a TV channel

* Channel 2 is the CATV channel designation and is the same as the Channel 2 on a TV set.

2.2.2 Quadrature Amplitude Modulation (QAM)

In the transmission of digital video signals, Quadrature Amplitude Modulation (QAM) is a popular modulation scheme for digital signal delivery because of its spectral efficiency. The general M-ary QAM signal can be mathematically represented by [12]

$$\begin{aligned} p_i(t) &= p'(t)\left[a_i \cos(\omega_c t) + b_i \sin(\omega_c t)\right] \\ p_i(t) &= p'(t)\left[r_i \cos(\omega_c t + \theta_i)\right], \qquad i = 1, 2, \ldots, M \end{aligned} \tag{2.1}$$

where $p'(t)$ is the pulse shape, a_i and b_i are signal amplitudes, $r_i = \sqrt{a_i^2 + b_i^2}$, and $\theta = -\tan^{-1}(b_i / a_i)$.

Let's take an intuitive approach in understanding the operating characteristics of QAM. With any modulation format, the data could be applied to a single frequency carrier signal by modulating its magnitude, frequency or phase relative to an arbitrary reference signal. QAM modulation is a combination of amplitude and phase modulation. The phase and magnitude of a QAM signal can be represented in polar or vector coordinates as a discrete point in the I-Q plane as shown in Fig. 2.5. "I" stands for "in-phase" (i.e., phase reference) and "Q" for "quadrature" (i.e., 90° out of phase). Each point can be represented by the vectorial sum of a certain magnitude of in-phase carrier and a certain magnitude of quadrature carrier. This is the principle of QAM modulation. Forcing the carrier phase and magnitude to satisfy one of the 64 predetermined positions in the I-Q plane shown in Fig. 2.5 [12] enables the video to be encoded as a 64 symbol digital signal.

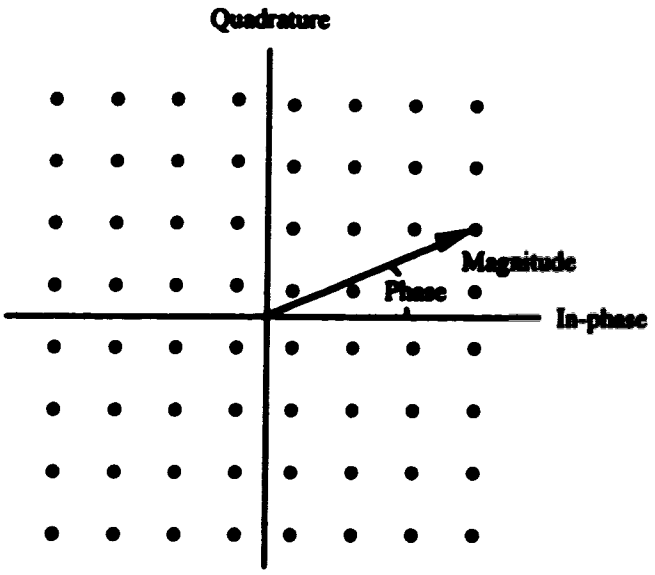

Fig. 2.5 64-QAM Constellation

As shown in Fig. 2.5, each of the diacrete values or states is called a symbol, and each symbol represents a particular word of binary data. In 64-QAM, each symbol represents one of 64 six-bit words. The effect of this modulation scheme is that six parallel binary data streams can be transmitted simultaneously, so the symbol rate is one-sixth of the bit rate. Because the symbol rate is less than the bit rate, the bandwidth required is reduced. As the number of states gets larger, the smaller the bandwidth becomes for a given information rate. However, disadvantages of high level QAM are: a) the complexity in circuitry and b) the signal has less immunity to noise and interference because the states are close together.

Another important requirement of QAM modulation is signal filtering. The unfiltered QAM signal occupies a very wide bandwidth, which is theoretically infinite, and is defined by the $\text{sinc}\left(fT_{symbol}\right)$ function (i.e. $\frac{\sin(\pi fT_{symbol})}{\pi fT_{symbol}}$) where T_{symbol} is the period of a symbol. This wide bandwidth output must be restricted to avoid interference with adjacent channels. In order to prevent data degradation, signal filtering is required

and the filters must conform to Nyquist's First Criterion for zero intersymbol interference (ISI) [13].

The ideal Nyquist filter has a flat response and a bandwidth equal to half the symbol rate as shown in Fig. 2.6. However, this filter is impractical. Therefore, a realizable filter is usually designed to approximate the raised cosine filters. These filters meet the zero intersymbol interference criterion, but they occupy more bandwidth than the ideal filter. Plots of the frequency response of the raised cosine family of filters are shown in Fig. 2.6 [13] for rolloff factors r = 0, r = 0.5, and r = 1.0.

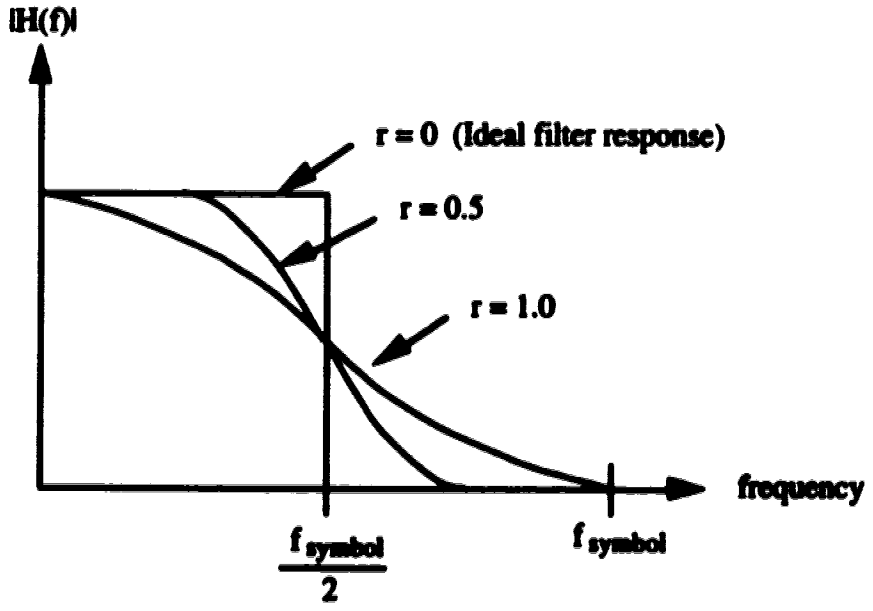

Fig. 2.6 Frequency response for different rolloff factors

As can be seen in Fig. 2.6, it is desirable to design a filter with a small rolloff factor. However, as the rolloff factor decreases, the transfer function of the filter is more difficult to approximate because of the steep rolloff in the filter transfer function. Furthermore, the clock timing requirements become more stringent because the impulse response decays slower.

Quadrature Amplitude Modulation is chosen as the modulation format for the transmission of digital video signals because of its bandwidth efficiency, hence the potential for transmitting a moderately compressed digital video signal within a 6 MHz TV channel. Digital video transmission depends on both video compression and digital modulation technologies. In compressed systems, the video signal is initially sampled. The resulting data is digitized and approximated by various algorithms in order to reduce the effective data transmission rate and yet maintaining the required video quality. However, in order to fit a digital video signal that has been compressed to ~ 30 Mb/s, into a 6 MHz bandwidth TV channel, the sampled data has to be further compressed using bandwidth efficient digital modulation formats. Using modulation schemes such as M-ary QAM, the digital signal is specially modulated to allow fast data transmission and bandwidth efficiency, therefore a moderately compressed digital video signal can be fitted into a TV channel. However, as the number of QAM levels increases, the signal becomes more susceptible to noise and interference because the symbol states are closer together. In essence, there is a trade-off between digital compression and the level of QAM in fitting a digital video signal within a 6 MHz bandwidth.

2.3 System Impairments

In order to effectively evaluate the performance of a system in which both analog and digital signals are transmitted simultaneously over an optical fiber, it is necessary to examine the effects that all the various components of the transmission chain have on the performance of the system. The two major undesirable effects are those of random noise and distortion arising from nonlinearities in electro-optic components, primarily the laser diode [6-9].

2.3.1 Noise

There are three dominant types of noise: receiver front-end thermal noise, shot noise , and relative intensity noise (RIN) [6-9]. Noise from the preamplifier in a receiver circuit is called front-end noise. It consists of resistor thermal noise (Johnson noise) and transistor noise. The quantum behavior of light and photocurrent gives rise to a random noise known as shot noise. RIN noise is normally referred to as laser excess noise. RIN can be further subdivided into noise intrinsic to the laser and extrinsic to it. For a single mode laser, the intrinsic RIN is caused by spontaneous emission coupled to a lasing mode [14-15]. The extrinsic RIN, on the other hand, is attributable to reflections from fiber discontinuities (e.g. fiber connectors/splices) back into the laser cavity, or by multiple reflections between fiber discontinuities. In practical systems, extrinsic RIN can be sufficiently suppressed using optical isolators, high return loss connectors such as APC/FC connectors, or fusion splices. The intrinsic RIN of a laser diode is a function of frequency and increases in amplitude with increasing frequency to a maximum at the laser's natural resonance frequency. The magnitude of the peak depends on the gain saturation and spontaneous emission rate of a particular diode.

2.3.2 Nonlinear Distortion

Because a semiconductor is a nonlinear device, the various microwave subcarriers mixed within the laser cavity form distortion products. The three types of distortion which we are most concerned with are cross modulation, harmonic distortion, and intermodulation distortion [6-9].

Cross modulation is a form of distortion where modulation from one channel is imposed onto other subcarriers in the system. It occurs as a result of the non-linear gain in the system. Variation in input signal level due to modulation in one channel causes

changes in the gain of the amplifier. This variation in gain effectively modulates other carriers being passed through the amplifier.

Harmonic distortion results in harmonic frequencies of other carriers being present in a channel passband. The harmonic products from a subcarrier at frequency f_1 appear at $2f_1$ for second order, $3f_1$ for third order and so on.

Intermodulation distortion arises from the interaction between two, three, or more different subcarrier frequencies resulting in products which may appear in the band of interest. Intermodulation between two frequencies f_1 and f_2 results in second order distortion products appearing at $|f_1 \pm f_2|$ and two tone third order distortion products at $|2f_1 \pm f_2|$ and $|2f_2 \pm f_1|$. Third order distortion can also arise from the combination of three different frequencies f_1, f_2, and f_3. These products are called triple beats which appear at frequencies $|f_1 \pm f_2 \pm f_3|$. Among the intermodulation products, generally only the second order and third order terms are considered, since higher order products tend to be insignificant. Fig. 2.7 illustrates a variety of distortion products.

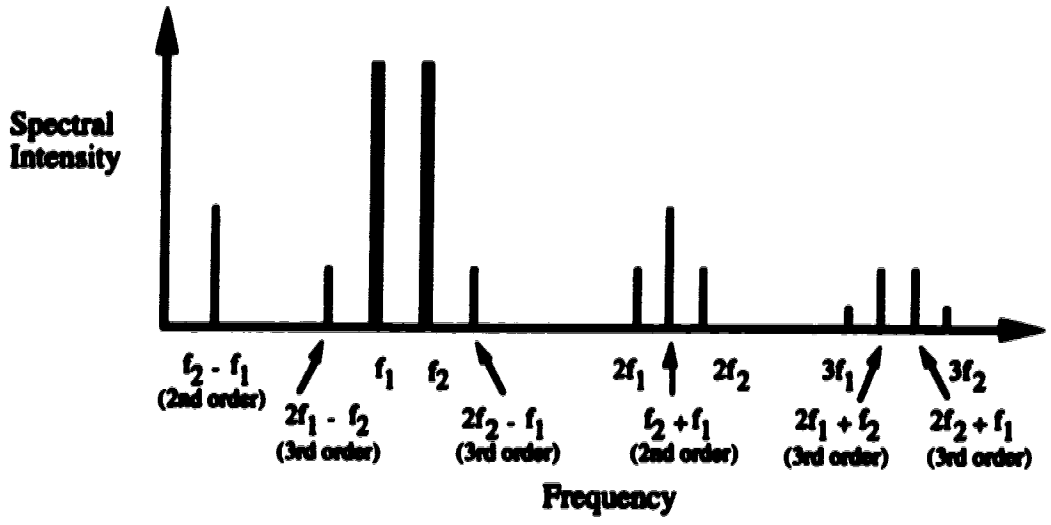

Fig. 2.7 Distortion products

Nonlinear distortion is caused by nonlinearity in the laser power-current curve, resonance distortion, and the nonlinear distortion produced by the laser diode chirp and fiber dispersion [6-9]. The light power versus current curve for a laser, shown in Fig. 2.8, exhibits a threshold current level below which the light output is close to zero and a rolloff or saturation of the light output at high levels of drive current. Therefore, large excursions in modulation current produce distortion. This type of distortion is independent of frequency within the modulation bandwidth of the laser and can be analyzed by a power series expansion about the bias point. The intrinsic nonlinearity from a laser diode is attributable to resonance distortion which results from nonlinear coupling between carriers and photons in the laser cavity. Resonance distortion is a function of frequency. It increases with frequency and can become dominant at frequencies close to the relaxation oscillation frequency of the laser [6]. The features of resonance distortion can be determined from the semiconductor laser rate equations.

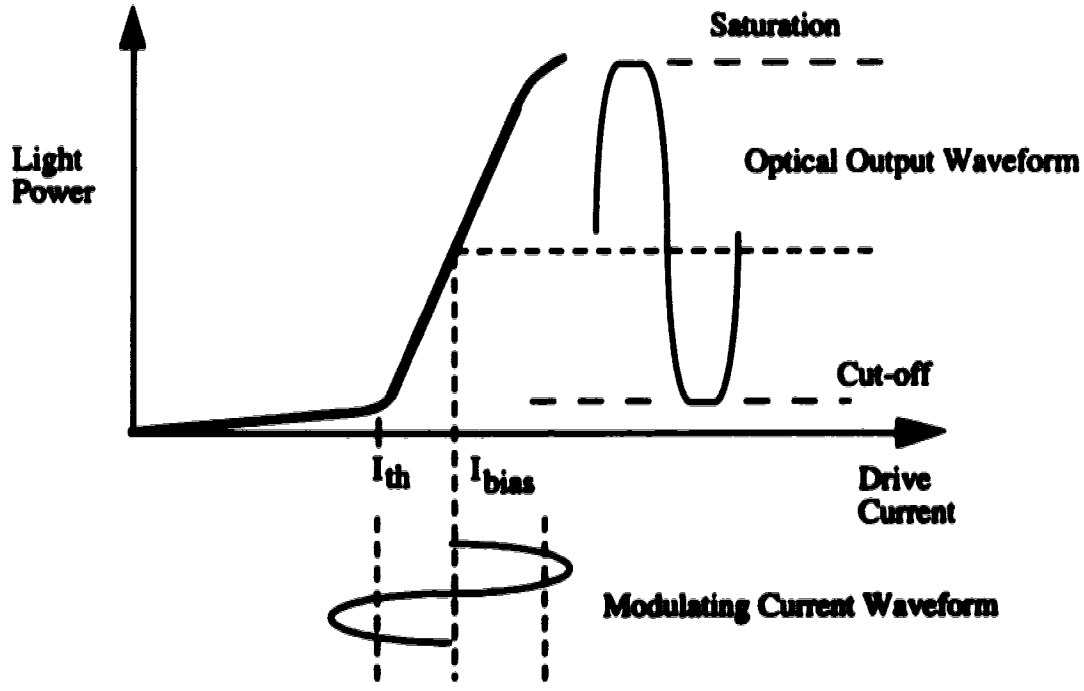

Fig. 2.8 Threshold and saturation clipping induced nonlinear distortion

2.4 System Performance Parameters and Requirements

2.4.1 Performance Parameters and Requirements for the AM-VSB Signals

Performance of multichannel AM-VSB signals is specified by the noise and nonlinear distortion associated with the video carrier. The noise performance is specified by the carrier-to-noise ratio (CNR). The nonlinear distortion is specified by the composite-second-order (CSO) and the composite-triple-beat (CTB) which are the intermodulation distortion products resulting from frequency beating of subcarriers [16-17]. In a multichannel system, several nonlinear distortion products will fall at or near the same frequency, resulting in beat stacking. The CSO and CTB are the strongest stack of the second order $(A \pm B)$ and the third order $(A \pm B \pm C)$ products within the 6 MHz channel bandwidth respectively. The CSO and CTB are the most dominant distortion products in multichannel AM SCM systems. Although other types of nonlinear distortion exist such as cross-modulation distortion and harmonic distortion products, they are relatively small compared to the CSO and CTB and usually ignored in system performance measurements.

In the standard CATV channel allocations, the CSO products fall 1.25 MHz above or below the video carriers because they are generated by sums and differences of two carriers whose frequencies are located at 1.25 MHz above the integer multiples of 6 MHz. The third-order intermodulation products fall on the video carrier frequencies themselves, and therefore CTB is measured at the video carrier frequency with the video carrier of the desired channel turned off. CSO and CTB are measured relative to that of the carrier power level and specified in terms of dBc.

The noise and distortion standards for the present coaxial CATV distribution systems require a CNR of 44 dB, and CSO and CTB of -52 dBc or better (i.e. at subscribers' TV sets) [18]. However, the requirements are more stringent for fiber

trunking/feeder distribution systems and are: CNR of approximately 50 dB, CSO and CTB from -55 dBc to -60 dBc (i.e. at the conversion nodes as shown in Fig. 1.2).

2.4.2 Performance Parameters and Requirements for the QAM Signals

The effects of noise and nonlinear distortion on the analog video signals have been thoroughly investigated over the years. Therefore, the performance parameters and requirements are well established for the analog signals. However, for a hybrid AM-VSB/QAM optical transmission system, one also has to be concerned with the impact of noise and nonlinear distortion on the QAM signals as well.

In a hybrid analog/digital optical transmission system, as the composite signal is distorted by the laser threshold nonlinearity, nonlinear distortion products are induced and spread over a wide spectrum. Some of these products fall into the QAM channel and interfere with the digital signals, thus acting as a source of degradation. In order to determine the feasibility of a hybrid AM-VSB/QAM optical fiber transmission system, a thorough knowledge of the impact of nonlinear distortion products on the performance of the QAM signals is required. Therefore, the core of this work involves a comprehensive experimental and theoretical treatment of the impact of nonlinear distortion products induced by laser clipping on the performance of the QAM signals. We will also qualitatively explore the random nature of nonlinear distortion products within a QAM channel bandwidth.

Performance of the QAM signals is specified by the bit error rate (BER). For a feasible hybrid AM-VSB/QAM optical transmission system, a BER of 10^{-5} before Forward Error Correction (FEC) is required in order to obtain at least 10^{-9} after error correction [19].

3. THEORY

As mentioned in Chapter 2, the two major impairments in a hybrid AM-VSB/QAM optical fiber transmission system are noise and nonlinear distortion. Specifications and performance criteria with respect to noise and nonlinear distortion are all well established for analog signals, but not for multilevel QAM signals due to the limited understanding of the effect that nonlinear distortion has on the digital signals. Thus, the objective of this chapter is to provide a theoretical treatment of the BER performance of 64-QAM signals in the presence of noise and nonlinear distortion.

3.1 Noise Analysis

Fig. 3.1 shows an equivalent circuit for the signal and noise sources in a lightwave multichannel SCM system. Since the PIN photodiode is modeled as a current source, it is appropriate to treat the noise sources as current sources. As shown in Fig. 3.1, the three dominant types of noise are : shot noise, RIN noise, and front end noise. In this section, we will examine each noise source and give an expression for CNR for the AM-VSB signals and SNR for the multilevel QAM signals.

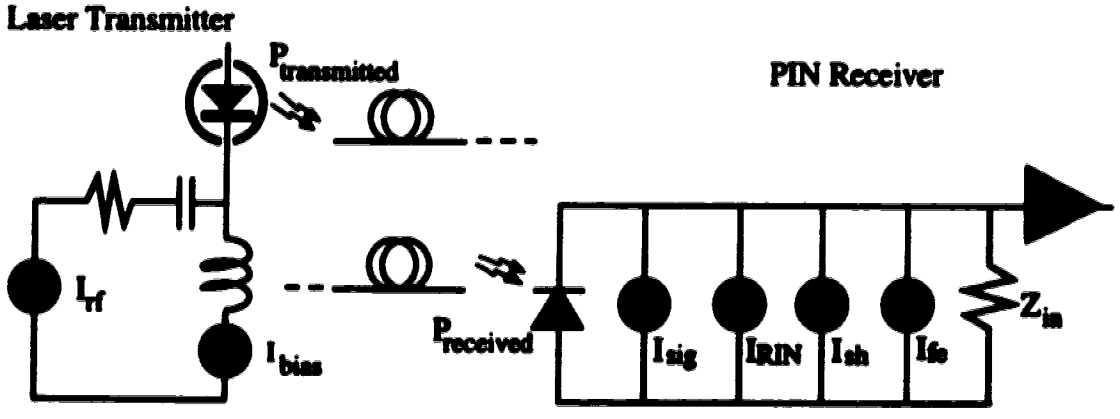

Fig. 3.1 Noise equivalent circuit for the lightwave multichannel SCM system

3.1.1 Modulation Index

In order to accurately account for the contribution of the carrier power for the analog signals and signal power for the digital signals in the noise analysis, it is important to concisely define the modulation index for both the analog and digital signals.

3.1.1.1 Modulation Index for AM-VSB Signals

Fig. 3.2 [20] illustrates the direct modulation of the optical source intensity with an input RF signal. Because the drive current consists of a fixed bias current and an intensity modulating signal, the transmitted optical power waveform can be written as

$$P(t) = P_{bias}(1 + m(t)) \tag{3.1}$$

where P_{bias} is the average optical power at the bias current level, I_{bias}, and $m(t)$ is the intensity modulating signal. In practice, the analog system performance analysis and tests are usually conducted with unmodulated sinusoidal carriers. Therefore, for a single channel, $m(t)$ can be represented as

$$m(t) = m \cdot \cos(2\pi ft) \tag{3.2}$$

where f is the carrier frequency and m is the peak modulation index which is given by

$$m = \frac{P_{peak}}{P_{bias}} , \tag{3.3}$$

where P_{peak} and P_{bias} are defined in Fig. 3.2.

However, since our highly linear laser has a very sharp threshold turn-on and generates negligible optical power when the bias current is below the threshold current value*, one can assume that

$$m = \frac{P_{peak}}{P_{bias}} = \frac{\Delta I}{I_{bias} - I_{th}} \quad , \tag{3.4}$$

where ΔI is the peak amplitude of the modulating current, I_{bias} is the bias current, and I_{th} is the threshold current. The modulation index m is often referred to as the peak modulation index per channel and is specified as a percentage (%).

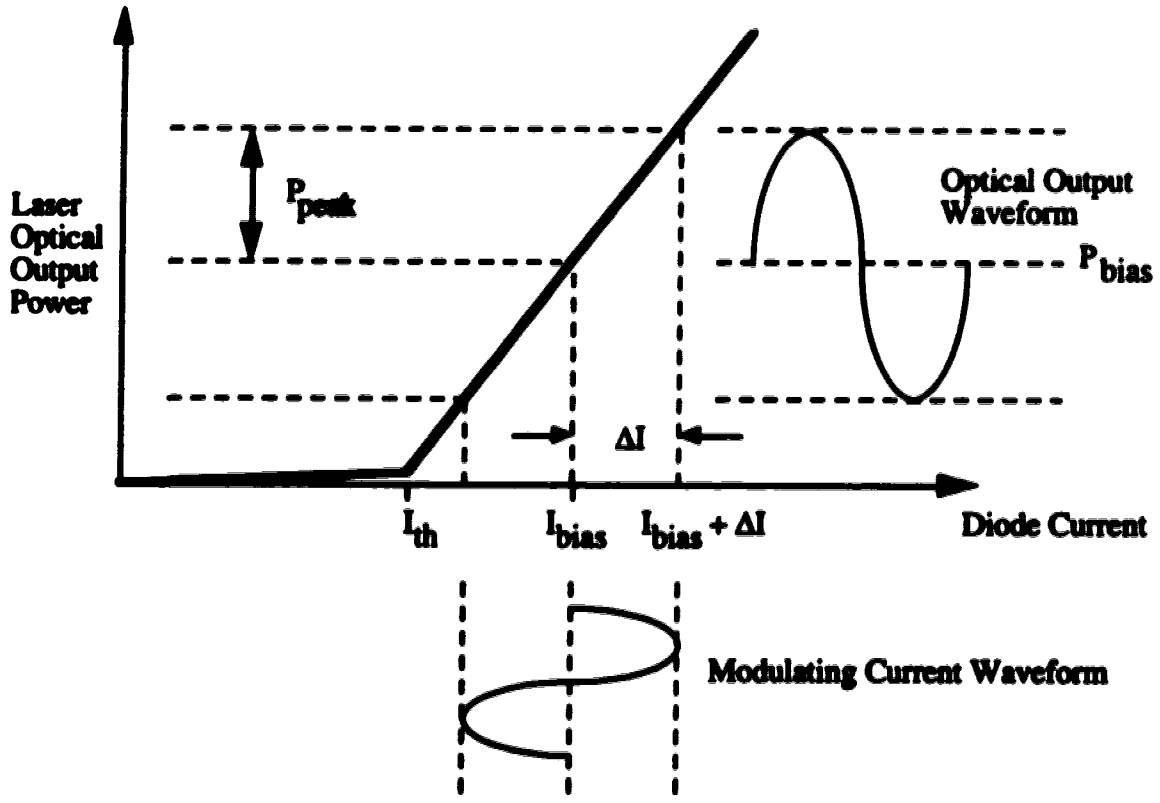

Fig. 3.2 Direct modulation of the optical source intensity

* See Fig. 5.2 for the Optical Power vs. Drive Current characteristic.

In the case of multichannel optical fiber transmission, where a large number of carriers are combined into a single composite signal to modulate the laser, the transmitted optical power waveform can be expressed as [21]

$$P(t) = P_{bias}\left(1 + \sum_{i}^{N} m_i \cos(2\pi f_i t + \theta_i)\right) \tag{3.5}$$

where N is the number of video carriers (TV channels), m_i, f_i, and θ_i are respectively the per channel modulation index, video carrier frequency, and phase of channel i. For random phases and carrier frequencies that are not harmonically related, and with N larger than 10, $P(t)$ can be modeled as a Gaussian random process with a mean value of P_{bias} and variance of $\sigma^2 = P_{bias}{}^2 \frac{Nm^2}{2}$. Thus, we can define the total rms modulation index μ as [21-22]

$$\mu = \sqrt{\frac{Nm^2}{2}} \tag{3.6}$$

which represents the ratio of the rms level of the composite multichannel signal with respect to the mean power level and is often the parameter that determines the nonlinear distortion.

The modulation index for analog signals can also be specified in terms of the rms drive current where

$$m_{rms} = \frac{I_{rms}}{I_{bias} - I_{th}}. \tag{3.7}$$

For sinusoidal carriers, m_{rms} can be related to the peak modulation index, m, by

$$m_{rms} = \frac{\left(\frac{I_p}{\sqrt{2}}\right)}{I_{bias} - I_{th}} = \frac{m}{\sqrt{2}}. \qquad (3.8)$$

Throughout this work, the modulation index for analog signals will refer to the peak modulation index, unless otherwise stated.

3.1.1.2 Modulation Index for the Multilevel QAM Signals

For the analog video signals, CSO and CTB measurements are usually conducted with unmodulated sinusoidal carriers whose envelopes are constant. A 64-QAM modulated signal, on the other hand, has many different envelope levels as shown in Fig. 3.3.

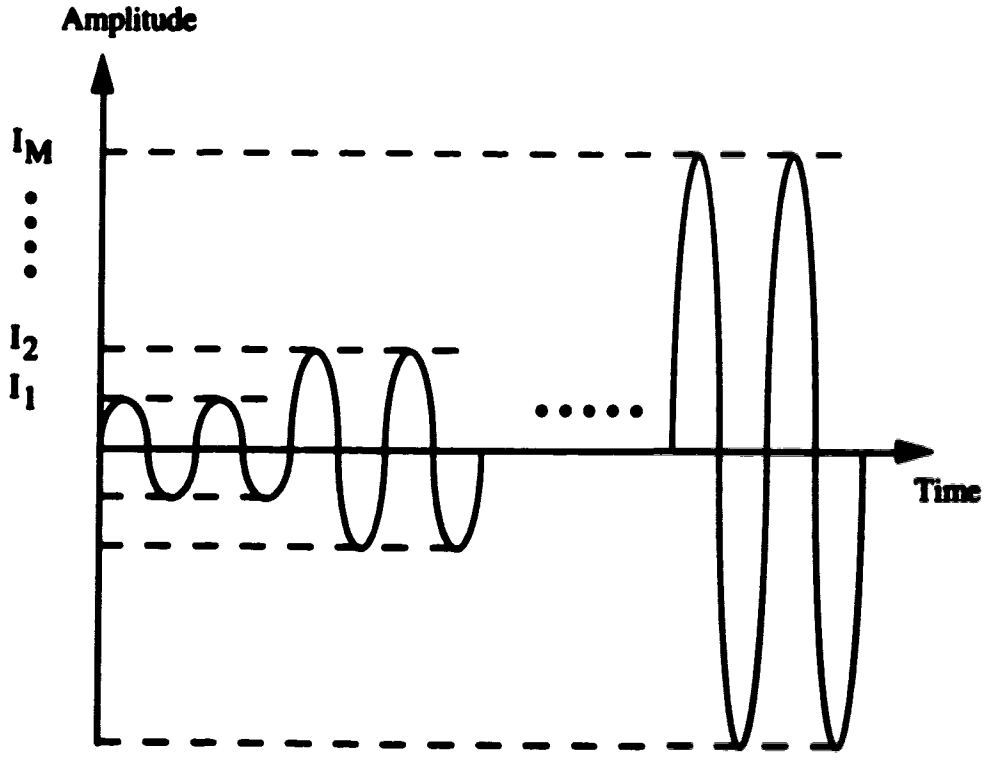

Fig. 3.3 Time domain waveform of a multilevel QAM signal

As can be seen in Fig. 3.3, the envelope of the drive current depends on the transmitted symbol. Therefore, it is convenient to define an effective rms drive current whose amplitude can be found by taking the average of all the symbols' rms currents, assuming that all M signal levels are equiprobable,

$$I_{eff,rms} = \sqrt{\frac{1}{M}\sum_{i=1}^{M}\frac{I_i^2}{2}} \tag{3.9}$$

where I_i is the peak current amplitude of the ith symbol and M is the number of signal levels. As a result, the corresponding effective rms modulation index for QAM signals, $m_{eff,rms}$, is given by

$$m_{eff,rms} = \frac{I_{eff,rms}}{I_{bias} - I_{th}}. \tag{3.10}$$

The effective rms drive current, $I_{eff,rms}$, can be related to the average transmitted QAM channel signal power, P_{QAM}, by

$$I_{eff,rms} = \sqrt{\frac{P_{QAM}}{R}}, \tag{3.11}$$

assuming that the signal voltage is converted directly to a driving current through a resistance R. The average QAM channel signal power, P_{QAM}, is the average RF QAM signal power and can be measured experimentally.

A more commonly used definition of the modulation index for the QAM signals is the effective peak modulation index [23-24] $m_{eff,p}$ which is related to the effective rms modulation index by

$$m_{eff,p} = \frac{I_{eff,p}}{I_{bias} - I_{th}} = \frac{\sqrt{2} \cdot I_{eff,rms}}{I_{bias} - I_{th}} = \sqrt{2} \cdot m_{eff,rms} \tag{3.12}$$

where $I_{eff,p}$ and $m_{eff,p}$ are the effective peak drive current and effective peak modulation index respectively.

Throughout this work, the term "QAM modulation index" will be used to mean the effective peak modulation index for a 64-QAM signal.

3.1.2 AM-VSB Carrier Power

The mean square carrier current at the output of the photodiode is given by [20]

$$\langle i_{AM-VSB}{}^2 \rangle = \frac{1}{2}(m\Re P_o)^2 \tag{3.13}$$

where $\Re$ is the photodiode responsivity, P_o is the average received optical power, and m is the peak modulation index per channel. The mean square signal current is in units of A^2. $\langle i_{AM-VSB}{}^2 \rangle$ can also be expressed in terms of the rms modulation index as

$$\langle i_{AM-VSB}{}^2 \rangle = (m_{rms}\Re P_o)^2 . \tag{3.14}$$

3.1.3 QAM Channel Signal Power

The mean square signal current for multilevel QAM signals is given by

$$\langle i_{QAM}{}^2 \rangle = \frac{1}{2}(m_{eff,p}\Re P_o)^2 \quad \textit{or equivalently,} \quad = (m_{eff,rms}\Re P_o)^2 \tag{3.15}$$

where $m_{eff,p}$ and $m_{eff,rms}$ are the QAM signal effective peak and rms modulation index respectively.

3.1.4 Front End Noise

In this analysis, the noise power for the preamplifier is converted to an equivalent mean square input current, and expressed as A^2. The general expression for the preamplifier noise is [20]

$$\langle i_T^2 \rangle = \frac{4kT}{R_{eq}} \cdot F \cdot B \tag{3.16}$$

where k is the Boltzmann's constant, T is the absolute temperature, R_{eq} is the equivalent resistance of the photodiode load, F is the noise factor of the preamplifier, and B is the effective noise bandwidth.

3.1.5 Shot Noise

This noise component is also often called quantum noise and is given by [20]

$$\langle i_{sh}^2 \rangle = 2q\Re P_e \cdot B \tag{3.17}$$

where q is the electronic charge, $\Re$ is the detector responsivity, and P_e is the average received optical power.

3.1.6 RIN Noise

Laser intensity noise is generally classified as relative intensity noise and is given by [20]

$$\langle i_{RIN}^2 \rangle = RIN \cdot (\Re P_o)^2 \cdot B \tag{3.18}$$

where RIN is defined as

$$RIN = \frac{\left\{(\Delta P(f))^2\right\}}{\langle P_{laser} \rangle^2} \tag{3.19}$$

where $\left\{(\Delta P(f))^2\right\}$ is the spectral density of the mean square deviation of the light output of the laser ($\frac{W^2}{Hz}$) and $\langle P_{laser} \rangle$ is the average light output power of the laser (W). The units of RIN are Hz^{-1}. The level of RIN is dependent on many factors such as the laser bias current, external optical feedback, and frequency. Therefore, RIN is usually specified for a particular frequency and bias current.

3.1.7 CNR

For the AM-VSB signals, the noise performance is often characterized by the ratio of the rms carrier power to the rms noise power referred to the input of the receiver. This ratio is known as Carrier-to-Noise ratio (CNR) and is given by

$$CNR = \frac{Carrier\ Power}{Shot\ Noise + RIN\ Noise + Front\ End\ Noise}. \tag{3.20}$$

By substituting equations (3.13), (3.16), (3.17), and (3.18) into the above equation, the Carrier-to-Noise ratio for a single channel is given by

$$CNR = \frac{\frac{1}{2} m^2 \Re^2 P_o^2}{RIN \cdot \Re^2 P_o^2 \cdot B + 2q\Re P_0 \cdot B + \left(\frac{4kT}{R_{eq}}\right) \cdot F \cdot B} \qquad (3.21)$$

3.1.8 SNR

For the multilevel QAM signals, the channel QAM signal power to noise ratio for a single channel is given by

$$SNR = \frac{\frac{1}{2} m_{eff.p}^2 \Re^2 P_o^2}{RIN \cdot \Re^2 P_o^2 \cdot B + 2q\Re P_0 \cdot B + \left(\frac{4kT}{R_{eq}}\right) \cdot F \cdot B} . \qquad (3.22)$$

3.2 Analysis of Nonlinear Distortion Due to Threshold Nonlinearity

In this section, we describe a nonlinear distortion analysis developed by Alameh et. al. [25] and give an expression for the ratio of signal power (or carrier power for AM-VSB signals) to the nonlinear distortion power in the signal band, or SNLD for short. The nonlinear distortion (NLD) is the total power of NLD components falling within the bandwidth of a single channel.

To analyze the clipping-induced nonlinear distortion, Alameh and Minasian employed a model that utilizes a Gaussian random process to represent the signals in all channels except the one reserved for measurement. This procedure is justified by the central limit theorem, which is that the superposition of a large number of independently varying small quantities yields a resultant with a Gaussian distribution of amplitude [26]. After distortion by the laser, nonlinear distortion power will appear over the bandwidth of

the channel. The carrier-to-nonlinear-distortion is then obtained by dividing the output signal power by the total nonlinear distortion power contained within the bandwidth of the channel under test.

The first step in this analysis is to determine the power spectral density of the nonlinear distortion from the autocorrelation function of the laser output. For rectangular input power spectral density, Alameh et. al. have shown that the autocorrelation function of the laser output consists of a signal term, ${}_{s}R_{o}(\tau)$, and a nonlinear distortion term, ${}_{NLD}R_{o}(\tau)$, which are given in terms of the received optical power as [25]

$$ {}_{s}R_{o}(\tau) = \frac{(m\Re P_{o})^{2}}{2} \cdot h_{o,1}{}^{2} \cdot \sum_{1}^{N} \cos(2\pi f_{n}\tau) \qquad (3.23) $$

$$ {}_{NLD}R_{o}(\tau) = \sum_{k=2}^{\infty} \frac{h_{o,k}{}^{2}}{k!} \cdot \sigma^{2k} \cdot \mathrm{sinc}^{k}(\pi NB\tau) \cdot \cos^{k}(2\pi f_{o}\tau) \qquad (3.24) $$

where N is the number of channels, f_o is the frequency of the centre channel, B is the channel bandwidth, and $\sigma^2 = \mu^2(\Re P_o)^2$ where μ is the total rms modulation index. The coefficients $h_{o,k}$ depend on the laser transfer characteristic. In this analysis, we are only concerned with threshold nonlinearity. Thus, for an ideal laser transfer characteristic,

$$ h_{o,k} = \frac{1}{2\pi} \cdot (-1)^{\frac{k-2}{2}} \cdot \left(\frac{\sqrt{2}}{\sigma}\right)^{k-1} \cdot \exp\left(-\frac{1}{2\mu^{2}}\right) \cdot G_{k-2}\left(\frac{-\sqrt{2}}{\mu}\right) \qquad (3.25) $$

where

$$G_{k-2}\left(\frac{-\sqrt{2}}{\mu}\right)=\sum_{i=0}^{k-2}\frac{(k-2)!}{i!(k-2-i)!}\cdot\left[\frac{\sqrt{(-1)}}{\sqrt{2}\cdot\mu}\right]^{i}\cdot\int_{-\infty}^{\infty}\left(y^{k-2-i}\cdot\exp(-y^{2})\right)dy \tag{3.26}$$

and $h_{o,1}=1$.

The output autocorrelation function given in equations (3.23) and (3.24) may be used to obtain two important results: 1) the total output power by setting τ=0, and 2) the output spectral density by taking the Fourier Transform. For our purposes, we are more interested in the output spectral density. Thus, by taking the Fourier Transform of the output nonlinear distortion autocorrelation function ${}_{NLD}R_{o}(\tau)$, the nonlinear distortion power spectral density ${}_{NLD}W(f)$ is given by [25]

$$\begin{aligned}{}_{NLD}W(f)&=\sum_{k=2}^{\infty}\frac{h_{o,k}^{\ 2}}{k!}\cdot\sigma^{2k}\cdot F\left[\operatorname{sinc}^{k}(\pi NB\tau)\cdot\cos^{k}(2\pi f_{o}\tau)\right]\\&=\sum_{k=2}^{\infty}\frac{h_{o,k}^{\ 2}}{k!}\cdot\sigma^{2k}\cdot\int_{-\infty}^{\infty}\operatorname{sinc}^{k}(\pi NB\tau)\cdot\cos^{k}(2\pi f_{o}\tau)\cdot\cos(2\pi f\tau)d\tau\end{aligned} \tag{3.27}$$

Although the above expression is not in a closed form and looks rather complex, it can be numerically evaluated. The integral in equation (3.27) can be calculated with high accuracy because the function $\operatorname{sinc}^{k}(\pi NB\tau)$ drops off rapidly with increasing τ and k. The computations for the NLD power spectral density also involve a summation of an infinite series. It was found that this series converges slowly and that 50 terms or more were needed to provide accurate estimation*.

Once the power spectral density is calculated, the total nonlinear distortion power within any particular channel can be obtained from

---

* See Appendix C for the calculation of the nonlinear distortion power spectral density.

$$NLD = {}_{NLD}W_o(f_p) \cdot 2B \,, \tag{3.28}$$

assuming that nonlinear distortion is uniformly distributed over the channel bandwidth. f_p is the frequency of the pth channel and B is the bandwidth of the channel.

If a QAM signal of modulation index $m_{eff,p}$ exists in the channel under test, the signal power can be calculated using equation (3.15). The SNLD at the pth channel is then obtained by dividing the output signal power by the nonlinear distortion power falling within the pth channel,

$$SNLD = \frac{\frac{1}{2}\left(m_{eff,p}\Re P_o\right)^2}{{}_{NLD}W_o(f_p) \cdot 2B} \,. \tag{3.29}$$

3.3 BER Analysis of 64-QAM Signals in the Presence of Gaussian Noise

Quadrature amplitude modulation digital signaling was introduced in Section 2.2.2. This type of digital signaling technique is commonly used in microwave digital communications and computer modem systems. In this section, we derive the probability of a bit error for 64-QAM signals in a Gaussian noise environment.

Fig. 3.4 [27] illustrates the first quadrant of a 64-QAM signal constellation in which the boundaries for the decision regions are given by the perpendicular bisectors (the dashed lines) separating the various signal states.

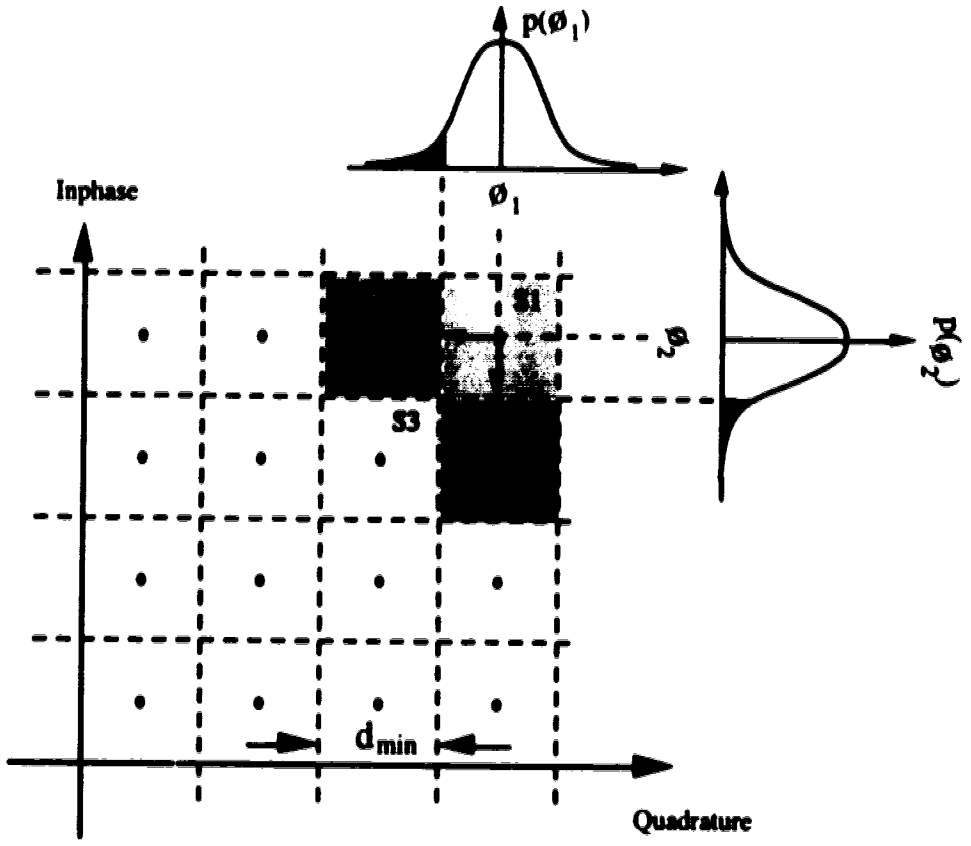

Fig. 3.4 64-QAM vector signal set

As can be seen in Fig. 3.4, a symbol error can occur in more than one direction depending on the number of neighboring signal states that surround the symbol. For example, when one of the corner symbols is transmitted, an error can only occur in two directions. However, errors can occur in three directions for the non-corner edge symbols (i.e. S2 and S4) and four directions for the interior symbols (i.e. S3). As a result, assuming that all the signals are equiprobable, the average symbol error probability for M-ary QAM signals is given by [28]

$$P(E_{symbol}) = 1 - \frac{1}{M} \cdot \sum_{i=1}^{M} P(C|m_i)$$

$$= 1 - \frac{1}{M} \cdot \begin{bmatrix} 4 \cdot P_{2-dir} + 4 \cdot (\sqrt{M} - 2) \cdot P_{3-dir} \\ + \left\{ M - 4 \cdot (\sqrt{M} - 1) \right\} \cdot P_{4-dir} \end{bmatrix} \qquad (3.30)$$

where $P(C|m_i)$ is the probability of a correct decision given that the symbol, S1, is transmitted. P_{2-dir}, P_{3-dir}, and P_{4-dir} are the probabilities of a correct decision for the symbols that are subject to two-directional, three-directional, and four directional errors respectively.

In general, P_{2-dir} is defined as [27]

$$P_{2-dir} = \left(1 - \int_{-d_{min}/2}^{-\infty} p(\theta_1) d\theta_1 \right) \cdot \left(1 - \int_{-d_{min}/2}^{-\infty} p(\theta_2) d\theta_2 \right)$$

$$= (1 - P_e)^2 \qquad (3.31)$$

where P_e is the one directional probability of a symbol error, $p(\theta_1)$ and $p(\theta_2)$ are the amplitude probability density functions of the quadrature and inphase components of the signal, respectively. In this analysis, these two p.d.f. functions are assumed to be equal. d_{min} represents the minimum distance between two neighboring states as shown in Fig. 3.4. Using similar arguments, we have

$$P_{3-dir} = \left(1 - 2 \cdot \int_{-d_{min}/2}^{-\infty} p(\theta_1) d\theta_1 \right) \cdot \left(1 - \int_{-d_{min}/2}^{-\infty} p(\theta_2) d\theta_2 \right)$$

$$= (1 - 2P_e) \cdot (1 - P_e) \qquad (3.32)$$

and

$$P_{4-dir} = \left(1 - 2\cdot \int_{-d_{min}/2}^{-\infty} p(\theta_1)d\theta_1\right)\cdot\left(1 - 2\cdot \int_{-d_{min}/2}^{-\infty} p(\theta_2)d\theta_2\right) \quad (3.33)$$
$$= (1-2P_e)^2$$

By substituting equations (3.31), (3.32), and (3.33) into the symbol error probability given in equation (3.30) yields the result

$$P(E_{symbol}) \cong \frac{4\cdot(M-\sqrt{M})}{M}\cdot P_e \quad . \quad (3.34)$$

In this analysis, we are only concerned with Gaussian noise. Therefore,

$$P(E_{symbol}) \cong \frac{4(M-\sqrt{M})}{M}\cdot\left(\frac{1}{\sqrt{2\pi N_o}}\int_{-d_{min}/2}^{-\infty}\exp\left(\frac{-n^2}{2N_o}\right)dn\right)$$
$$\cong \frac{4(M-\sqrt{M})}{M}\cdot\left(\frac{1}{2}\cdot erfc\left(\frac{d_{min}}{2\sqrt{2N_o}}\right)\right) \quad (3.35)$$
$$\cong \frac{2(M-\sqrt{M})}{M}\cdot erfc\left(\frac{d_{min}}{2\sqrt{2N_o}}\right)$$

where N_o is the noise power. For M-ary QAM signaling, the energy per symbol or power is a function of the signal amplitude (i.e. symbol state), and it is more appropriate to express d_{min} in terms of the average QAM channel signal power [28],

$$d_{min} = \frac{\sqrt{2}\cdot S}{\sqrt{M}-1}$$
$$= \frac{2\cdot\sqrt{P_{ave}\cdot PF_n}}{\sqrt{M}-1} \quad (3.36)$$

where S is the peak signal envelope. P_{ave} is the received QAM channel signal power. PF_m is the ratio of the QAM signal peak power to the average QAM channel signal power. For 64-QAM signals, $PF_{64} = 2.328$. If we define the average QAM channel signal power to noise ratio as

$$SNR = \frac{P_{ave}}{N_o} = \frac{\left[d_{min} \cdot \left(\sqrt{M} - 1\right)\right]^2}{4 \cdot N_o \cdot PF_m} \tag{3.37}$$

then $P(E_{symbol})$ can be expressed in terms of the SNR by

$$P(E_{symbol}) \cong \frac{2(M - \sqrt{M})}{M} \cdot erfc\left(\frac{\sqrt{SNR \cdot PF_M}}{\sqrt{2} \cdot (\sqrt{M} - 1)}\right) . \tag{3.38}$$

So far, we have obtained the probability of a symbol error for M-ary QAM signals. However, the quality of a digital transmission system is often measured by the probability of a bit error which is commonly referred to as the bit error rate (BER). In order to determine BER, one needs to know the relationship between a symbol error and a bit error.

With M-ary QAM signaling, if an error occurs, it is far more likely that a symbol is mistaken for one of its neighbors rather than for the more distant symbols. Therefore, it is desirable to implement a coding scheme such that any two adjacent symbols in the constellation differ by only one bit. This type of code is called a Gray code [29]. Using a Gray code, a symbol error causes only a single bit error, thus minimizing the number of bit errors for a fixed number of symbol errors. Since a M-ary QAM symbol represents a

$\log_2(M)$-bit code, the probability of a bit error for Gray coded M-ary QAM signals is given by

$$P(E_{bit}) = \frac{1}{\log_2(M)} \cdot P(E_{symbol}) = \frac{2(M-\sqrt{M})}{M \cdot \log_2(M)} \cdot erfc\left(\frac{\sqrt{SNR \cdot PF_M}}{\sqrt{2} \cdot (\sqrt{M}-1)}\right) \quad (3.39)$$

Throughout this work, equation (3.39) will be used extensively to evaluate the BER performance of 64-QAM signals in a Gaussian noise environment. Since the SNR is a function of the QAM modulation index and the received optical power, equation (3.39) can also be used to find the BER analytically with respect to the QAM modulation index and the received optical power.

3.4 BER Analysis of 64-QAM Signals in the Presence of Non-Gaussian Impulsive Noise Combined with Gaussian Noise

In a hybrid AM-VSB/QAM optical fiber transmission system, the digital signals are degraded not only by Gaussian noise, but also by the laser threshold nonlinear distortion which exhibits impulsive characteristics in the time domain*. In order to accurately analyze the performance of 64-QAM signals in any system, it is critical to have a realistic noise model. In this case, because the nonlinear distortion products within the channel bandwidth appear impulsive in the time domain, the noise model should be a mixture of Gaussian and non-Gaussian impulsive noise.

In this analysis, Middleton's class A noise model, which is a generalized analytical model of Gaussian noise combined with non-Gaussian impulsive noise, is used.

---

* Experimental results supporting this claim are provided in Section 6.3.1.

This model is applicable to systems in which the frequency components of the impulsive noise are constrained within the bandwidth of the receiver bandpass filter . In this model, the signal amplitude probability distribution function, $p_{I+G}(n)$, is given by [28][30-33]

$$p_{I+G}(n) = e^{-A} \cdot \sum_{j=0}^{\infty} \frac{A^j}{j!} \cdot \frac{1}{\sqrt{2\pi N_{total}\sigma_j^2}} \cdot \exp\left(-\frac{n^2}{2N_{total}\sigma_j^2}\right) \qquad (3.40)$$

where N_{total} is the total noise power $(\sigma_G^2 + \sigma_I^2)$, $\sigma_j^2 = [(j/A) + \Gamma]/(1+\Gamma)$, Γ is the mean power ratio of the Gaussian noise component (σ_G^2) to the non-Gaussian impulsive noise component (σ_I^2), and A is the impulsive index (i.e. the product of the received average number of impulses in a second and the duration of the impulse).

The procedure used to derive the probability of a bit error for 64-QAM signals in the presence of Gaussian noise combined with non-Gaussian impulsive noise is similar to that described in Section 3.3. Let us start with the generalized expression for the average probability of a symbol error for M-ary QAM signals

$$P(E_{symbol}) \cong \frac{4 \cdot (M - \sqrt{M})}{M} \cdot P_e \qquad (3.41)$$

where

$$P_e = \int_{-d_{min}/2}^{-\infty} p(n)dn \qquad (3.42)$$

where $p(n)$ is the signal amplitude probability distribution function.

Since the p.d.f. given in equation (3.40) is different from that of Gaussian noise, P_e has to be recalculated [28].

$$P_e = \int_{-d_{min}/2}^{-\infty} p_{I+G}(n)dn$$

$$= e^{-A} \cdot \sum_{j=0}^{\infty} \frac{A^j}{j!} \cdot \frac{1}{\sqrt{2\pi N_{total}\sigma_j^2}} \cdot \int_{-d_{min}/2}^{-\infty} \exp\left(-\frac{n^2}{2N_{total}\sigma_j^2}\right)dn \quad . \quad (3.43)$$

$$= \frac{e^{-A}}{2} \cdot \sum_{j=0}^{\infty} \frac{A^j}{j!} \cdot \mathrm{erfc}\left(\frac{d_{min}}{2\sqrt{2N_{total}}\sigma_j}\right)$$

In terms of the SNR, P_e can be expressed as

$$P_e = \frac{e^{-A}}{2} \cdot \sum_{j=0}^{\infty} \frac{A^j}{j!} \cdot \mathrm{erfc}\left(\frac{\sqrt{SNR \cdot PF_M}}{\sqrt{2}\left(\sqrt{M}-1\right)\sigma_j}\right) \quad (3.44)$$

where PF_M is the ratio of the QAM signal peak power to the average QAM channel signal power. For 64-QAM signals, $PF_{64} = 2.328$.

Finally, assuming Gray coding, the probability of a bit error for 64-QAM signals in the presence of Gaussian/non-Gaussian impulsive noise is given by [28]

$$P_{I+G}(E_{bit}) \cong \frac{2(M-\sqrt{M})}{M \cdot \log_2(M)} \cdot e^{-A} \cdot \sum_{j=0}^{\infty} \frac{A^j}{j!} \cdot \mathrm{erfc}\left(\frac{\sqrt{SNR \cdot PF_M}}{\sqrt{2}(\sqrt{M}-1)\sigma_j}\right) . \quad (3.45)$$

It is important to note here that the SNR used in the above equation is the ratio of the average QAM channel signal power to the total noise power (Gaussian noise power + impulsive noise power). Thus, SNR can be expressed as

$$SNR = \frac{1}{(SNR_G^{-1} + SNLD^{-1})} . \tag{3.46}$$

Similarly, Γ', which is defined as the mean power ratio of the Gaussian noise component (σ_G^2) to the non-Gaussian impulsive noise component (σ_I^2), can also be expressed in terms of SNR_G and $SNLD$ and is given by

$$\Gamma' = \frac{\sigma_G^2}{\sigma_I^2} = \frac{SNLD}{SNR_G} . \tag{3.47}$$

Substituting equations (3.46) and (3.47) in equation (3.45) yields an expression for the probability of a symbol error that is a function of SNR_G and $SNLD$.

$$P_{I+G}(E_{bit}) \cong \frac{2(M-\sqrt{M})}{M \cdot \log_2(M)} \cdot e^{-A} \cdot \sum_{j=0}^{\infty} \frac{A^j}{j!} \cdot \operatorname{erfc}\left(\frac{\sqrt{\frac{1}{(SNR_G^{-1} + SNLD^{-1}} \cdot PF_M}}{\sqrt{2}(\sqrt{M}-1)\sqrt{\frac{\left(\frac{j}{A} + \frac{SNLD}{SNR_G}\right)}{\left(1 + \frac{SNLD}{SNR_G}\right)}}} \right) . \tag{3.48}$$

This mathematical manipulation is important in that it enables one to determine the impact of each source of degradation on the performance of 64-QAM signals.

Furthermore, since SNR_G and $SNLD$ can be expressed in terms of the modulation index and the parameters, σ_j, depends on Γ' and A which are functions of the modulation index as well, the BER of 64-QAM signals in a hybrid AM-VSB/QAM optical fiber system can also be analyzed with respect to the modulation index.

4. DESIGN AND IMPLEMENTATION OF A HYBRID AM-VSB/QAM OPTICAL FIBER TRANSMISSION SYSTEM

This chapter introduces the experimental AM-VSB/QAM optical fiber transmission system which was designed and implemented in order to test the performance of QAM signals in a hybrid analog/digital environment. A block diagram of the system is shown in Fig. 4.1.

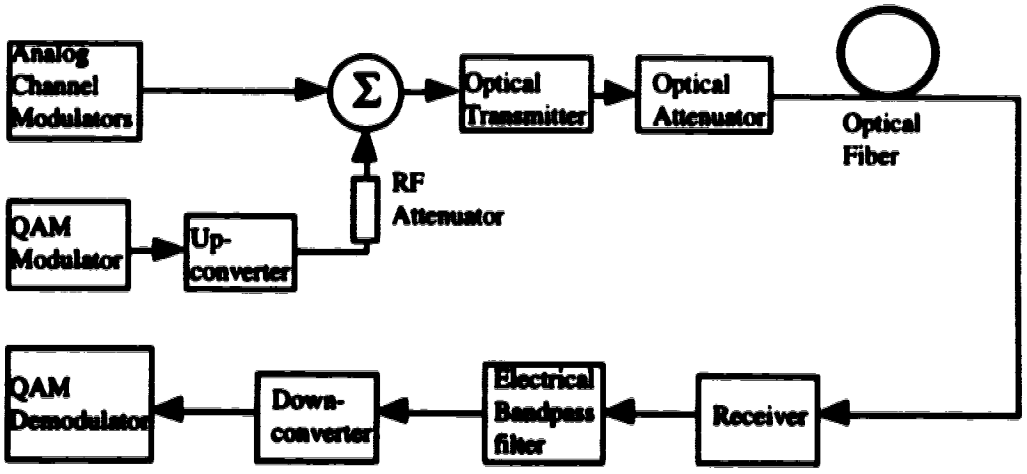

Fig. 4.1 Block diagram of a AM-VSB/QAM optical fiber transmission system

A fiber-optic AM/VSB - QAM transmission system consists of the following components:

i) QAM modulator and demodulator
ii) Analog channel modulators
iii) Up-converter and down-converter
iv) Analog optical transmitter
v) Analog optical receiver

The following sections contain descriptions of each component, in detail. Where possible, an explanation for the techniques or designs used in the construction will be given.

4.1 QAM Modulator and Demodulator

Digital transmit and receive shelves from the Northern Telecom RD-6 digital radio system were modified Bob Thomas of BNR, Dept. 7R15, in order to fit a QAM signal spectrum within a 6 MHz bandwidth TV channel. The system originally operates at a symbol rate of 25.219 Msymbol/second, in a channel 29.65 MHz wide. With the objective of operating within a 6 MHz TV channel, the QAM digital radio system was modified to operate at a symbol rate of 4.5833 Msymbol/second which provides a QAM signal spectrum well within 6 MHz bandwidth [34].

4.1.1 Transmit Shelf

The modified RD-6B transmit shelf contains the following modules: Common Control Unit, Modulator Unit, and Monitor & Alarm Unit. The Common Control Unit receives, scrambles, and Forward Error Correction (FEC) encodes the information bits. The FEC algorithm used is the Double Error Correction Binary Block Code. Data streams are then Gray-to-Binary encoded and routed to the Modulator Unit.

The Modulator Unit accepts six binary data streams from the Common Control Unit, three for the Inphase (I) axis and three for the Quadrature (Q) axis. On each path, a three-bit data symbol is converted to an eight-level Pulse Amplitude Modulation (PAM) signal by a three-bit D/A converter. The PAM signal is then passed through a low pass filter whose response can be approximated by that of a root-Nyquist filter. Next, the QAM linear IF modulator multiplies the Inphase analog signal by the 70 MHz carrier and the Quadrature analog signal by the same carrier shifted by 90 degrees. The result is two 70 MHz Double Sideband, Amplitude Modulated Suppressed Carrier (DSB-AM-SC)

signals which are summed to form the IF output. A block diagram of the modified 64-QAM Modulator Unit is given in Fig. 4.2 [35].

The last module in the transmit shelf is the Monitor and Alarm Unit. It provides alarm indications and an alpha-numeric display of performance monitoring parameters.

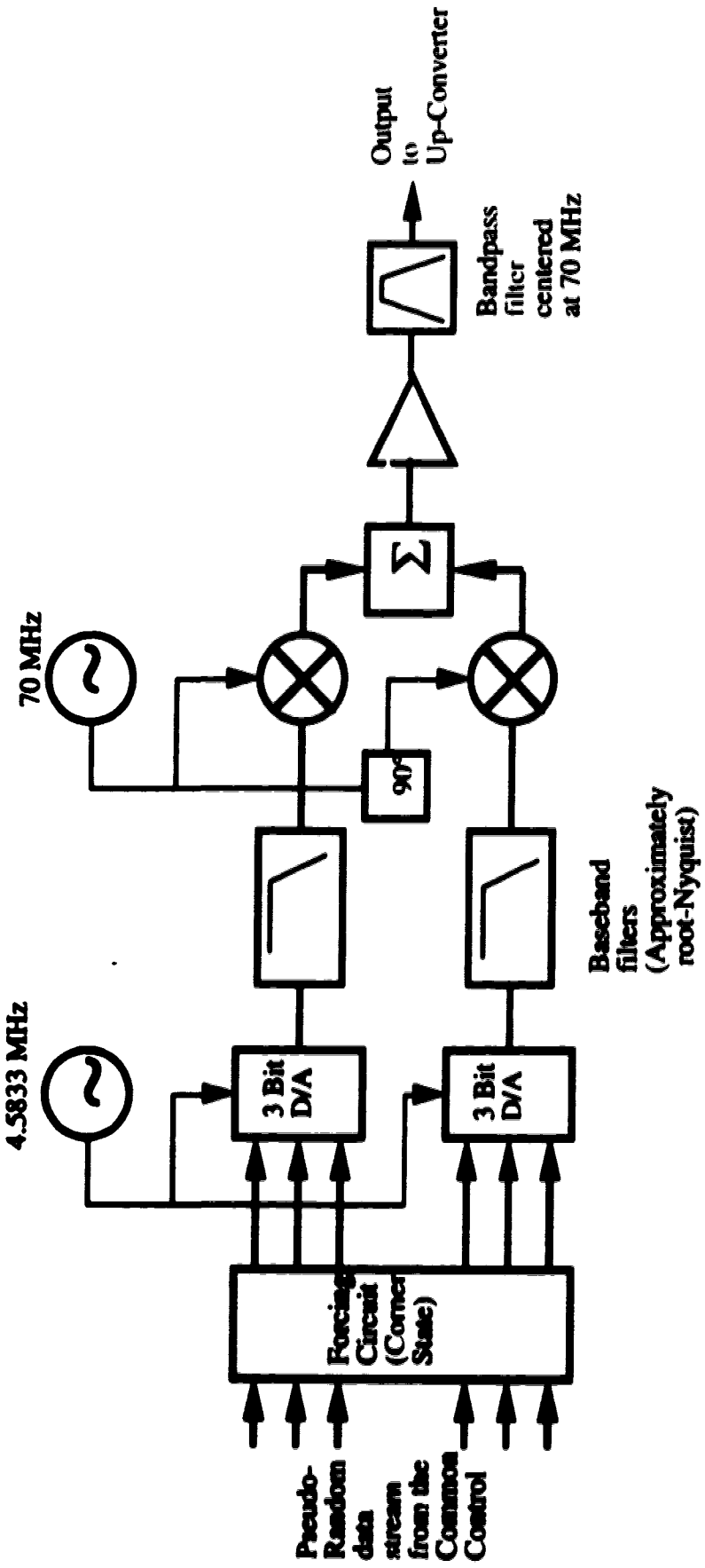

Fig. 4.2 Block Diagram of 64-QAM Modulator Unit

4.1.2 Receive Shelf

Like the transmitter, the modified receive shelf also contains three main modules but in this case they are a Demodulator Unit, a Common Control Unit, and a Monitor and Alarm Unit.

The Demodulator Unit accepts the 64-QAM modulated 70 MHz IF signal. After passing through an Automatic Gain Control (AGC) circuit, the IF signal enters a linear QAM demodulator where it is mixed with a locally generated 70 MHz IF signal. This results in Inphase and Quadrature baseband signals. The next stage is a low pass filter which attenuates the harmonics and equalizes the pulse shape to present an open eye for data regeneration. The primary function of the low pass filters, however, is to reject adjacent channel interference and define the noise bandwidth. The baseband signal is then passed on to the Adaptive Time Domain Equalizer (ATDE) which was designed to minimize the intersymbol interference distortion caused by multipath fading. Finally, the equalized 8-level PAM baseband signals are converted to binary signals by the A/D converters which are controlled by a clock in order to sample the baseband signal at the instant of maximum EYE opening. A block diagram of a 64-QAM Demodulator Unit is given in Fig. 4.3 [35].

The Common Control Unit in the receiver undoes what the Common Control Unit in the transmitter did. It accepts data from the Demodulator Unit. This data is then Binary to Gray decoded, FEC decoded and corrected for any single or double bit errors present within a frame, and finally descrambled and distributed. It is important to note here that even though the QAM digital system has FEC capability, the experimental study presented in Chapter 6 was conducted without FEC correction. The Monitor and Alarm Unit of the receiver has the same function as that in the transmitter.

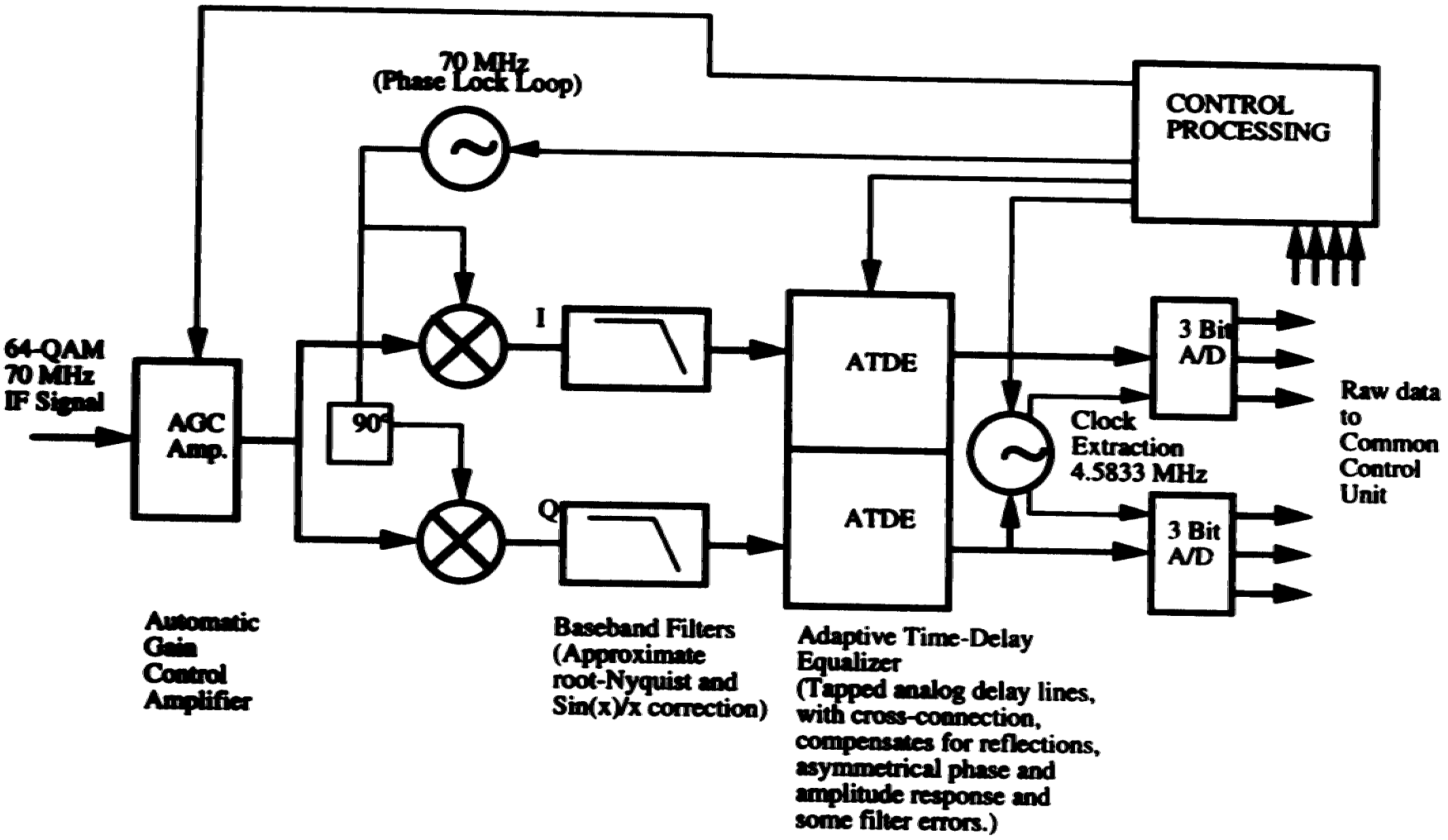

Fig. 4.3 Block diagram of 64-QAM Demodulator Unit

4.2 Analog Channel Modulators

The AM/VSB analog video signals are emulated with the carriers generated by 42 independent Blonder-Tongue modulators. Each modulator generates two carriers, video and audio. The audio carrier is 4.5 MHz higher than the video carrier and approximately 15 dB lower in power. The frequency allocation of these carriers follows that used in CATV systems and is given in Appendix A.

4.3 Up-converter and Down-converter

One of the main objectives in the design of a fiber-optic AM/VSB - QAM transmission system is to build into the system the capability to place the QAM signal spectrum anywhere in the CATV band (50 MHz to 450 MHz) and to recover the signal efficiently without physically altering the system set-up. At first, it seems that a single-stage up-converter and down-converter are capable of such a task. However, this scheme requires a tunable bandpass filter in the up-converter to eliminate the image frequencies and another one in the down-converter to recover the desired signal and at the same time attenuate all other adjacent channels. Tunable bandpass filters that are presently available are tunable over a small frequency range. In order to cover the entire CATV band, a minimum of three such filters is required. A realizable and practical alternative is to use two-stage up-converters and down-converters.

4.3.1 Up-converter

A block diagram of the two-stage up-converter is shown in Fig. 4.4 [34]. At the first frequency mixer, the input 64-QAM 70 MHz IF signal is mixed with a 650 MHz local oscillator carrier. This results in a 64-QAM signal at 580 MHz and an undesired spurious response at 720 MHz which is then eliminated by the 10 MHz wide bandpass filter centered at 580 MHz. At the second frequency mixer, the 64-QAM 580 MHz signal can now be shifted to anywhere in the CATV band (50 MHz to 450 MHz) by mixing with

the local oscillator signal of frequency in the range of 630 MHz to 1030 MHz. The spurious response at this stage is located quite high up in frequency (580 MHz + f_{LO}) and can be easily rejected by the 450 MHz low pass filter in the up-converter.

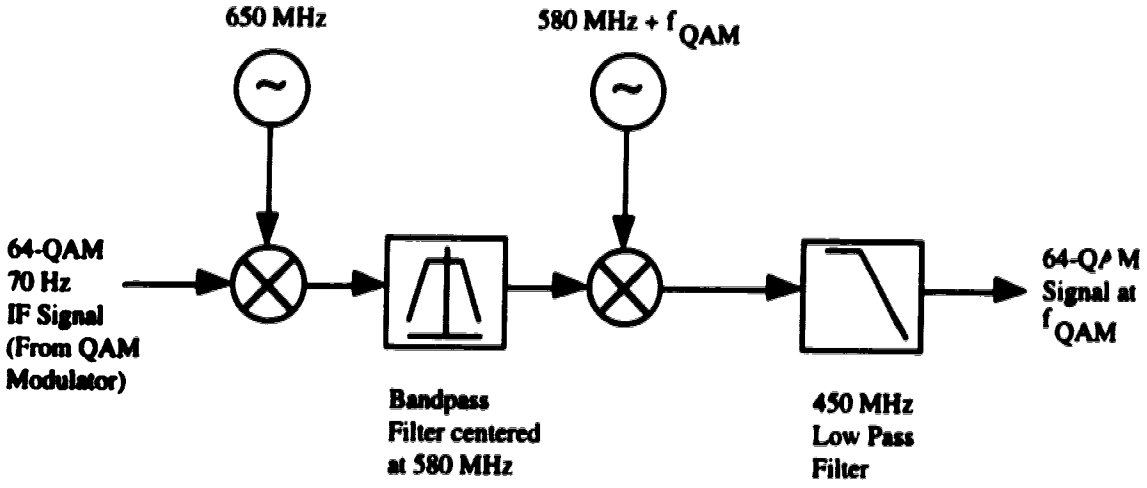

Fig. 4.4 Block diagram of the up-converter

The local oscillator carriers are generated by Hewlett Packard 8656A and Rohde & Scharz signal generators. The two mixers, bandpass filter, and low pass filter used in the design are all from Mini-Circuits. Description and model numbers are given in Table 4.1.

Table 4.1: Up-converter component description and model numbers

Model Number	Description
Mini-Circuits ZLW-2	First mixer in the up-converter
Mini-Circuits ZLW-5	Second mixer
K&L 4B341-580/u12	Bandpass filter centered at 580 MHz
Mini-Circuits SLP-450	Low pass filter with 3dB frequency of 440 MHz

4.3.2 Down-converter

The block diagram of the down-converter is shown in Fig. 4.5 [34]. The purpose of the down-converter is two-fold. Its first task is to shift the received 64-QAM signal back to a 70 MHz IF signal which is the carrier frequency that the QAM demodulator was designed to receive. The second task is to amplify the power of the signal to a level within the dynamic range of the QAM demodulator.

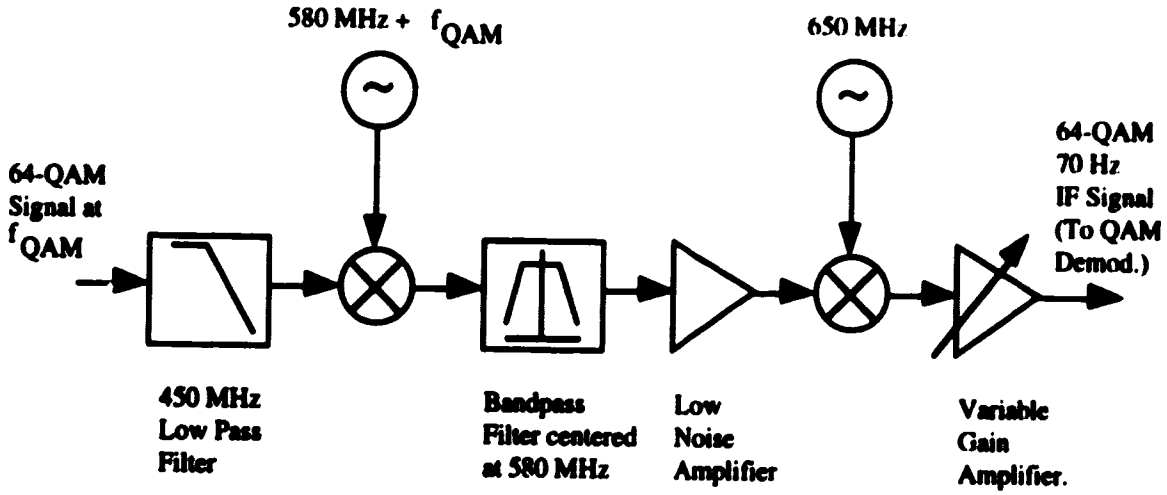

Fig. 4.5 Block diagram of the down-converter

The first component in the down-converter is the 450 MHz low pass filter which is used to attenuate any unwanted high frequency signals that were accidentally picked up during the transmission. The 64-QAM received signal is then mixed with a local oscillator carrier of frequency of 580 MHz + f_{QAM}. This results in a 64-QAM 580 MHz signal which is then filtered out by a 10 MHz wide bandpass filter centered at 580 MHz. After going through two filters and a mixer that has an insertion loss of approximately 9 dB, the signal power level at this point is low. A Low Noise Amplifier (LNA) is used to boost the power of the signal. At the second mixer, the 64-QAM 580 MHz signal is

frequency shifted back to 70 MHz. The local oscillator carrier frequency used for this frequency mixing process is 650 MHz. The final stage of the down-converter is the variable gain amplifier which is used to amplify the signal power to a level that is within the dynamic range of the QAM demodulator.

The local oscillator carriers are generated using Hewlett Packard 8656B and Systron Donner signal generators. Components such as filters, LNA amplifiers, and mixers are from Mini-Circuits. Description and model numbers are given in Table 4.2.

Table 4.2: Down-converter component description and model numbers

Model Number	Description
Mini-Circuits ZLW-5	First mixer in the down-converter
Mini-Circuits ZLW-2	Second mixer
K&L 4B341-580/u12	Bandpass filter centered at 580 MHz
Mini-Circuits SLP-450	Low pass filter with 3dB frequency of 440 MHz
Mini-Circuits ZFL-1000LN	Low Noise Amplfier
Mini-Circuits ZFL-1000GHz	Variable Gain Amplifier

4.4 Analog Optical Transmitter

The transmission of CATV signals in fiber based distribution systems imposes very demanding performance requirements on the optical modulation components. At the transmitter, a linear transfer is needed relating the electrical input to the optical output. The linearity of the transmitter is influenced not only by the laser linearity, but also by the supporting matching, biasing, and amplifying circuits. This section will concentrate on the design of the transmitter and the operation of the supporting circuits.

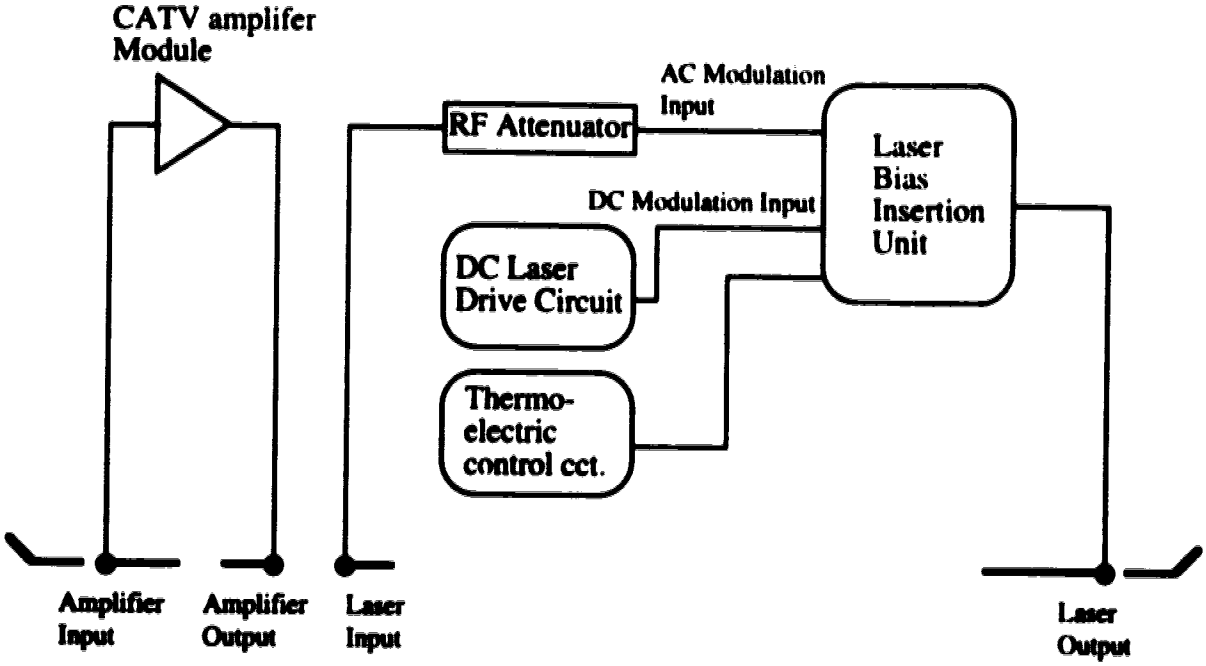

Fig. 4.6 Layout of the analog optical transmitter

The layout of the analog optical transmitter is shown in Fig. 4.6. The diagram indicates that there are three main modules. These are: Laser Bias Unit, DC Laser Drive Unit, and Thermoelectric Cooler Control Unit. Also, incorporated into the transmitter package is a CATV amplifier module which is used to boost the power of the AC modulation signal in cases of weak input signal. The CATV amplifier module, Philips BGY1085A, has a power gain of 19 dB and a bandwidth from 40 to 1000 MHz. All the modules including the laser are packaged in an aluminum box which acts as an EMI shield.

4.4.1 Laser Bias Unit

The schematic diagram of the Laser Bias Unit is shown in Fig. 4.7. This is the module that the laser is mounted on. Because the unit involves the processing of AC signals, it is designed as a microstrip circuit and built on a two-sided printed circuit

board. The diagram shows that there are two input branches. The AC modulation branch consists of a 0.1 μF capacitor which, in combination with a 67 Ω resistor, forms a high pass filter and therefore provides DC isolation. The reason for the choice of 67 Ω value is that of impedance matching. A series combination of a 67 Ω resistor and the laser dynamic impedance which is approximately 8 Ω provides an input resistance of 75 Ω. Therefore, the transmitter input impedance is matched to the 75Ω line impedance of the coaxial cables used in CATV. The DC drive current branch consists of a ferrite bead and a 100 μH inductor which function as an AC block. The bias current is supplied and controlled by the DC Laser Drive Unit.

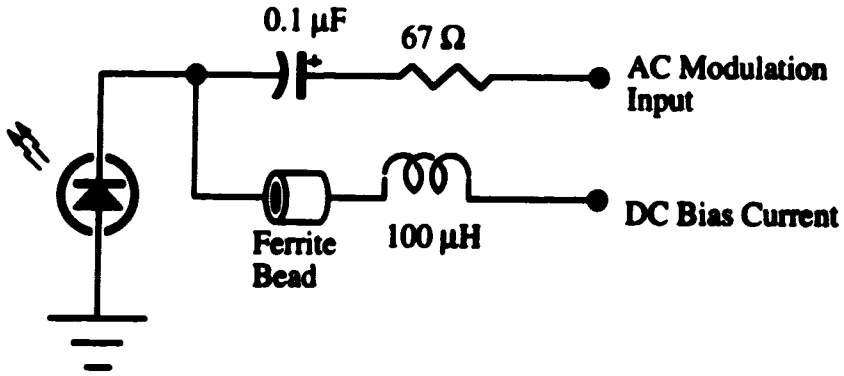

Fig. 4.7 Schematic diagram of the laser bias unit

The laser used in this project is a highly linear distributed feedback (DFB) laser developed by FUJITSU (model FLD150F3ACH-AL). Its peak wavelength is at 1543 nm. A detailed characterization of the laser is given in Section 5.1.

4.4.2 DC Laser Drive Unit

The DC Laser Drive Unit was designed by David D. Clegg of TRLabs. It has several monitor points and safety features. One of the safety features is that of start-up delay circuits which were designed to ensure that the bias current rises up to the preset

value slowly. This is done to avoid bias current over-shoot which can cause permanent damage to the laser. Another safety feature is the current limit circuit. It was designed to protect the laser in cases where the bias current rises up out of control or is accidentally set at a value beyond the current specification of the laser.

The laser bias current control is accomplished with a feedback loop in which the back facet photocurrent is the feedback signal. Key elements of this loop are the back facet photodiode which is built into the laser package, an error amplifier, and an output driver amplifier. The back facet photocurrent is measured and scaled. This current is then compared to a set point current, to produce an error signal proportional to the difference. This signal is then routed to a transistor, the output driver, which controls the magnitude of the laser bias current. The DC Laser Drive Unit also provides a numeric LED display of the laser bias current and the back facet photocurrent.

4.4.3 Thermoelectric Cooler Control Unit

The principles behind the design of the temperature control circuit are similar to that of the laser bias current control unit. Both designs use feedback control. In the case of temperature control, the feedback loop consists of a thermistor temperature sensor, an error amplifier, and the output driver. The temperature is measured by a thermistor which is a device whose resistance varies with temperature. This temperature is then compared to a set point temperature. The difference results in a proportional error signal. This signal then controls the output driver that regulates the amount of current passing through the thermoelectric cooler. The thermoelectric cooler is a junction of dissimilar metals that can heat or cool small thermal loads by passing an electric current through the junction [36].

4.5 Analog Optical Receiver

The purpose of the optical receiver in an optical fiber video transmission system is to convert the optical signal into an equivalent electrical signal. For optimum link performance, the receiver module must have low distortion and low noise. A schematic diagram of the receiver used in the measurements described in this documents is shown in Fig. 4.8.

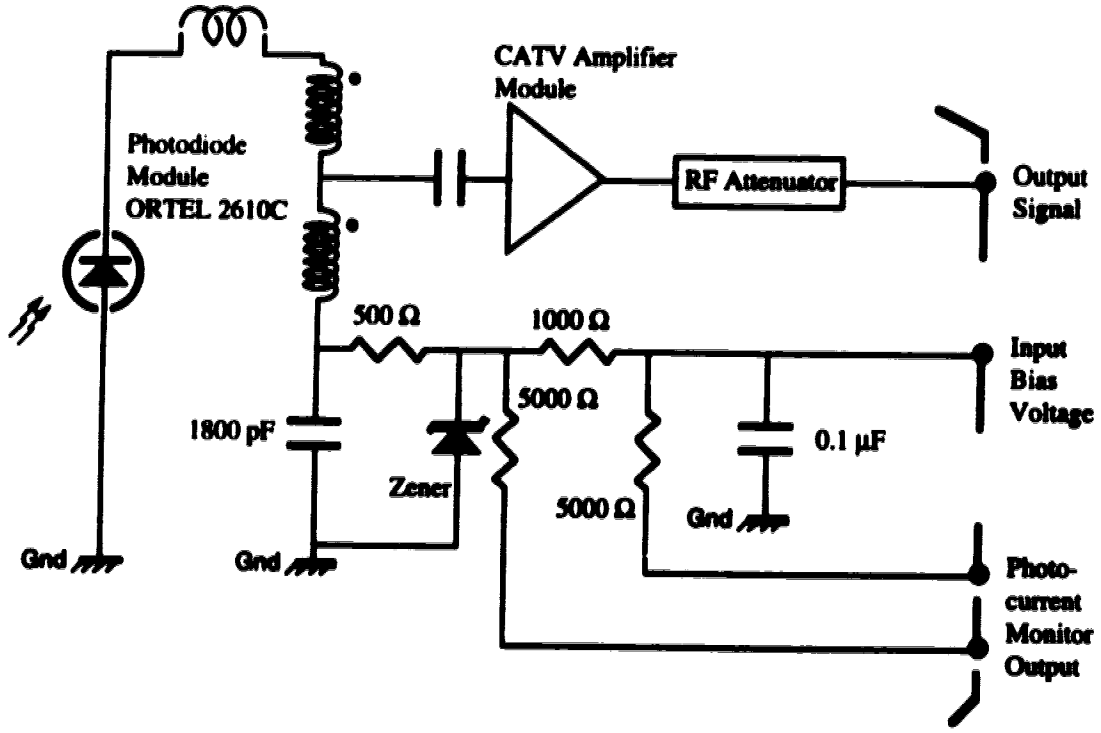

Fig. 4.8 Schematic diagram of the analog optical receiver

This receiver involves direct coupling between a photodiode module (Ortel 2610C) and a CATV hybrid amplifier. This high dynamic range push-pull amplifier is commonly used for video transmission through coaxial cables.

The Ortel 2610C Broadband Photodiode Module has a bandwidth from 40 to 600 MHz. It has a built-in impedance transformer which was designed to improve noise performance and to transform the photodiode high output impedance to the 75 Ω CATV

amplifier input impedance. The receiver also provides a photocurrent monitor output. The photocurrent is proportional to the voltage across the 1000 Ω resistor. The Philips BGY1085A CATV amplifier module has a bandwidth of 1000 MHz and a gain of approximately 19 dB. The noise figure for this amplifier is 6.5 dB.

5. OPTICAL LINK CHARACTERIZATION

In order to analyze the experimental results and correctly assess the performance of a hybrid AM/VSB-QAM SCM system, a firm knowledge of the characteristics of the optical link and its components, particularly the laser, is required. This chapter begins with the measured fundamental characteristics of the laser such as the L-I curve and spectrum scan, and then proceeds on to the laser linearity results. The frequency response of the optical link is also presented in this chapter.

5.1 Laser Characteristics

The laser used in the analog transmitter was purchased from Fujitsu Microelectronics, Inc. This highly linear distributed feedback (DFB) laser is packaged with a short fiber pigtail. At room temperature (~ 25 deg. C), the operating peak wavelength is around 1542.9 nm as shown in Fig. 5.1. The spectrum was scanned using a CVI Digikrom 240 Digital Monochromator which is controlled by a Macintosh II Si computer using the software package called LabVIEW™.

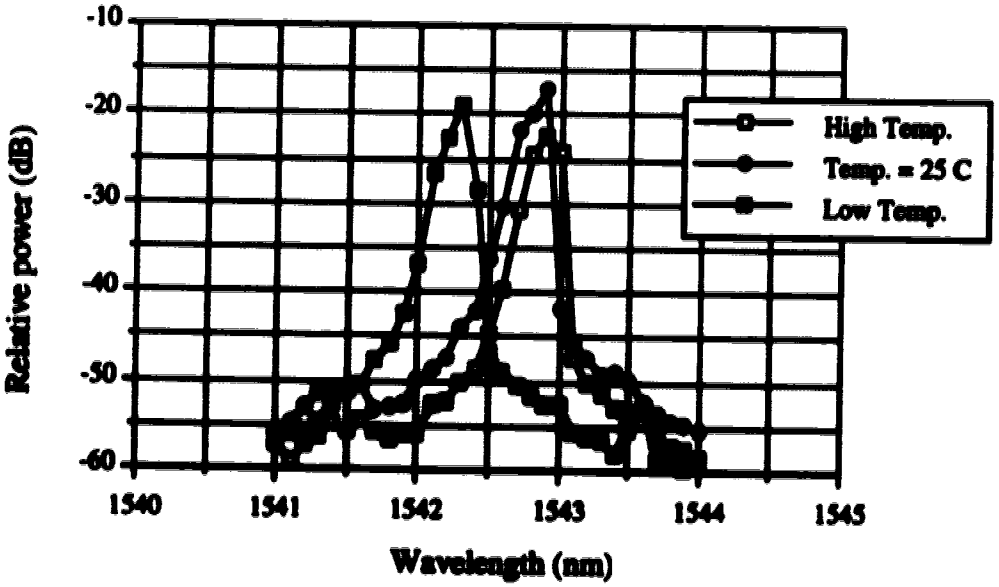

Fig. 5.1 Spectrum of the Fujitsu DFB laser, resolution = 0.1 nm, I_{bias} = 50 mA

As shown in Fig. 5.1, the laser wavelength is approximately 1542.9 nm. In addition, it is tunable over 1 nm range by varying the temperature of operation with the temperature control unit. The laser has a RIN specification of -160 dB/Hz and -165 dB/Hz at 50 MHz and 550 MHz respectively. Its internal dynamic resistance is approximately 7 Ω. The laser threshold current rating was 18.5 mA which is confirmed by the measured L-I curve shown Fig. 5.2. The optical power vs. backfacet monitor photocurrent plot is given in Fig. 5.3.

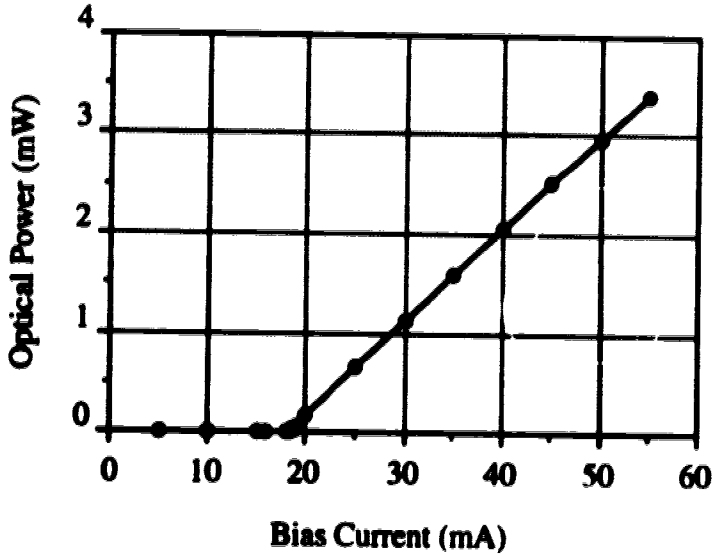

Fig. 5.2 Optical power vs. drive current for Fujitsu 1550 nm DFB laser

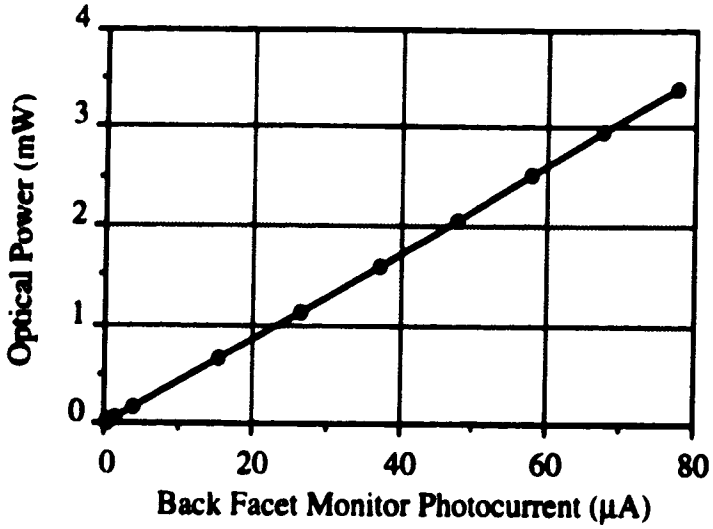

Fig. 5.3 Optical power vs. back facet monitor photocurrent for Fujitsu 1550 nm DFB laser

5.2 Laser Linearity

The nonlinear distortion performance of the system is mainly dictated by the nonlinear distortion performance of the laser diode. In this section, the linearity of the laser diode is examined by measuring the CSO at Channel 2 for various bias current levels using the experimental set-up shown in Fig. 5.4.

Fig. 5.4 Block diagram of the laser linearity experimental set-up

The power level of the composite 42 CATV carrier signal generated by the matrix generator is set at -20.6 dBm per channel, or equivalently 1.9 % modulation index per channel at bias current of 50 mA. The CSO in Channel 2 is then measured as the bias current is varied from 30 mA to 58 mA. Fig. 5.5 shows CSO measurements as a function

of the laser diode bias current. As can be seen in the figure, the laser is most linear at the bias current of approximately 51 mA. It also shows that CSO increases at low bias current. This increase is attributed to the signal distortion caused by the threshold nonlinearity. Because of the laser's uncertain reliability at high output optical power, no measurements were made at a bias current level beyond 60 mA.

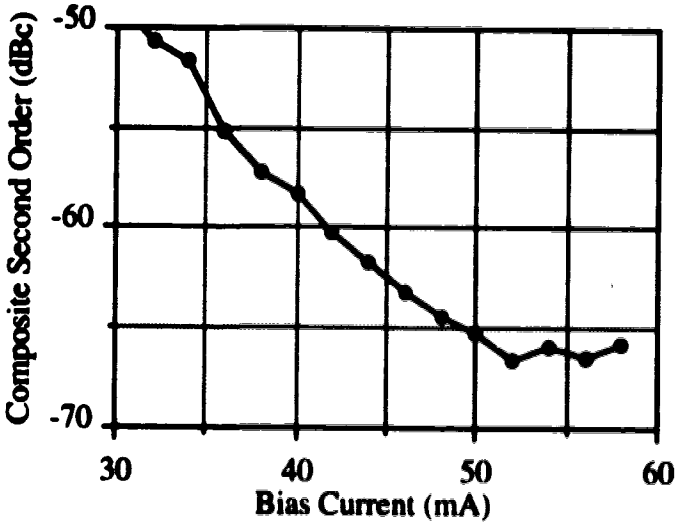

Fig. 5.5 Laser linearity as a function of the bias current

5.3 Frequency Response

The frequency response of an optical link is dependent on the frequency response of its components such as the laser diode, photodiode, CATV amplifier modules, and also the supporting circuits and the electrical connections. The set-up shown in Fig. 5.6 was used to obtain the frequency response of the optical link.

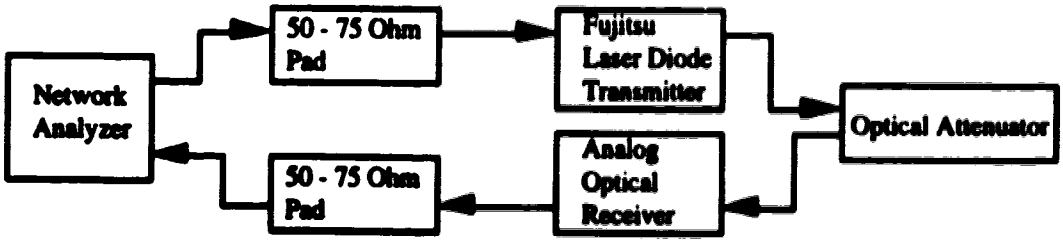

Fig. 5.6 Set-up used to obtain the optical link's frequency response

A pair of 50-75 Ω attenuation pads was used to provide the impedance matching between the Network Analyzer's 50 Ω terminals and the transmitter and receiver's 75 Ω input/output impedance. These pads have an insertion loss of 5.7 dB. The laser is biased at 50 mA. The optical attenuator is set at 0 dB attenuation and has an insertion loss of 2.1 dB.

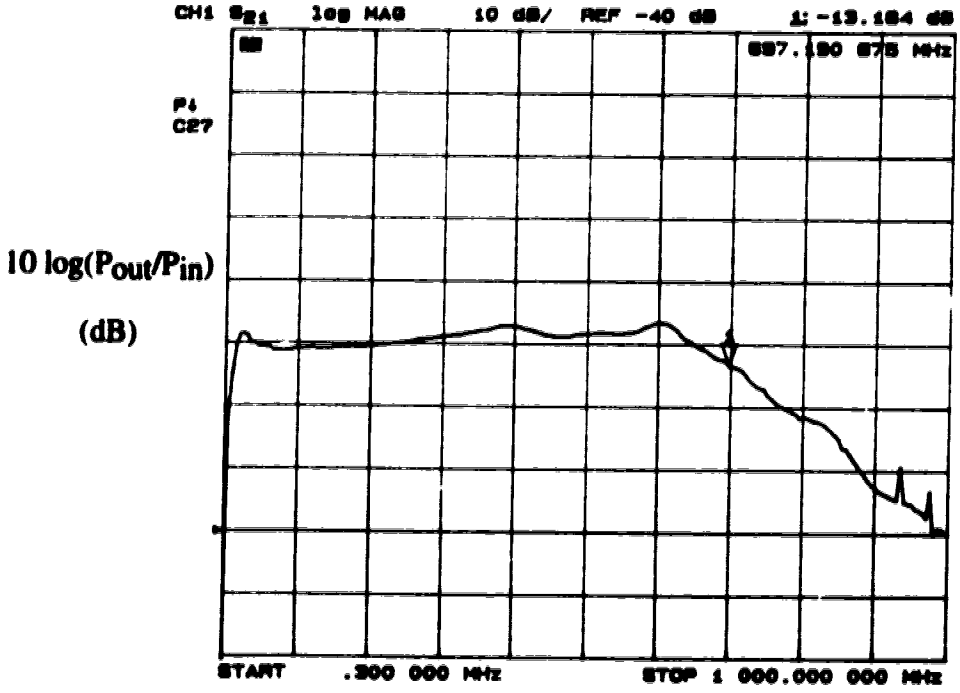

Fig. 5.7 Frequency response of the optical link

The frequency response of the optical link is shown in Fig. 5.7. This Figure indicates that the 3 dB bandwidth ranges from approximately 40 MHz to 700 MHz which is sufficient for this project. The optical link bandwidth is essentially limited by that of the photodiode module. It is also observed that midband gain is not constant. This is critical in the calibration of the modulation index and, therefore, will be taken into account in the calibration process which is described in Appendix B. The gain fluctuation in the passband is less than 3 dB.

6. RESULTS

In this chapter, the performance of 64-QAM signals in a hybrid fiber-optic AM/VSB-QAM transmission system is investigated based on experiments and the theoretical analysis described in Chapter 3. Noise and nonlinear characterizations for analog carriers are first presented, followed by BER calibrations for digital signals. Next, the performance of 64-QAM signals in a hybrid analog/digital environment is investigated. This section investigates the two fundamental sources of degradation which are distortion interference due to laser clipping and noise, and determines the extent to which the BER performance of a 64-QAM signal is degraded by each source. In addition, results of a study of the effects of fiber dispersion and EDFA's non-flat gain spectrum on BER performance are presented. Finally, the experimental results are analyzed and used in a channel capacity study which demonstrates the feasibility to simultaneously transmit AM/VSB and 64-QAM signals over optical fiber.

6.1 Noise and Nonlinear Distortion Performance of AM/VSB Carriers

In this section, we consider the performance of the analog AM-VSB signals when there are no QAM signals present. The quality of the analog AM/VSB signals is determined by three parameters: CNR (for noise), CSO and CTB (for nonlinear distortions).

6.1.1 CNR Performance

As stated in Section 3.1, the noise performance of an analog system is often characterized by the Carrier-to-Noise Ratio which is given by

$$CNR = \frac{\frac{1}{2} m^2 \Re^2 P_o^2}{RIN \cdot \Re^2 P_o^2 \cdot B + 2q\Re P_o \cdot B + \left\{ i_{th}^2 \right\} \cdot B} \qquad (6.1)$$

where m is the peak modulation index per channel, $\Re$ is the photodiode responsivity, P_o is the averaged received optical power, B is the effective noise bandwidth, q is the electron charge, and $\left\{ i_{th}^2 \right\}$ is the receiver mean square thermal noise current spectral density. The first term in the denominator of equation (6.1) accounts for the CNR limitation caused by RIN. The second term accounts for shot noise and the third term accounts for receiver thermal noise.

In order to compare the CNR performance prediction based on equation (6.1) with that of the actual system, the system CNR was measured using the experimental set-up as shown in Fig. 6.1. The set-up consists of a composite signal of 42 video carriers modulating the output optical intensity of our highly linear 1550 nm Fujitsu DFB laser. Because this laser has an optical isolator built into its package, the RIN contribution is limited to the intrinsic RIN of the laser diode. The optical signal is then received by the ORTEL 2610C photodiode module, amplified, and routed to a spectrum analyzer for measurements. The modulation index per channel* is 0.04. The laser diode has RIN specification of -160 dB/Hz at a bias current of 50 mA. The photodiode module has a responsivity of 0.94 A/W and a thermal noise current density referred to the output of the photodiode of [37]

$$\left\{ i_{th} \right\} = 7.3 \cdot 10^{-12} \cdot 10^{\frac{(F-G)}{20}} \quad A/\sqrt{Hz} \qquad (6.2)$$

---

* A detailed description of the calibration procedure for the modulation index is provided in Appendix B.

where F is the amplifier noise figure and G is the current gain of the transformer. Typical values for the amplifier noise figure and the current gain are 6.5 and 7 dB respectively.

The first step in the CNR measurement procedure is to measure the carrier power. With the spectrum analyzer adjusted to the following settings: resolution bandwidth of 30 KHz, video bandwidth of 100 Hz, frequency span of 10 MHz, and automatic sweeptime, the carrier power is measured by tuning the marker to the carrier and recording the power level read-outs. For noise measurements, it is critical to make sure that the noise observed on the spectrum analyzer monitor is from the system under test and NOT from the spectrum analyzer itself. A simple test to determine the noise source is to observe the changes in the noise level when the system under test is disconnected from the spectrum analyzer. If the noise floor remains unchanged, this indicates that the noise from the spectrum analyzer is the dominant source of noise. On the other hand, a large decrease in the noise level indicates that noise from the system under test is dominant. One can increase the difference between the spectrum analyzer noise floor and the system noise floor by decreasing the spectrum analyzer input attenuator. However, low input attenuation can cause overloading, thus distorting the composite 42 CATV carrier signal. Using the HP-8568A spectrum analyzer's built-in noise measurement function, noise is measured in units of dBm/Hz. This built-in function takes into account the shape of the resolution bandwidth filter in the spectrum analyzer. Therefore, the total noise in a 4.25 MHz bandwidth is given by

$$N = \langle N \rangle + 10 \cdot \log(4.25 \cdot 10^6) \qquad (6.3)$$

where $\langle N \rangle$ is the noise density (dBm/Hz). Finally, CNR is obtained by taking the difference in decibels between the carrier power and noise power.

Fig. 6.1 CNR measurement experimental set-up

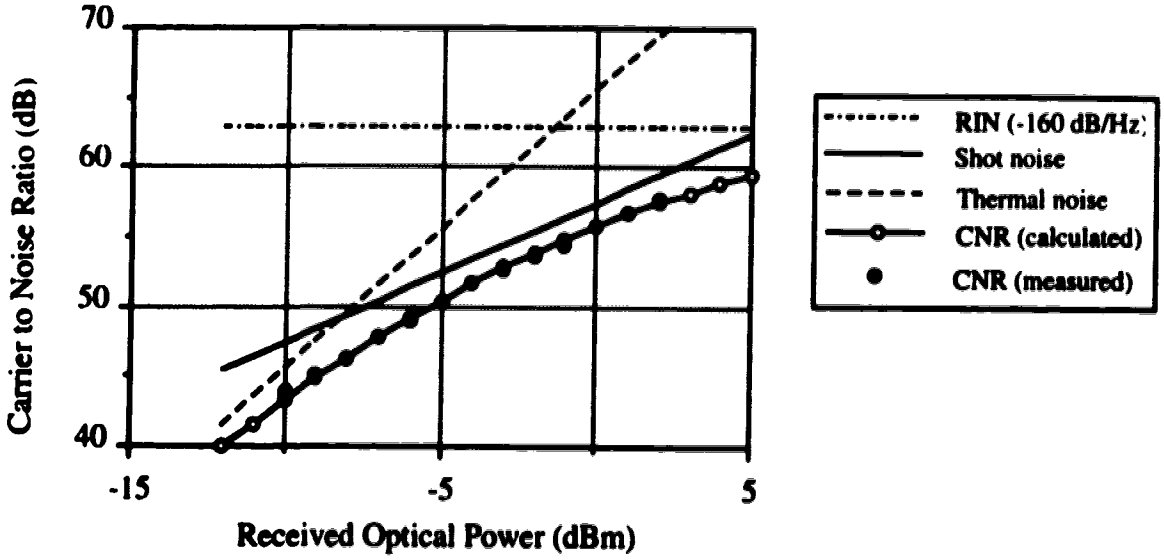

Fig. 6.2 CNR performance with respect to received optical power level
$m_{AM\text{-}VSB}$ = 4% per channel, I_{bias} = 50 mA

The measured CNR with respect to various received optical power levels is plotted in Fig. 6.2 along with the results calculated from equation (6.1). In addition, the individual contributions from laser diode RIN, photodetector shot noise, and receiver thermal noise are also plotted showing different noise limited regimes for different received optical power levels. As can be seen from Fig. 6.2, there is close agreement between the measured and calculated results. This indicates that the CNR equation and the various noise parameters are valid and can be used to predict the noise performance of the system. Comparisons between the system CNR and the individual noise contributions show that there are three distinct noise limited regimes: a) the RIN noise limited region

which limits the maximum attainable CNR at high received optical power levels; b) the thermal noise limited region which limits the maximum attainable CNR at low received optical power levels; c) the shot noise limited region which limits the maximum attainable CNR at the intermediate received optical power levels.

6.1.2 Nonlinear Distortion Performance

Distortion exists in the system due to nonlinearities in the operating characteristics of the components which make up the distribution link. The three main nonlinear mechanisms that significantly affect the performance of an optical analog system are 1) intrinsic nonlinearity of the laser, 2) the threshold nonlinearity of the laser, and 3) the nonlinear distortion due to the combination of chirp of the laser diode and fiber dispersion.

6.1.2.1 Characterization of Intrinsic and Threshold Nonlinearity

For conventional CATV signals, nonlinear distortion performance is specified in terms of CSO and CTB requirements. The nonlinear distortion products within the 6 MHz video channel bandwidth of Channel 2, shown in Fig. 6.3, indicates that nonlinear distortion appears at discrete frequencies. For the standard CATV channel allocations, the CSO products fall 1.25 MHz above and below the video carriers whereas the CTB products fall on the video carrier frequency. Both CSO and CTB are measured relative to the carrier power level and specified in terms of dBc.

For the measurements of CSO and CTB, a bank of Blonder-Tongue modulators was used to generate 42 CATV carriers whose frequency allocations are given in Appendix A. A bandpass filter is added between the receiver and the spectrum analyzer to the experimental set-up shown in Fig. 6.1. The purpose of the bandpass filter is to reject signals from the channels that are not being tested, thus preventing overloading of

the spectrum analyzer. Using NCTA recommended procedures [38] for measuring CSO and CTB, the spectrum analyzer is adjusted to the following settings: resolution bandwidth of 30 KHz, video bandwidth of 100 Hz, span of 10 MHz, and sweeptime of 0.2 sec per division.

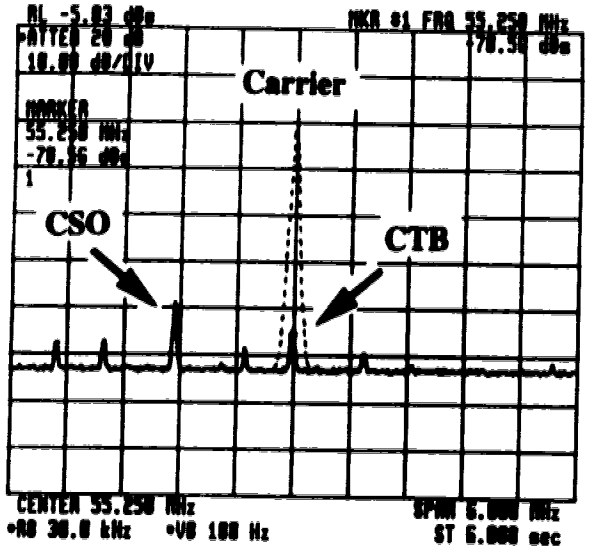

Fig. 6.3 Nonlinear distortion products in Channel 2

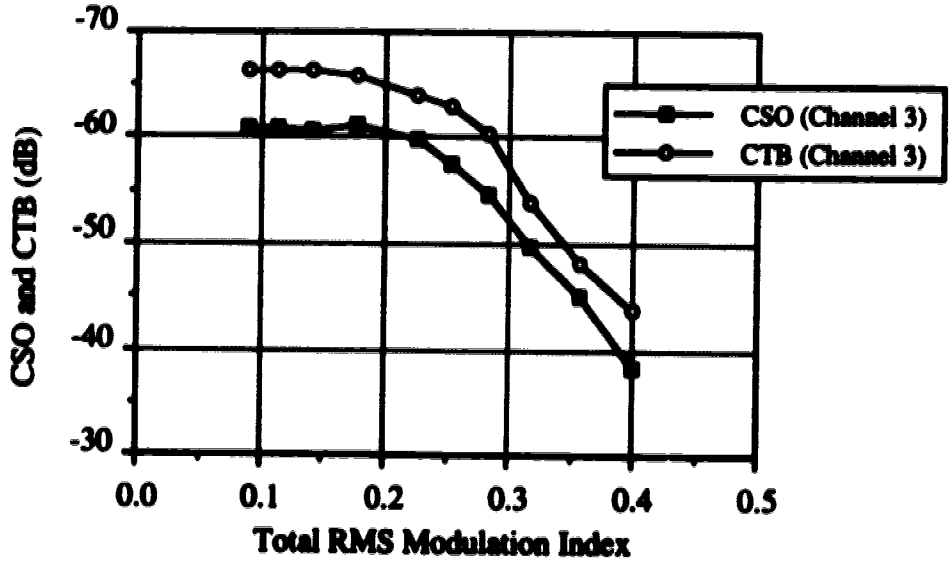

Fig. 6.4 CSO and CTB in Channel 3 as function of total rms modulation index
$P_{received}$ = -1 dBm, I_{bias} = 50 mA

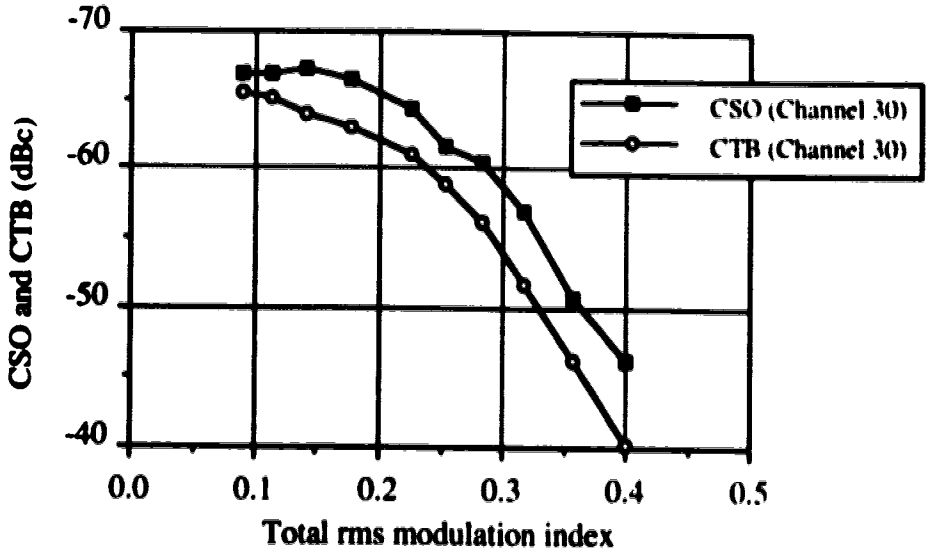

Fig. 6.5 CSO and CTB in Channel 30 as function of total rms modulation index
$P_{received}$ = -1 dBm, I_{bias} = 50 mA

Fig. 6.4 and 6.5 show the measured CSO and CTB of Channel 3 and Channel 30. To measure CSO and CTB degradation due to signal clipping, the modulation index per channel, m, is initially set to a small value such that the composite current level does not fall below threshold. The modulation index per channel is gradually increased by increasing the input current level, thereby effectively increasing the total rms modulation index μ which is given by

$$\mu = \sqrt{\frac{m^2 \cdot N}{2}} \tag{6.4}$$

where N is the number of channels. The modulation index level will eventually be large enough to cause signal clipping. Fig. 6.4 and 6.5 indicate that at low total rms modulation index μ, the intrinsic CSO and CTB are observed. As the rms modulation index is increased, distortion due to laser clipping occurs and dominates over the intrinsic CSO and CTB for u > 0.25.

6.1.2.2 Nonlinear Distortion Due to Laser Chirp and Fiber Dispersion.

In an AM/VSB optical fiber system, particularly when operating at 1550 nm wavelength which is away from the minimum dispersion wavelength of 1300 nm, the fiber chromatic dispersion and the laser diode chirp under modulation produce excess second order distortion which degrades the CSO performance. In this section, the mechanism which produces this type of second order type distortion is described and its impact on system performance is studied.

When the laser diode is under direct intensity modulation, the optical frequency (or wavelength) of the output is also modulated. This phenomenon is called laser diode frequency chirp or, simply, laser chirp which is a consequence of the optical frequency being dependent on the refractive index of the laser's active layer. Modulation of the injection current causes variations in carrier density, which in turn yields a variation in the active layer refractive index and hence a variation in the lasing mode optical frequency.

Fiber dispersion causes light of different wavelengths to travel at different group velocities resulting in wavelength-dependent delay. As the intensity modulated light is transmitted through a dispersive medium, such as optical fiber, the laser frequency modulation is converted to a modulation of the transmission delay and, consequently results in distortion.

For experimental measurements of the nonlinear distortion produced by laser chirp and fiber dispersion, 1310 nm single-mode optical fiber of 10 km in length was added to the experimental set-up shown in Fig. 6.1 in order to introduce fiber chromatic dispersion to the system. The experimental procedures and parameters are basically the same as those described in Section 6.1.2.1. Fig. 6.6 and 6.7 show the measured CSO and CTB of Channel 3 and Channel 30 as functions of the rms modulation index. Also

plotted in the same figures are the CSO and CTB performances obtained from systems with negligibly short fiber link.

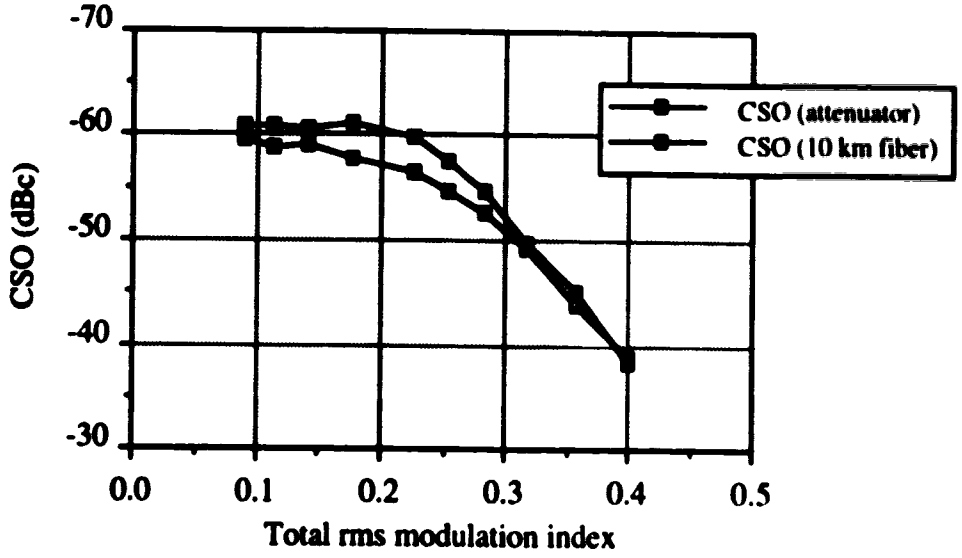

Fig. 6.6(a) CSO in Channel 3 with and without fiber transmission
$P_{received}$ = -1 dBm, I_{bias} = 50 mA

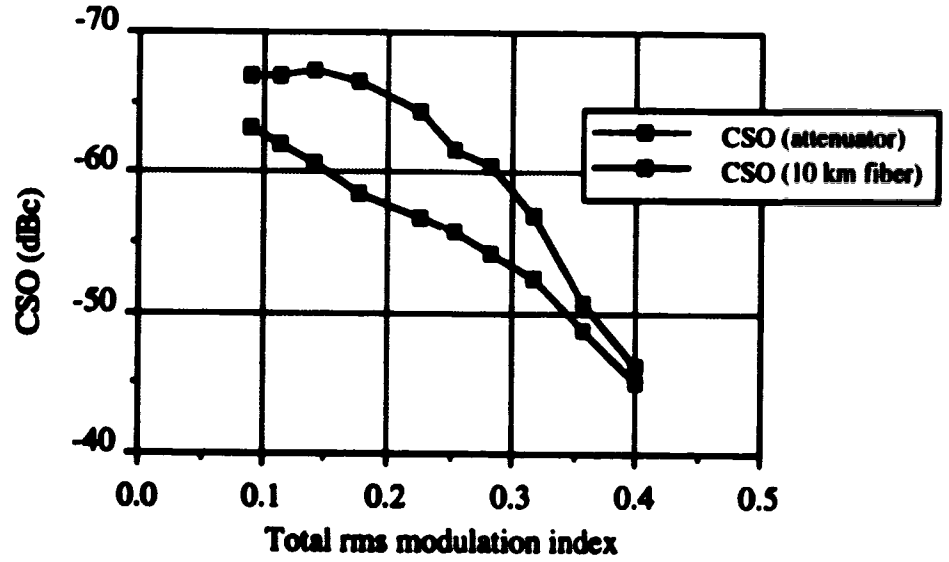

Fig. 6.6(b) CSO in Channel 30 with and without fiber transmission
$P_{received}$ = -1 dBm, I_{bias} = 50 mA

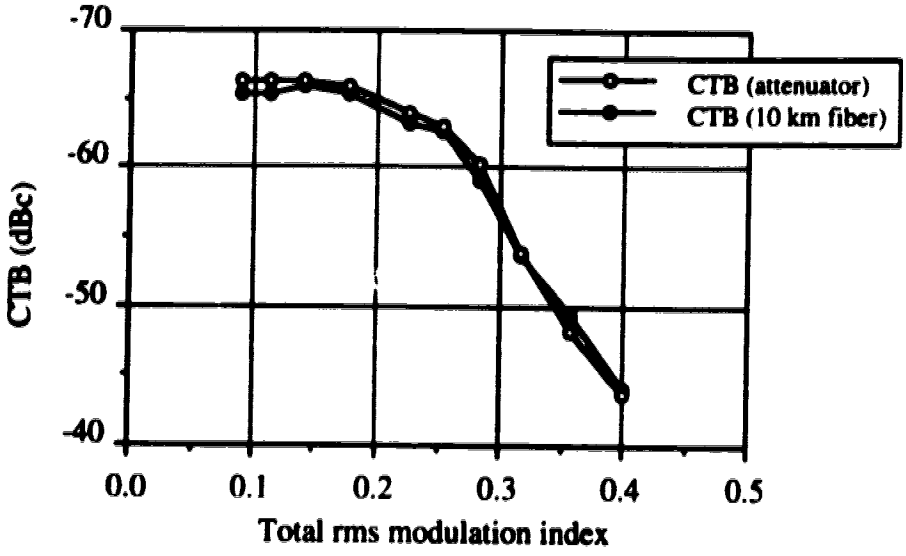

Fig. 6.7(a) CTB in Channel 3 with and without fiber transmission
$P_{received}$ = -1 dBm, I_{bias} = 50 mA

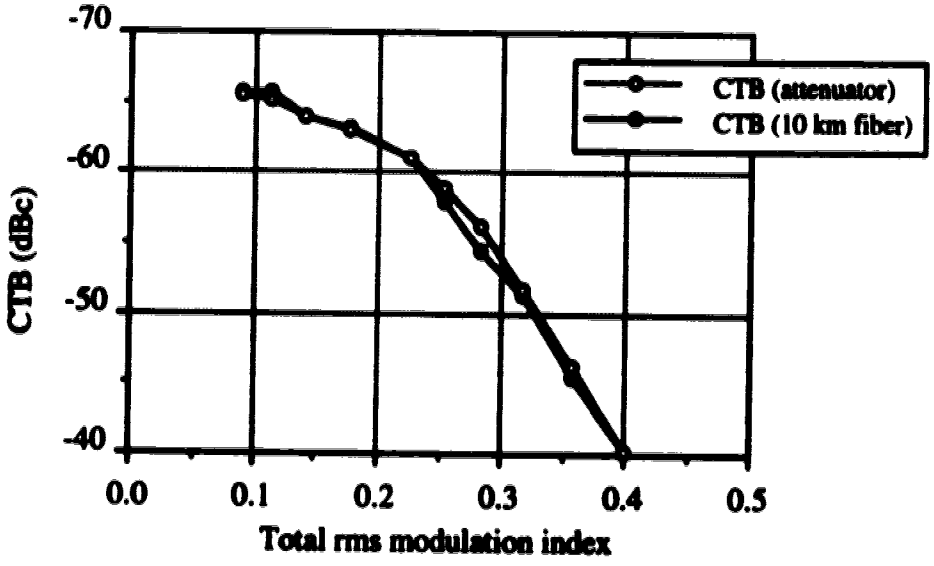

Fig. 6.7(b) CTB in Channel 30 with and without fiber transmission
$P_{received}$ = -1 dBm, I_{bias} = 50 mA

As can be seen in Figs. 6.6(a) and (b), the CSO performance is degraded significantly after 10 km of optical fiber transmission, particularly at low rms modulation index. This degradation is due to the combined effect of laser chirp and fiber dispersion. At high rms modulation index, the difference in CSO performance for systems with and without fiber is reduced because nonlinear distortion due to signal clipping dominates over the intrinsic and chirp/dispersion-induced distortion. It is also interesting to note that distortion due to chirp and dispersion is more severe in Channel 30 than in Channel 3. In order to understand the cause of this phenomenon, one has to perform a two-tone analysis of the nonlinear distortion. Blauvelt et al. [39] have performed the analysis and shown that second order distortion can be expressed as indicated below

$$S_i(t) = \cos(\omega_1 t) + \cos(\omega_2 t) \tag{6.5}$$

$$\begin{aligned} S_o(t) = S_i(t) &+ \omega_1 \delta \sin(2\omega_1 t) + \omega_2 \delta \sin(2\omega_2 t) \\ &+ (\omega_1 + \omega_2)\delta \sin(\omega_1 + \omega_2)t \\ &+ (\omega_1 - \omega_2)\delta \sin(\omega_1 - \omega_2)t \end{aligned} \tag{6.6}$$

where $S_i(t)$ is the input signal, $S_o(t)$ is the distorted output signal, and δ is the proportionality constant. Comparing the coefficients, the sum $(\omega_1 + \omega_2)$ terms are larger than the difference $(\omega_1 - \omega_2)$ terms. Consequently, distortion due to chirp and fiber dispersion is more severe at higher frequency channels than at lower frequency channels for multichannel system.

Fig. 6.7(a) and (b) also show that there is little degradation in CTB after 10 km of optical fiber transmission. This confirms the fact that laser diode chirp and fiber dispersion only contribute second order type distortion and, therefore, degrade CSO performance only.

6.2 BER Calibration of the Modified 64-QAM Digital Radio System

As mentioned in Chapter 4, a set of 64-QAM transmit and receive shelves from a Northern Telecom RD-6 digital radio system was modified in order to fit a QAM spectrum within a 6 MHz TV channel. Because of the modifications, it was important to calibrate and determine the extent to which BER performance of the modified system deviated from the designed performance due to the sources of degradation internal to the system such as imperfections in filter design and clock recovery. In this section, BER performance with respect to SNR, QAM modulation index, and received optical power are presented. A detailed description of the method used to measure QAM power level is also given.

6.2.1 QAM rms Signal Power Measurement Technique

One of the most commonly used parameters in system performance studies is the rms signal power. In most cases, this parameter can be measured directly by either a spectrum analyzer or a RF power meter. However, complications arise in using these instruments to obtain the rms power of 64-QAM signal in a hybrid analog/digital transmission system directly. The bandwidth of the spectrum analyzer is essentially limited by the resolution bandwidth which can be adjusted to a maximum of 3 MHz. The 64-QAM signal, for this work, has a bandwidth of approximately 5 MHz. Therefore, a portion of the signal power is filtered out by the spectrum analyzer, causing inaccuracy in the readings. The RF power meter, on the other hand, does not have the same problem because its bandwidth is typically in the GHz range. Unfortunately, in a hybrid transmission set-up where the 64-QAM signal is frequency multiplexed with the analog video signals, the RF power meter measures the rms power of the composite signal instead of only the 64-QAM signal.

A more practical and effective alternative is to indirectly obtain the rms power from the measured maximum steady state (mss) power. The mss power, also commonly referred to as the corner state power, is the power of the farthest state which is located at one of the four corners in a rectangular constellation shown in Fig. 6.8.

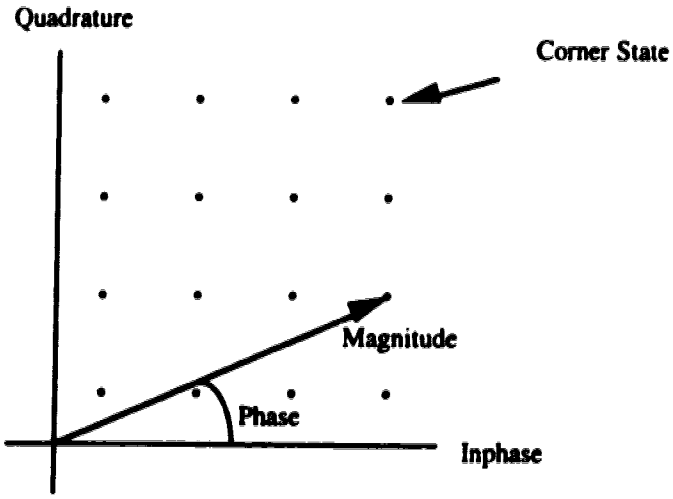

Fig. 6.8 64-QAM signal constellation

By forcing the QAM modulator to transmit the signal at one of the corner states continuously, the transmitted signal is effectively a carrier whose power can be accurately measured by a spectrum analyzer, independent of the resolution bandwidth. This measured corner state power is then converted to a QAM rms signal power by accounting for the conversion factor. Using Hewlett Packard 436A RF power meter, the conversion factor for a 64-QAM signal is found to be approximately 5.1 dB which is the measured difference in decibels between the QAM corner state power and the average rms power. It is important to recognize that this conversion factor takes into account not only the rms averaging but also the shape of the pulse shaping filter in the QAM modulator as well.

6.2.2 Calibration Results

BER performance of the modified 64-QAM digital radio system is evaluated for four different configurations: i) Electrical back-to-back, ii) Optical back-to-back, iii) through 10 km of optical fiber, and finally iv) through an EDFA and 10 km of optical fiber. The experimental set-up for each of these configurations is shown in Fig. 6.9(a) and (b).

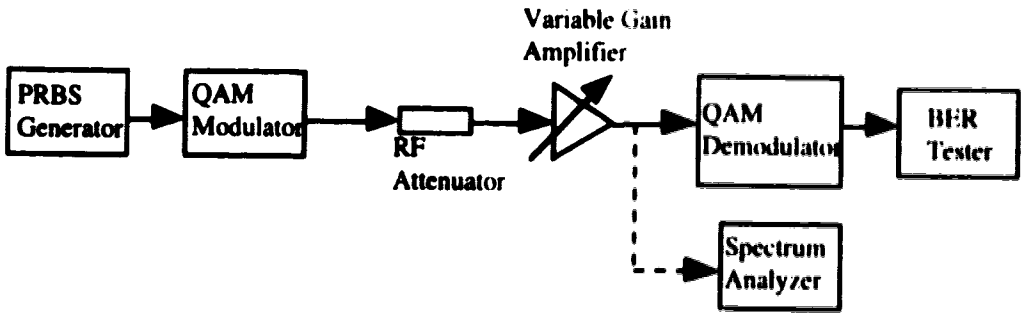

Fig. 6.9(a) Experimental set-up for electrical back-to-back measurements

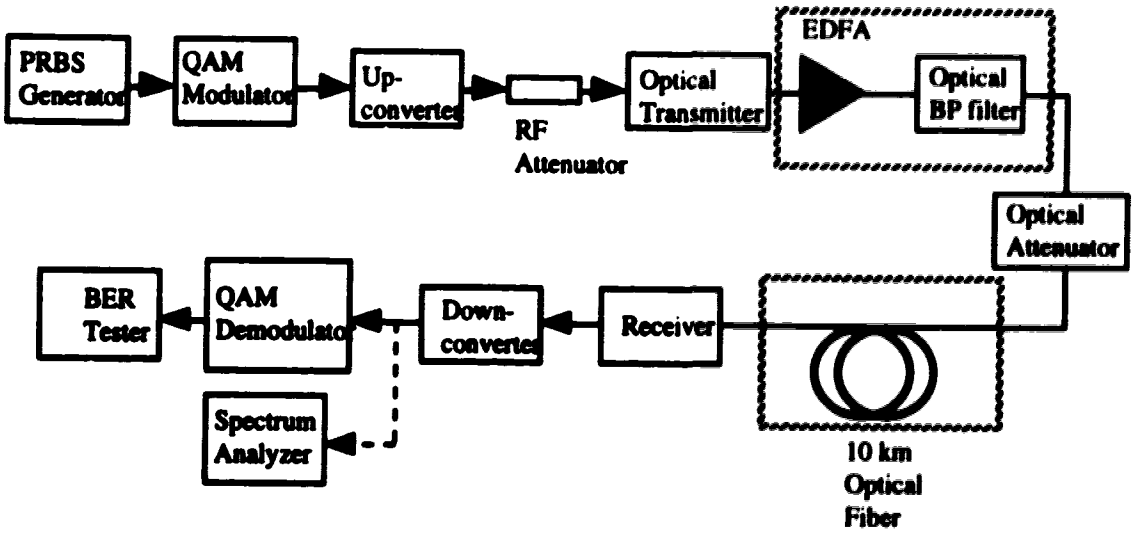

Fig. 6.9(b) Experimental set-up for optical back-to-back, 10 km of optical fiber, and EDFA plus 10 km of optical fiber configurations.

For the electrical back-to-back experimental set-up, a variable gain amplifier is used to amplify the power of the received signal to a level within the dynamic range of the QAM demodulator. More importantly, it also acts as a noise generator. For the optical configurations shown in Fig. 6.9(b), noise is generated by amplifiers in the down-converter and optoelectronic devices such as the laser and receiver. In these experiments, SNR is adjusted by varying the signal power at the output of the QAM modulator and is measured using a spectrum analyzer at the node before the QAM demodulator.

The measured BER results with respect to SNR are plotted in Fig. 6.10 along with the theoretical results calculated from equation (3.39) in Chapter 3. The fundamental BER performance of the 64-QAM transmit/receive set is obtained from the electrical back-to-back results. In this configuration, the experimental results are shown to be within 2 dB of the theoretical BER performance. This discrepancy is attributed mainly to the imperfections in the pulse shaping filter. The ideal filter has a vestigial spectrum characteristic, satisfying Nyquist's first criterion for zero intersymbol interference (ISI). However, a realizable filter can only be, at best, a close approximation of the ideal Nyquist filter. Because of non-ideal filter response and other internal imperfections, most practical M-ary QAM digital radio systems require higher SNR than theoretically predicted. In essence, the electrical back-to-back results represent the best possible BER performance of the 64-QAM transmit/receive set.

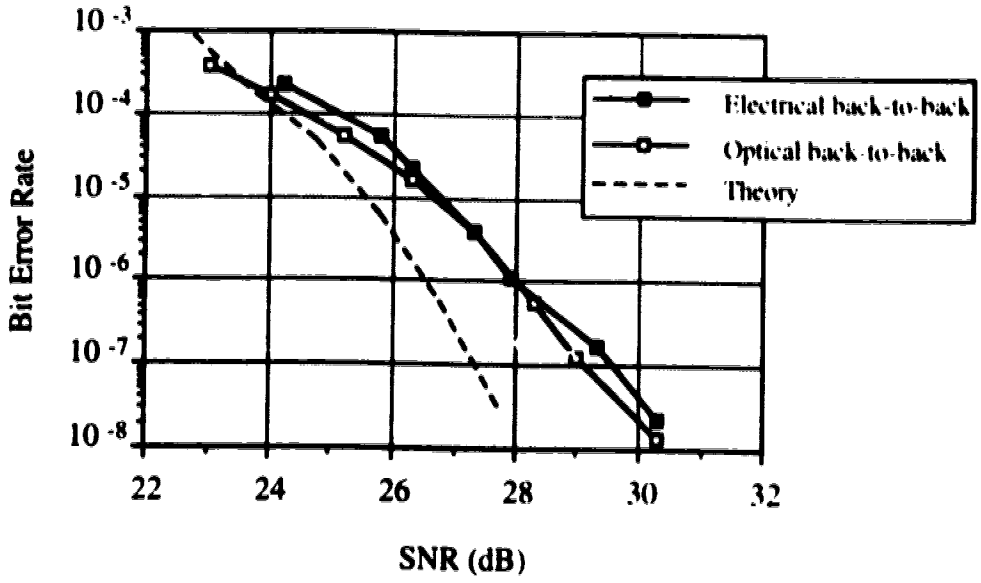

Fig. 6.10 64-QAM Bit Error Rate Performance Calibration
For optical back-to-back measurements, $P_{received}$ = -1 dBm
I_{bias} = 50 mA

BER measurements were also made for the configurations involving optical conversion. For these measurements, the laser bias current was set at 50 mA and the received optical power maintained at -1 dBm. SNR is adjusted by varying the signal power at the output of the QAM modulator using an RF attenuator, or equivalently the modulation index of the QAM signal. As can be seen in Fig. 6.10, the experimental results for the optical back-to-back set-up are the same as that of the electrical back-to-back. This demonstrates that the optical transmitter and receiver are linear and have negligible effect on the BER performance. However, with the latter two configurations, Fig. 6.11 indicates that the addition of 10 km of fiber and an EDFA cause further degradation in BER performance. The presence of the 10 km fiber and an EDFA distorts the QAM signal, deviating the signal spectral shape further from the ideal vestigial spectrum characteristic, thus causing degradation in BER.

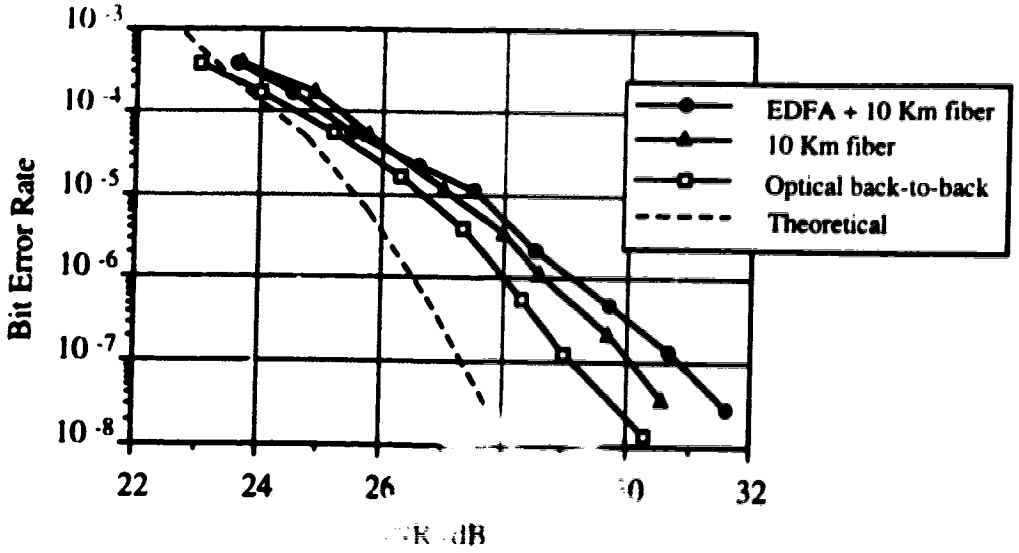

Fig. 6.11 64-QAM BER p[illegible]ce calibration with optical link
Preceived = [illegible] - 10 dB, I_{bias} = 50 mA

In addition, BER perfo[illegible]ce was also evaluated with respect to received optical power and QAM effective modulation index. For the measurements of BER versus received optical power, the effective modulation index was set at 5.5% and the laser biased at 50 mA.

The experimental results are plotted in Fig. 6.12 and 6.13. The difference between the experimental and theoretical BER performance shown in these figures is consistent with that of the previous BER versus SNR results. For example, the BER versus received optical power plot shows 1 dB difference between the experimental and theoretical BER performance. Because the electrical signal power is proportional to the optical signal power squared, a discrepancy of 1 dB in the optical domain is equivalent to an electrical discrepancy of 2 dB which is consistent with the results shown in Fig. 6.10. In Fig. 6.13, the BER versus QAM effective modulation index plot shows that at 10^{-8} BER, the required modulation index is 0.25% as compared to 0.2% calculated from

theory. This difference in decibels 20 log (0.25/0.2) is approximately 1.9 dB which further verifies the results shown in Fig. 6.10.

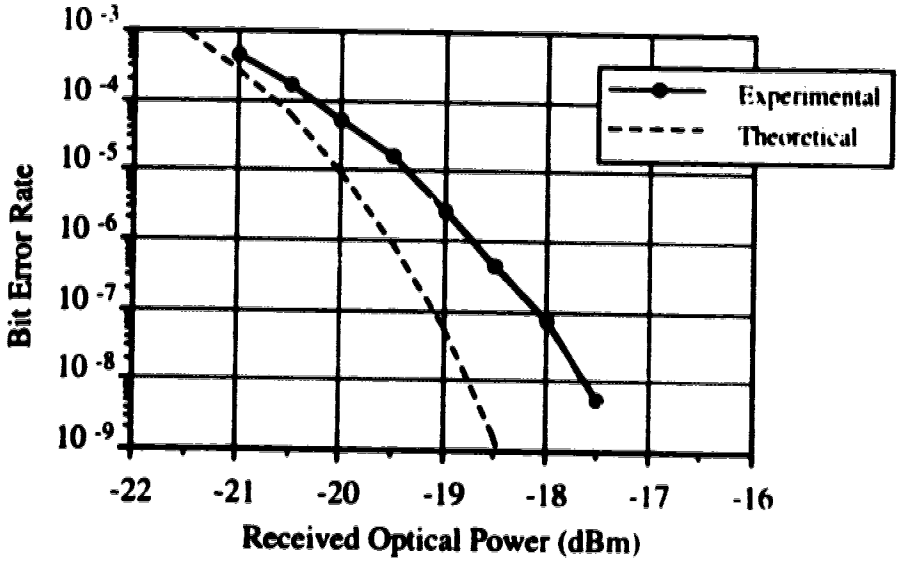

Fig. 6.12 BER versus Received Optical Power
m_{QAM} = 5.5 %, I_{bias} = 50 mA

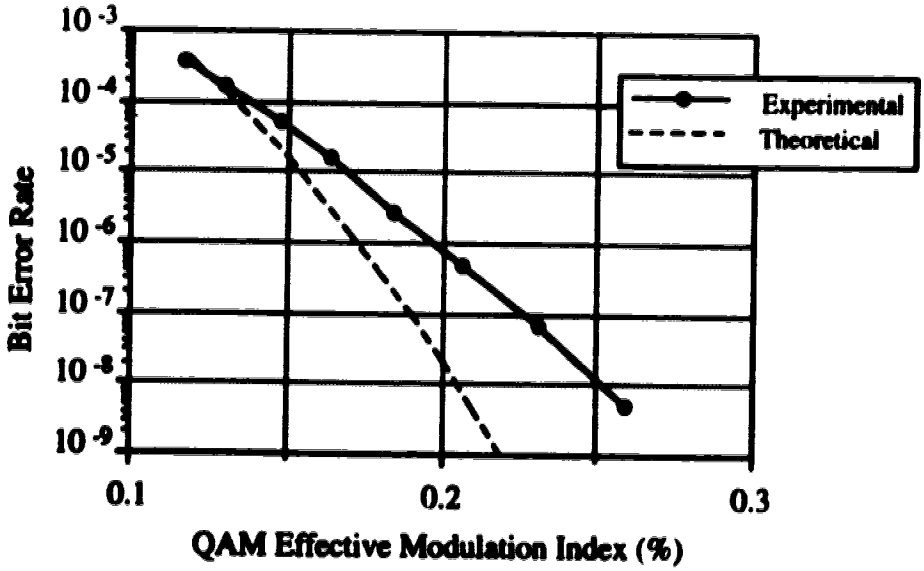

Fig. 6.13 BER versus QAM effective modulation index
$P_{received}$ = -1 dBm, I_{bias} = 50 mA

The main objective of the calibration process just described was to evaluate the BER performance of the modified 64-QAM transmit/receive equipment and to determine its suitability for further studies. As pointed out in the preceding paragraph, the measured BER performance is within 2 dB of the theoretical prediction. Obviously, performance of the 64-QAM transmit/receive equipment could be improved. However, the effort required for such small gain is intensive, time-consuming and, hence, probably impractical. Furthermore, in a hybrid AM-VSB/QAM optical transmission system, degradation caused by other effects such as laser clipping is far more severe. In conclusion, the modified 64-QAM transmit/receive set is considered suitable for the hybrid AM-VSB/QAM optical transmission experiments.

6.3. Performance of 64-QAM in a Hybrid AM-VSB/QAM Optical Transmission System

Optical fiber transmission of digital multi-level QAM and analog AM-VSB television signals is of interest to both the telecommunication and CATV industries. However, a review of current literature [23-24, 28, 33, 40-43] indicates that technical issues such as the randomness of nonlinear distortion products, effects of distortion and noise on BER performance of digitally modulated signals, relative QAM power level with respect to that of AM-VSB carriers for acceptable transmission quality, and etc... are not yet adequately investigated. This section addresses the above issues in detail both qualitatively and quantitatively.

6.3.1 Qualitative Study

In a SCM system, there are two major sources of degradation which are noise and distortion. Distortion is caused by the nonlinearity of the laser diode and clipping which

occurs when the modulating composite signal is below threshold. A spectrum of a distorted AM-VSB/QAM composite signal is illustrated in Fig. 6.14.

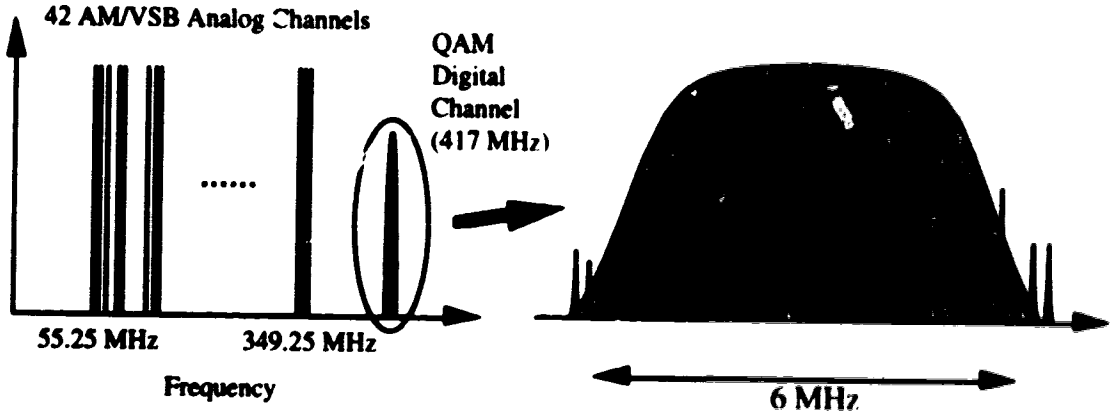

Fig. 6.14 Channel allocation for AM-VSB/QAM hybrid optical transmission and spectrum of 64-QAM signal and distortion products interference

Nonlinear distortion appears as discrete intermodulation products spread over the entire spectrum. Many of these products fall into each 6 MHz wide QAM channel as shown in Fig. 6.14 and, therefore, act as a source of degradation to this QAM signal. It is also observed that the spectral structure of nonlinear distortion is very different from that of Gaussian noise which does not have discrete frequency components but rather appears as a flat signal level over a broad band. The difference in spectral appearance between these two sources of degradation leads to the hypothesis that nonlinear distortion cannot be treated as noise and that the impact of each impairment on system performance has a different degree of severity. The first step in proving that this hypothesis is correct is to study the random nature of nonlinear distortion. Such knowledge can help one determine the appropriate theory that can be used to accurately predict the performance of M-ary QAM signals in a hybrid environment.

Observations of nonlinear distortion in the time domain should provide useful insights into this study. A HP-15631 Digitizing Oscilloscope was used to observe the time domain response of distortion products within a 10 MHz band. Fig. 6.15(a) and (b) show the time-domain output response respectively of noise and of nonlinear distortion products and noise combined.

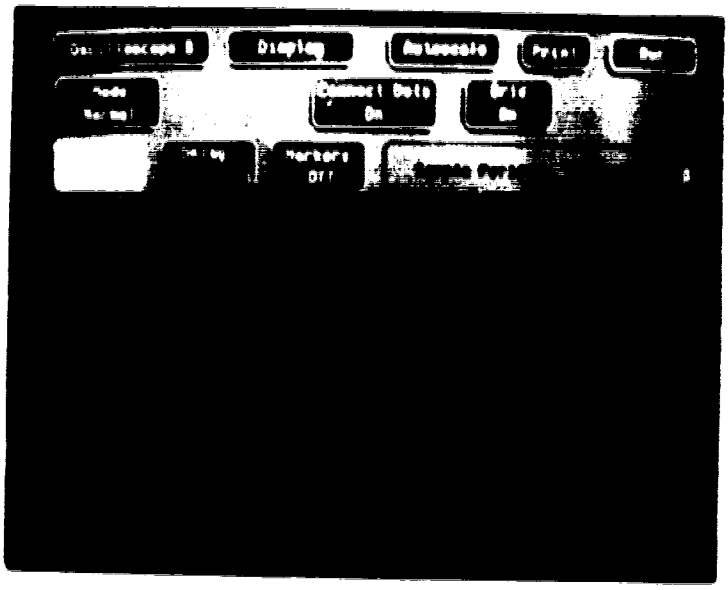

Fig. 6.15(a) Time domain response of noise

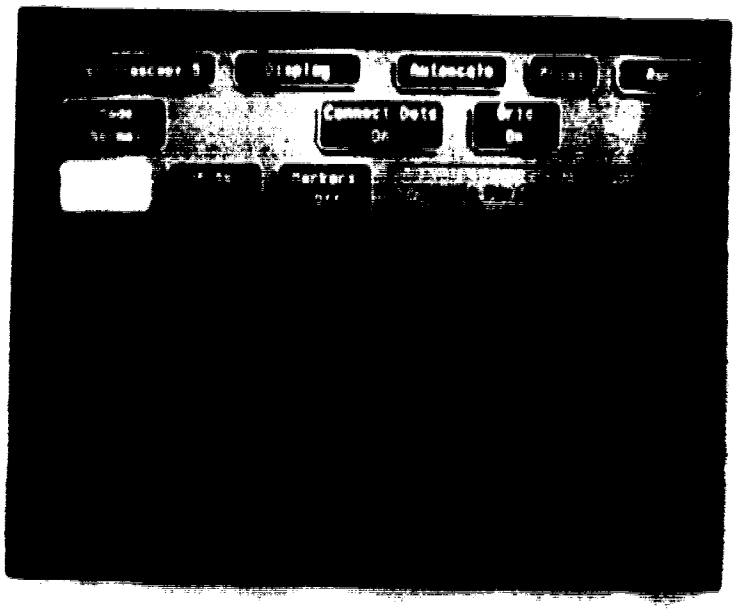

Fig. 6.15(b) Time domain response of noise and nonlinear distortion products

Some large impulse responses were observed in the latter case. This indicates that distortion products appear impulsive in the time domain and seem to have an amplitude distribution different from that of Gaussian noise. To confirm the above observations, histograms of the amplitude of noise and distortion samples were obtained with Tektronix CSA 803 Communication Signal Analyzer and are shown in Fig. 6.16(a) and (b). As expected, the noise histogram has a distribution similar to a Gaussian distribution function. With noise, there is a finite probability of a large excursion, but the possibility of that happening is extremely remote. On the other hand, the histogram for nonlinear distortion products plus noise indicates that occurrences of large impulses are more frequent, thus illustrating the impulsive nature of distortion products. Based on these observations, it is concluded that, for a hybrid AM-VSB/QAM optical transmission system, a realistic and accurate noise model should be a mixture of Gaussian and non-Gaussian impulsive noise.

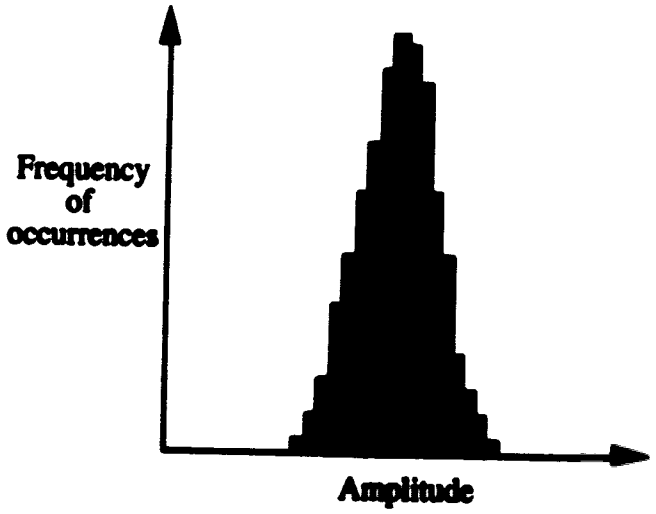

Fig. 6.16(a) Amplitude histogram of noise

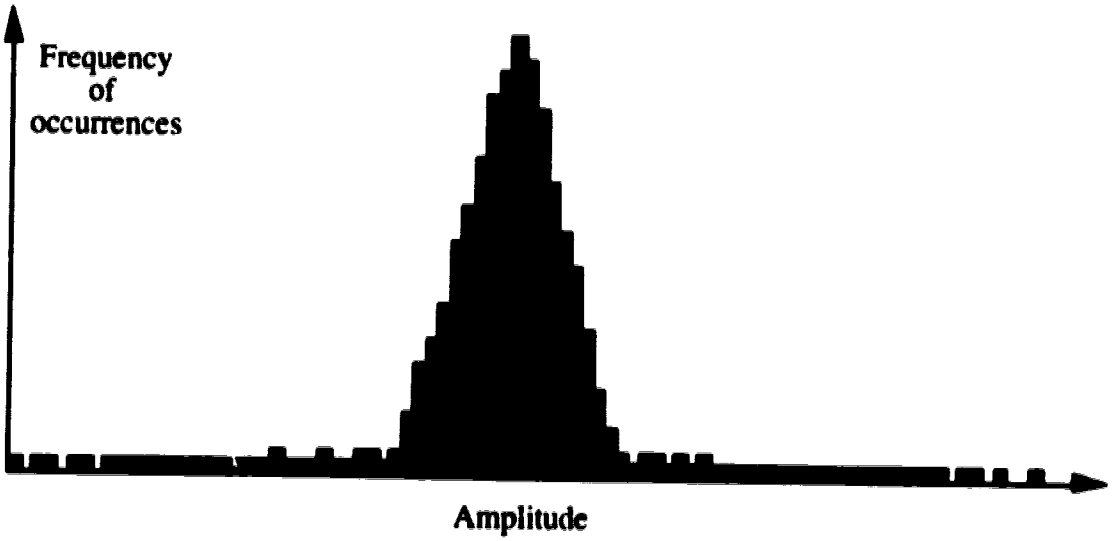

Fig. 6.16(b) Amplitude histogram of noise and nonlinear distortion products

6.3.2 Quantitative Study

In Section 6.3.1, the impulsive nature of nonlinear distortion was discussed and compared to that of Gaussian noise. In this section, the results from a comprehensive experimental study of the effects that nonlinear distortion and noise have on BER performance of 64-QAM signal are presented and compared to the theoretical results. The theoretical results are calculated based on the Middleton's Class A noise model which is a generalized model of Gaussian noise combined with non-Gaussian impulsive noise. Through out this study, it is important to recognize that the experimental results were obtained for a particular configuration in which 42 AM-VSB carriers are located from 55.25 MHz to 349.25 MHz and a QAM signal at 417 MHz.

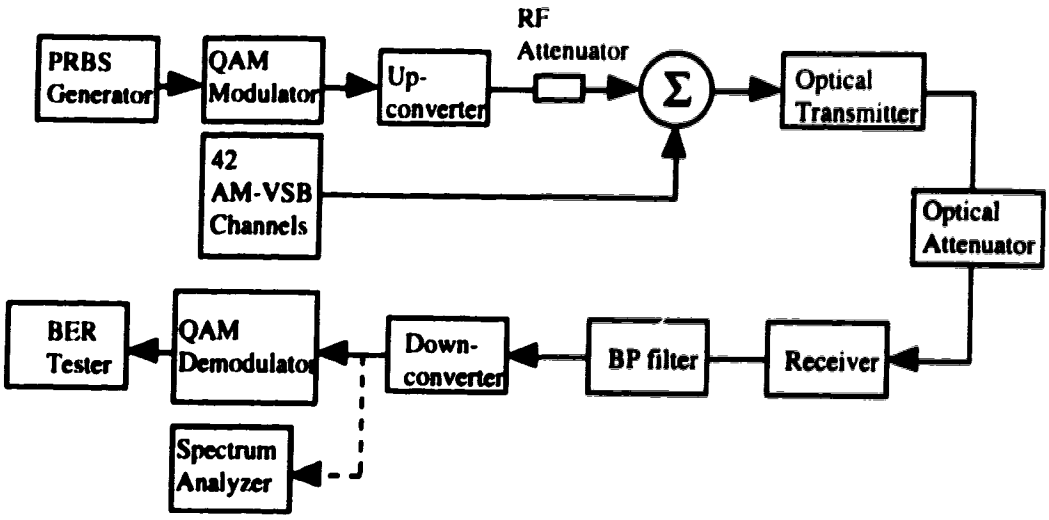

Fig. 6.17 Hybrid AM-VSB/QAM optical transmission experimental set-up

A block diagram of the experimental set-up is shown in Fig. 6.17. It consists of two signal sources which are a QAM modulator and a bank of Blonder-Tongue CATV modulators. The QAM modulator driven by a pseudo-random sequence generator generates a signal at 70 MHz which is subsequently up-converted to 417 MHz The bank of Blonder-Tongue modulators generate 42 AM-VSB video carriers whose frequencies range from 55.25 MHz to 349.25 MHz. The signals are then combined by a power combiner and used to intensity modulate a highly linear DFB laser. The QAM signal is then received, filtered, and down-converted back to 70 MHz before entering the demodulator and BER tester. This set-up allowed us to perform hybrid AM-VSB/QAM optical transmission experiments. The objective of these experiments was to study the effects of analog CATV carriers on digital signals by evaluating the BER performance of the 64-QAM signal with respect to various parameters such as modulation index, SNR, and SNLD. The results from these experiments are presented in the following sections.

6.3.2.1 BER as a Function of QAM and AM-VSB Modulation Index per Channel

The results given in Fig. 6.18 are of BER as a function of 64-QAM effective modulation index with AM-VSB carrier modulation indices of 6%, 5%, and 0% (no AM-VSB carrier). The modulation indices of both the QAM signal and the AM-VSB carriers were adjusted by varying the RF power at the output of the modulators.

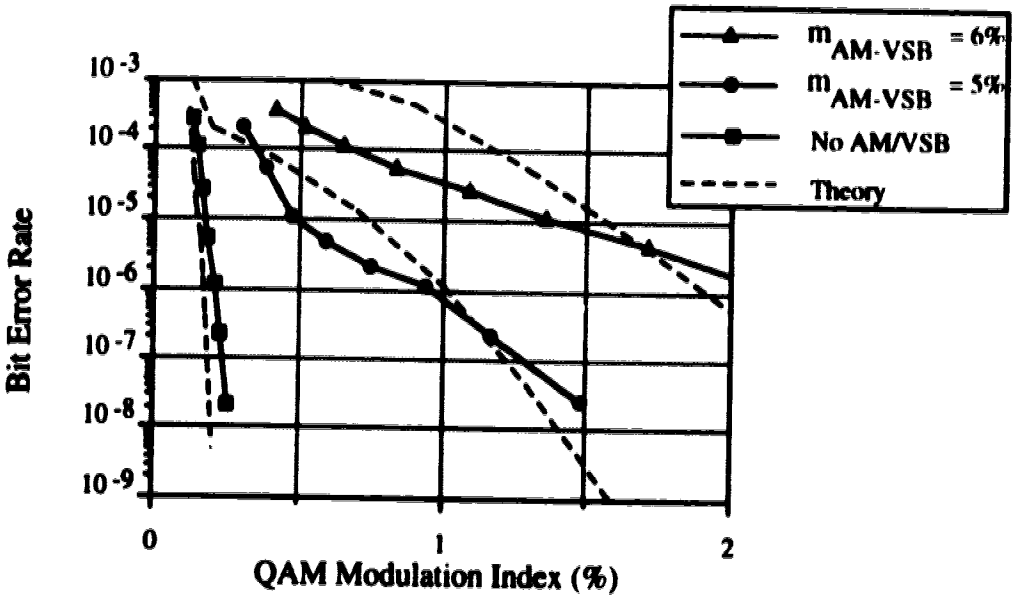

Fig. 6.18 BER versus 64-QAM modulation index for AM/VSB modulation index per channel of 6%, 5%, and 0% at received optical power of -1 dBm

The dashed curves in Figure 6.18 show the results calculated using the BER analysis described in Section 3.4* . The BER for M-ary QAM signals is given by equation (3.45) of Section 3.4, viz.

---

* Refer to Appendix C for the calculation of BER for 64-QAM signals in a mixed Gaussian noise combined with non-Gaussian impulsive noise environment.

$$P_{I+G}(E_{bit}) \cong \frac{2(M-\sqrt{M})}{M \cdot \log_2(M)} \cdot e^{-A} \cdot \sum_{j=0}^{\infty} \frac{A^j}{j!} \cdot \mathrm{erfc}\left(\frac{\sqrt{SNR \cdot PF_M}}{\sqrt{2}(\sqrt{M}-1)\sigma_j} \right) \tag{6.7}$$

where

$$SNR = \frac{1}{SNR_G^{-1} + SNLD^{-1}} \ , \tag{6.8}$$

$$\sigma_j^2 = \frac{\frac{j}{A} + \Gamma}{1+\Gamma} \ , \tag{6.9}$$

and

$$\Gamma = \frac{\sigma_G^{\ 2}}{\sigma_{NLD}^{\ 2}} = \frac{SNLD}{SNR_G} \ . \tag{6.10}$$

where SNR_G and $SNLD$ are functions of the modulation index and given by equations (3.22) and (3.29) in Chapter 3. PF_M is the ratio of the QAM signal peak power to the average QAM channel signal power. For 64-QAM signals, $PF_M = 2.328$.

A is the impulsive index which is defined as the product of a received average number of impulses in unit time and the duration of the impulse (i.e. the probability of an impulse). It can be determined experimentally by taking the ratio of the total number of samples containing impulses to the total number of samples. Using Tektronix CSA 803 Communication Signal Analyzer, the impulsive indices for the cases of 5% and 6% modulation index per AM carrier were measured to be 0.0012 and 0.022 respectively.

Using the measured impulsive index parameters, we obtained reasonable agreement between the theoretical and experimental results as can be seen in Fig. 6.18. This figure shows that BER performance is degraded due to the presence of analog carriers and that the severity of degradation depends on the AM-VSB modulation index

per channel. CATV analog carriers induce clipping distortion which interferes with the 64-QAM signal. As the AM-VSB modulation index per channel is increased, the output of the intensity modulated signal begins to produce additional distortion owing to signal clipping, thereby causing further degradation in BER performance.

In addition, Fig. 6.18 also shows that the QAM modulation index must increase significantly to compensate for the additional distortion induced by the increase in AM-VSB modulation index per channel in order to maintain BER at a certain value. In other words, for a certain QAM BER the relative difference in power between the AM-VSB carriers and the QAM signal diminishes as the modulation index of the video carriers increases. For example, with m_{AM} of 5%, for 10^{-5} BER, the 64-QAM power level is approximately 20 dB below that of the AM-VSB carriers. For the same BER but with m_{AM} of 6%, the difference in power level is now only 12 dB.

It is also important to note that even though the BER is severely degraded by distortion, no true BER floor was observed. In other words, as the QAM effective modulation index is increased, BER continues to improve and is not constrained to a fixed value. In order to qualitatively explain this observation, one has to recognize that the square of the modulation index is directly proportional to electrical signal power. For each BER curve shown in Fig. 6.18, the distortion and noise in the system are constant because of the constant AM-VSB modulation index. By increasing the QAM modulation index, the signal power goes up, thereby increasing both SNR and SNLD. As a result, BER performance continues to improve and no BER floor is observed.

6.3.2.2 BER as a Function of SNR and SNLD

Next, we investigate BER performance with respect to SNR and SNLD. Specifically, BER is measured as a function of SNR with SNLD of 41 dB, 44 dB, and infinity (negligible distortion). The experimental set-up used for these measurements is

similar to the one shown in Fig. 6.17 with the only difference being that an attenuator is added between the receiver and down-converter.

The measurements were made as follows. First, the AM-VSB modulation index per channel was set at 6% in order to induce distortion which is then measured by summing the power of all distortion products in a 64-QAM channel. Knowing the distortion power, any value of SNLD can be obtained by appropriately adjusting the 64-QAM signal level. As for adjusting SNR without affecting SNLD in the system, the most convenient method is to vary the signal power at the output of the receiver using an attenuator because major sources of noise in the system come from amplifiers in the down-converter. SNLD, meanwhile, remains constant because both signal and distortion power are attenuated proportionally. Equivalently, the experimental set-up can be thought to include two generators which add distortion and noise to the signal after the laser and receiver respectively. Fig. 6.19 presents an equivalent set-up that helps explain the above measurement procedure.

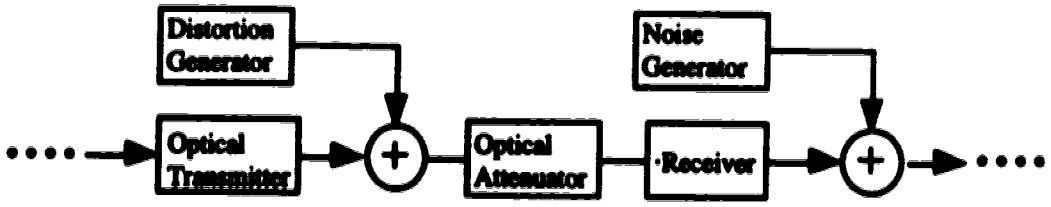

Fig. 6.19 Equivalent Set-up

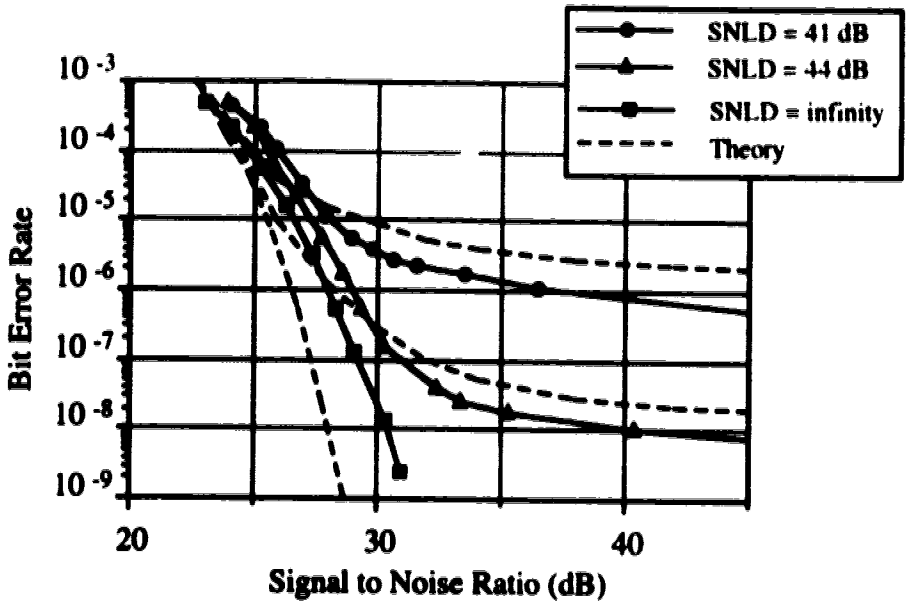

Fig. 6.20 BER as a function of SNR with SNLD of 41 dB, 44 dB, and infinity. $m_{AM\text{-}VSB} = 6\%$, $P_{received} = -1$ dBm, $I_{bias} = 50$ mA

The theoretical results are obtained using equation (6.7). However, the variables are *SNR* and *SNLD*, instead of the modulation index. Since the AM-VSB modulation index per channel was set at 6%, the corresponding impulsive index, A, of 0.022 was used for the calculation.

The results are shown in Fig. 6.20. This figure shows a greater tendency toward BER floors. It indicates that in the high SNR regime, the BER performance of the 64-QAM signal is limited by distortion because the level of BER floors depends on SNLD. It is also observed that the 64-QAM signal requires lower SNR than SNLD in order to obtain a certain BER. For example, BER levels out at approximately 10^{-6} for SNLD of 41 dB. To obtain the same BER in a system where there is no distortion, the required SNR is approximately 27 dB. This observation demonstrates that distortion degrades 64-QAM signal performance more severely than noise.

6.3.2.3 BER as a Function of SNLD

Hypothetically speaking, if one extrapolates BER curves illustrated in Fig. 6.20 to SNR of infinity and plots the values of BER against SNLD, one can effectively determine the impact of distortion on BER performance of the 64-QAM signal. In practice, SNR cannot equal infinity because there is always noise in the system. However, a close approximation to that condition can be obtained by operating the system in a SNR regime in which noise has negligible effect on BER. From the calibration results shown in Section 6.2, a SNR of 32 dB gives a BER of 10^{-9}. Therefore, the BER of the QAM signal in the SNR range from 40 to 45 dB has an acceptably low value and the effect of noise on the QAM signal can be considered negligible. This is the principle behind the next set of BER results which were measured with respect to SNLD with SNR in the range of 40 to 45 dB. The results are plotted in Fig. 6.21.

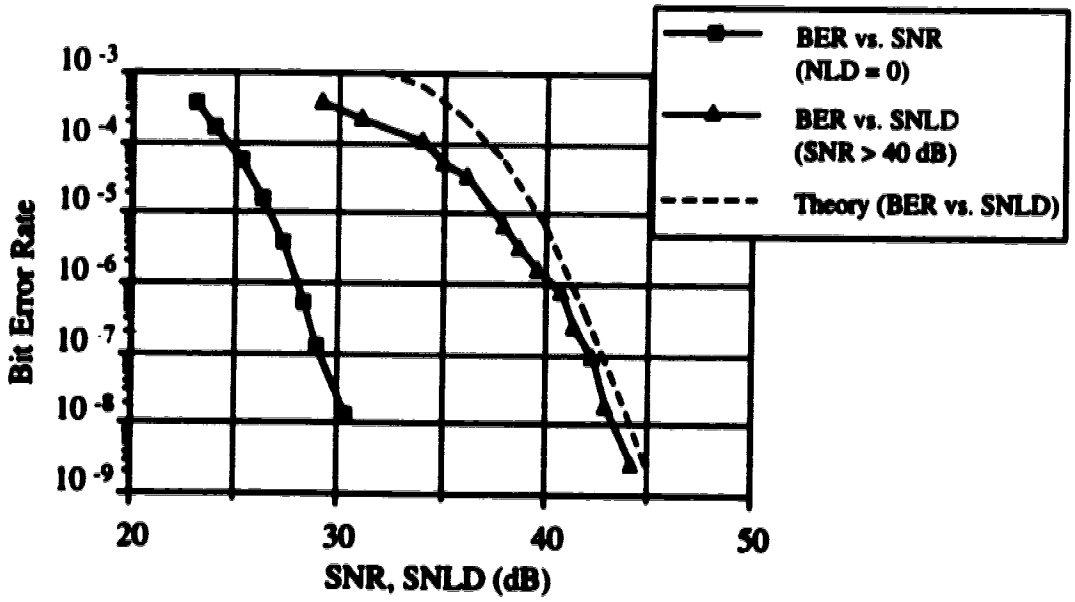

Fig. 6.21 BER versus SNR and BER versus SNLD.
$m_{AM\text{-}VSB}$ = 6%, $P_{received}$ = -1 dBm, I_{bias} = 50 mA

Fig. 6.21 shows that the 64-QAM signal requires a SNLD of 10 to 12 dB higher than SNR to obtain a certain BER. This result indicates that distortion is more detrimental to the BER performance of a 64-QAM signal than noise and, therefore, is consistent with the observation made earlier in Section 6.3.2.1.

In summary, the measurements and the theoretical predictions provide important insights and knowledge on the performance of a 64-QAM signal in a hybrid AM-VSB/QAM optical transmission system, and in particular the impact of distortion and noise on BER. It is often assumed that distortion and noise degrade the signal equally, and are treated as additive noise power signals. However, it is consistently shown in Figs. 6.18, 6.20, and 6.21 that distortion degrades BER more severely than noise. Therefore, the assumption that the two impairments are additive in power significantly underestimates the effect of distortion on BER and should be considered inappropriate. In addition, the close agreement between the experimental results and theoretical predictions calculated using the Gaussian/non-Gaussian impulsive noise model further confirms our conclusion that distortion is impulsive in the time domain, and that its impact on BER can be adequately predicted if the distortion is considered as non-Gaussian impulsive noise.

6.3.2.4 Interpretation of the Impulsive Index Parameter, A

The impulsive index parameter, A, is defined as the product of the received average number of impulses in a unit time and the average duration of the impulse [30-32]. In other words, A is the probability of an impulse or equivalently the duty cycle of the impulses. In the context of threshold nonlinear distortion, Maeda et. al. [33] assumed in their BER analysis of a 16-QAM signal in an AM-VSB/QAM hybrid optical transmission system that the impulsive index A is equivalent to the probability of clipping. They also assumed that the instantaneous optical power is distributed in a

Gaussian manner about P_{bias} with the rms signal power σ^2 being given by $\sigma^2 = \mu^2 \cdot P_{bias}{}^2$. Thus,

$$A = \int_{-\infty}^{P_{th}} \frac{\exp\left(\frac{-(x - P_{bias})^2}{2 \cdot \sigma^2}\right)}{\sqrt{2\pi\sigma^2}} dx \qquad (6.11)$$

where μ is the total rms modulation index and P_{bias} is the average bias optical power. This assumption is based on the fact that the nonlinear distortion products, which appear as impulses in the time domain, are caused by clipping. Although it is true that the impulsive distortion is a direct result of clipping, this does not justify assuming that the probability of an impulse is the same as the probability of clipping. Let us take an intuitive approach to show that the assumption made by Maeda et. al. is inappropriate.

Without loss of generality, we can consider the clipped composite signal as the sum of a undistorted signal and a distortion-induced error signal. In the frequency domain, this error signal is represented by discrete nonlinear distortion products. Some of these products will fail into a QAM channel and interfere with the QAM signal. Hence, the impulsiveness of this interfering signal strongly depends on the phases, frequencies, and magnitudes of all the distortion products within a QAM channel, and the sum of these will be dependent on the particular QAM channel. Throughout the whole process, there is no physical evidence supporting the one-to-one relationship between the probability of clipping and the probability of an impulse in a particular channel, or that for each clipping event an impulse within a given channel will occur. Therefore, the assumption made by Maeda et. al. is unjustified.

As mentioned in Section 6.3.2.1, we take an experimental approach in determining the impulsive index parameter. Using a digitizing oscilloscope, we can approximate A by taking the ratio of the total number of samples containing impulses to

the total number of samples. The impulsive indices for the cases of 5% and 6% modulation index per AM-VSB carrier were measured to be 0.0012 and 0.022 as compared to 6.87×10^{-6} and 1.06×10^{-4} calculated from Maeda's assumption (eqn (6.11)).

In order to show that Maeda's assumption is inappropriate and that our experimental approach in determining the impulsive index parameter is valid, we will compare three sets of results: i) experimental results, ii) theoretical results calculated with the measured impulsive indices, and iii) theoretical results calculated with the impulsive indices obtained from Maeda's assumption. Fig. 6.22 shows BER as a function of 64-QAM effective modulation index with AM-VSB carrier modulation indices of 6% and 5%. Fig. 6.23 shows BER as a function of SNR with SNLD of 41 dB, 44 dB, and infinity.

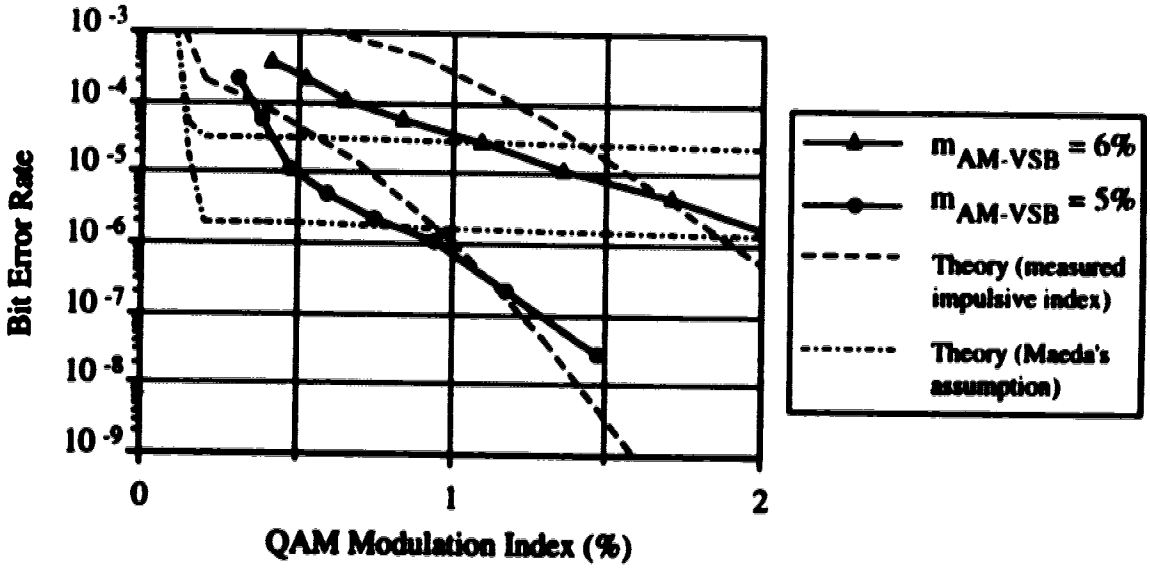

Fig. 6.22 Comparison of BER vs. QAM modulation index experimental results with two sets of theoretical results, one calculated with the measured impulsive index parameters and the other with impulsive index parameters obtained from Maeda's assumption. The impulsive indices for 5% and 6% modulation index per AM-VSB carrier were measured to be 0.0012 and 0.022 as compared to 6.87×10^{-6} and 1.06×10^{-4} from Maeda's assumption. $P_{received} = -1$ dBm, $I_{bias} = 50$ mA.

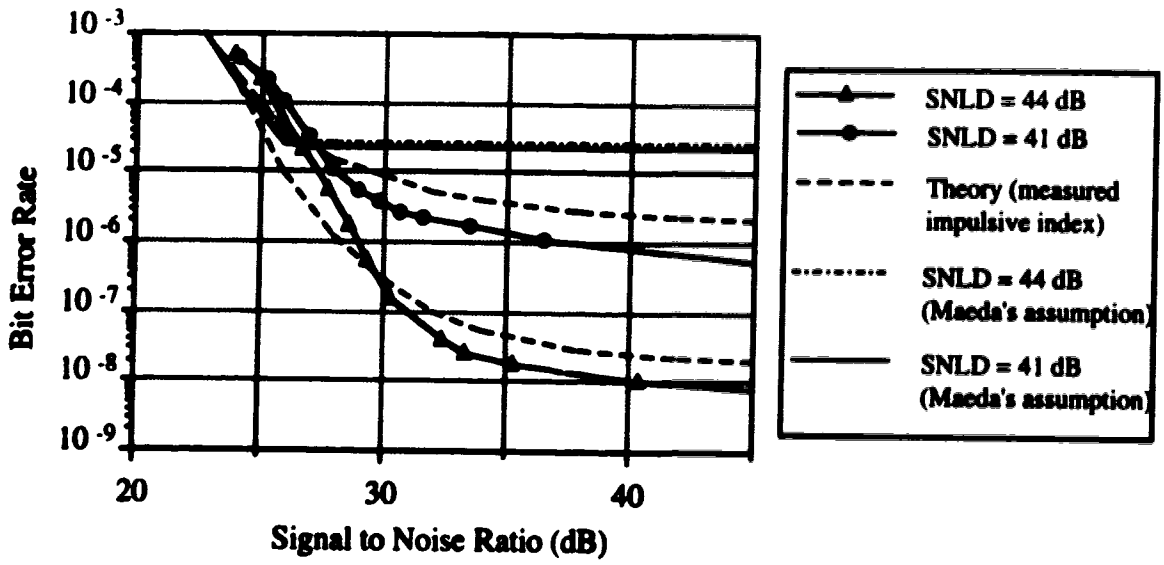

Fig. 6.23 Comparison of BER vs. SNR for different levels of SNLD experimental results with two sets of theoretical results, one calculated with the measured impulsive index parameters and the other with impulsive index parameters obtained from Maeda's assumption. $m_{AM\text{-}VSB} = 6\%$, $A_{measured} = 0.022$, $A_{Maeda} = 1.06 \times 10^{-4}$, $P_{received} = -1$ dBm, $I_{bias} = 50$ mA.

As can be seen in Fig. 6.22 and 6.23, we obtained close agreement between the experimental and theoretical results using the measured impulsive index parameters. On the other hand, the results calculated with the impulsive indices obtained from Maeda's assumption are vastly different from the experimental results. These calculated results show distinctive BER floors in both figures and that in the latter figure, the level of the BER floors is the same for SNLD of 41 dB and 44 dB. These characteristics are the consequence of the fact that Maeda's assumption significantly underestimates the impulsive index parameter.

In order to understand the physical meaning behind the results shown in Fig. 6.22 and 6.23, we have to understand the relationship between the impulsive index and the

peak amplitude of an impulse. Let us consider two scenarios in which the non-Gaussian impulsive noise power is constant. In one scenario, the impulsive index is 0.022 (i.e. measured value), whereas the other scenario has an impulsive index of 1.06×10^{-4} (i.e. from Maeda's assumption). In other words, the occurrence of an impulse is far more frequent or equivalently the time duration of the impulses is longer in the first scenario than the latter one. Since the non-Gaussian impulsive noise power is the same for both cases, the peak amplitude of an impulse for the second case, which has a very small impulsive index (i.e. 1.06×10^{-4}), must be extremely high and far above the signal level; such that, as the signal power is increased, the BER performance of the QAM signal does not improve. In this small impulsive index range, the BER performance is, therefore, highly dependent on the impulsive index and much less on the signal power. This phenomenon is evident in Figs. 6.22 and 6.23 in which the BER performance is clamped to a fixed value as the QAM modulation index and SNLD are increased. The level of the BER floors is also shown to be highly dependent on the impulsive index parameter.

The experimental results, on the other hand, indicate that the BER performance of a QAM signal continues to improve and is not constrained to a fixed value as the QAM modulation index is increased, as shown in Fig. 6.22. In addition, the experimental results plotted in Fig. 6.23 show that the level of the BER floors depends on SNLD and, hence, the signal power. These observations are clearly in contradiction with that obtained from the results calculated using Maeda's assumption. Therefore, the assumption that the impulsive index is the same as the probability of clipping is, indeed, inappropriate.

In this work, we measured the impulsive index, A, by taking the ratio of the total number of samples containing impulses to the total number of samples. With this direct approach, no assumption is made. As shown in Figs. 6.22 and 6.23, a close agreement between the experimental results and the theoretical results calculated with the measured

impulsive index parameters is obtained. On this basis, we conclude that our approach in determining the impulsive index is valid.

6.4 BER versus QAM modulation index for different received optical power levels.

In this section, we explore how the BER of a 64-QAM signal is affected by variations in received optical power. Figs. 6.24(a), (b), and (c) show BER as a function of QAM modulation index for received optical power of -1, -4, and -7 dBm. The results were obtained for the cases with no AM-VSB carrier, an AM-VSB modulation index of 5%, and 6%.

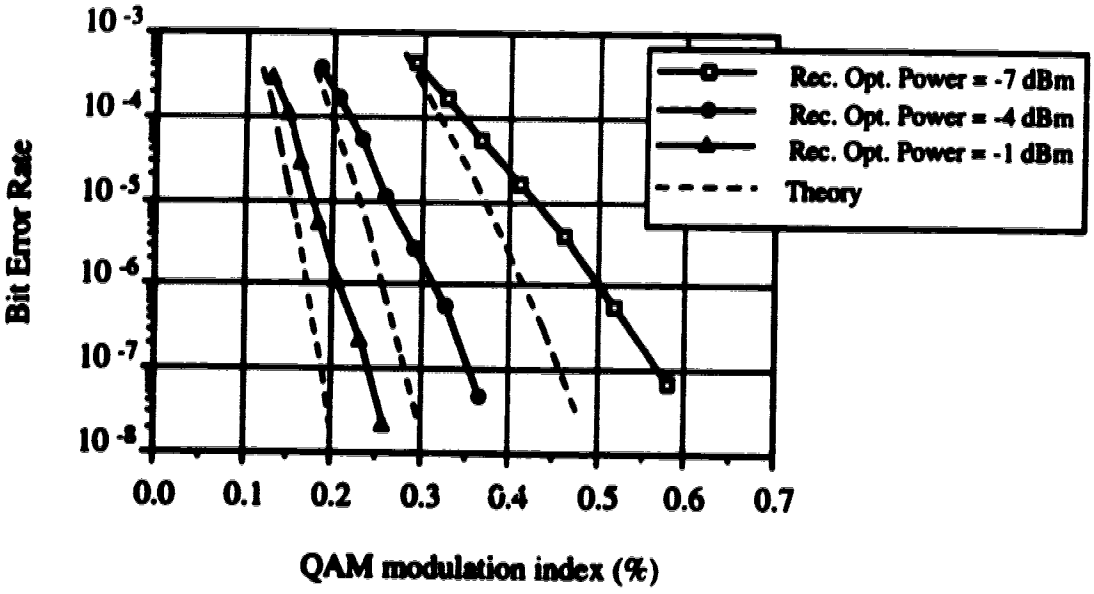

Fig. 6.24(a) No AM-VSB

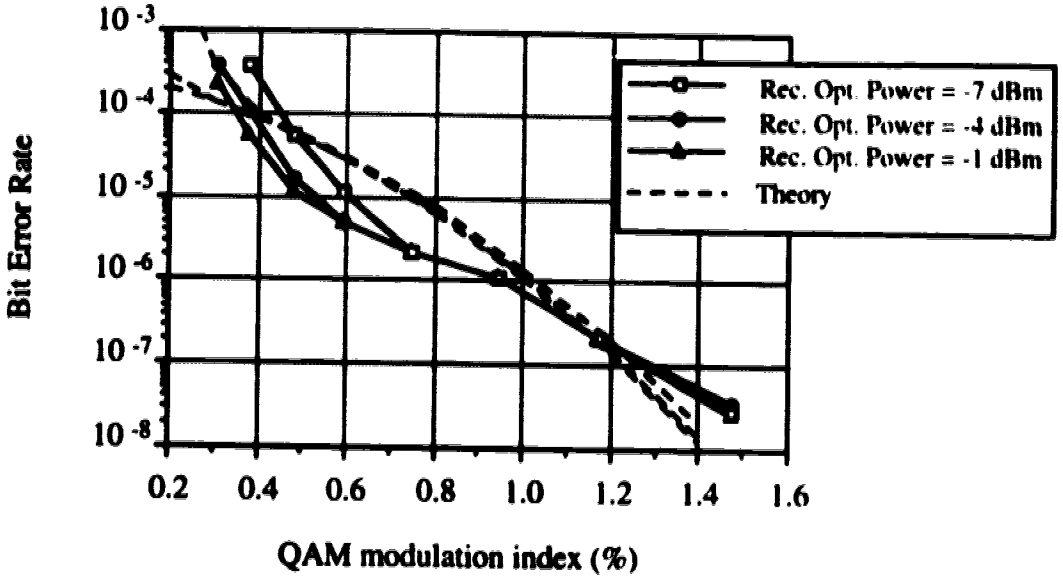

Fig. 6.24(b) $m_{AM\text{-}VSB} = 5\%$

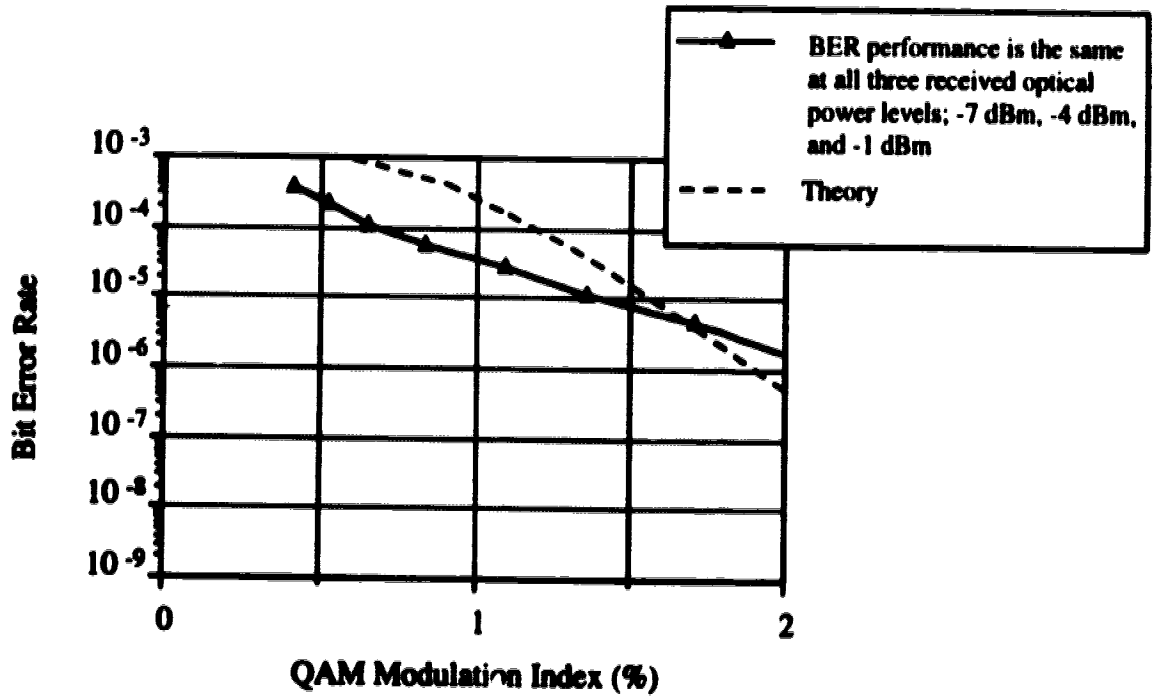

Fig. 6.24(c) $m_{AM\text{-}VSB} = 6\%$

In the thermal noise and shot noise limited regime, SNR in general increases as more optical power is received. Therefore, one intuitively expects that signal performance is highly dependent on optical power. In the case of no distortion as illustrated in Fig. 6.24(a), the results are shown to be consistent with what was expected; that is, received optical power has a strong influence on the BER performance.

However, in the case of mixed analog/digital optical transmission with $m_{AM\text{-}VSB}$ = 5% and 6%, it is shown that there is little variation in the performance when received optical power is attenuated from -1 dBm to -7 dBm. This observation can be explained as follows. In Section 6.3, it was shown that distortion is the predominant source of degradation in a hybrid analog/digital SCM system. Therefore, signal performance is limited by SNLD rather than SNR. As the received optical power is varied from -7 dBm to -1 dBm, SNR is increased but not SNLD because distortion is generated at the laser. For this reason, BER performance remains unchanged.

In addition, Fig. 6.24(b) also shows that BER is mildly affected by the variation in received optical power at low QAM modulation index. This observation may seem to contradict with the explanation given in the above paragraph. However, if one recognizes that in this low QAM modulation index region, SNR is also low such that BER performance is now limited not only by distortion, but by both noise and distortion. As a result, BER changes as the received optical power is varied.

6.5 Effect of Fiber Dispersion and Erbium Doped Fiber Amplifier (EDFA) on 64-QAM Signal Performance

With recent advances in EDFAs, it is desirable to operate the system at 1550 nm wavelength because the gain spectrum lies in that wavelength region. However, the optical fibers present deployed in the telecommunication networks are usually 1310 nm dispersion minimized single mode fibers; 1550 nm systems will suffer from fiber dispersion caused by operating away from the minimum dispersion wavelength. The

combination of fiber dispersion and laser diode frequency chirp produces nonlinear distortion which degrades the BER performance of 64-QAM signal.

The addition of an optical amplifier introduces extra noise and nonlinear distortion which is mostly caused by the combined effect of the amplifier's non-flat gain spectrum and laser diode chirp. A typical gain spectrum of an EDFA is shown in Fig. 6.25. The non-flat gain characteristic of an EDFA combined with laser chirp, which is modulation in optical wavelength, results in light of different wavelengths experiencing different gain, thus, causing nonlinear distortion [44-45].

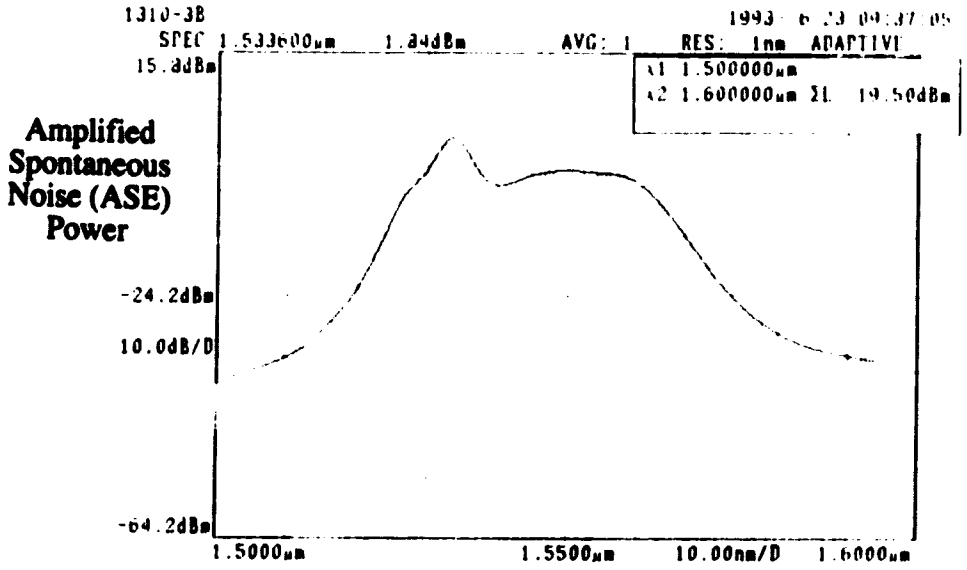

Fig. 6.25 Typical EDFA's gain spectrum

In this section, we investigate the effect of fiber chromatic dispersion and an EDFA's non-flat gain spectrum on QAM signal performance. In the following experiments, BER is measured with respect to QAM modulation index for three experimental systems. The first system uses an optical attenuator to emulate fiber loss. The dominant distortion mechanism in this system is laser clipping. In the second system, a 10 km length of 1310 nm minimum dispersion single moded fiber is added to the set-up. The presence of this fiber introduces additional distortion which is caused by

fiber dispersion and laser chirp. Finally, the third system is basically the same as the second, but with an EDFA added to the link as post amplifier. In this system, the EDFA's non-flat gain spectrum and laser chirp provide an additional distortion mechanism. The block diagram of the experimental set-up is shown in Fig. 6.26.

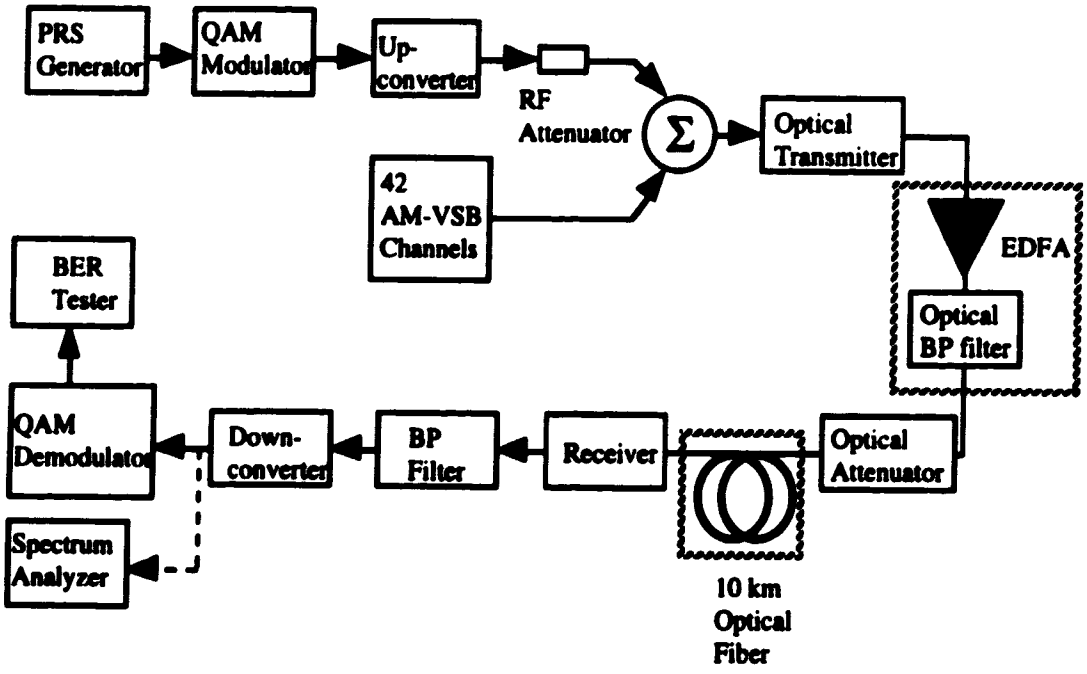

Fig. 6.26 Experimental Set-up with 10 km of fiber and an EDFA

As shown in Fig. 6.26, the EDFA is cascaded with an optical transmitter to generate the maximum transmitted optical power. The transmitter, at the bias current of 50 mA, produces approximately 5 dBm of optical power. At this input power level, the EDFA is well into saturation and has a gain of 10 dB. The optical bandpass filter is used to minimize the out-of-band Amplified Spontaneous Emission (ASE) noise. At the output of the filter which has 2.6 dB insertion loss, the optical power level was measured to be 12.7 dBm. The optical attenuator was set at 10 dB attenuation, emulating a one-to-ten splitter. The 10 km of fiber has a total loss of about 3.7 dB which, with the splitter loss, reduces the received optical power to -1 dBm. The results of BER versus QAM

modulation index for all three experimental set-ups with $m_{AM\text{-}VSB}$ = 4%, 5%, and 6% are shown in Figs. 6.27(a), (b), and (c).

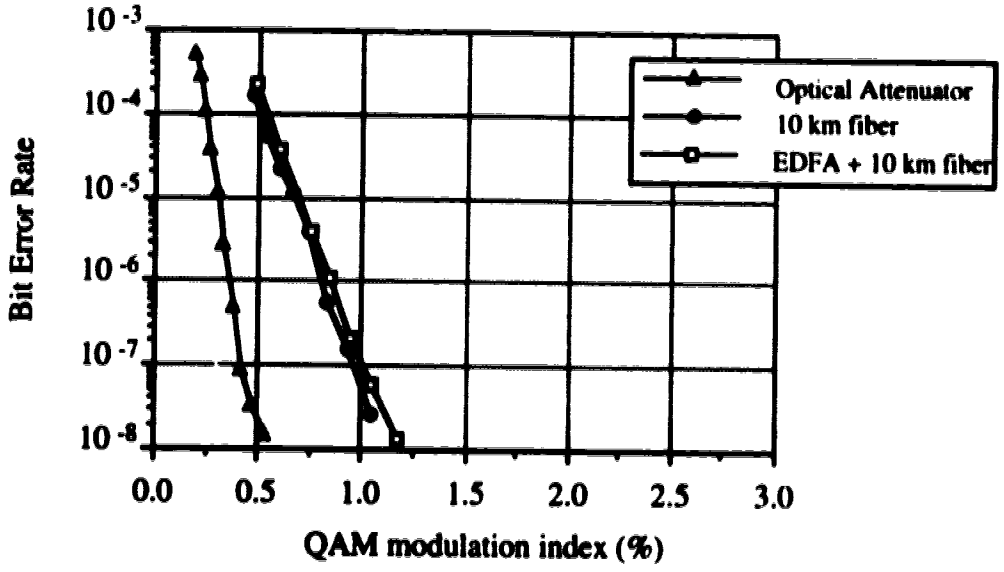

Fig. 6.27(a) $m_{AM\text{-}VSB}$ = 4%, G_{EDFA} = 10 dB, P_{tx} = 5 dBm, $P_{received}$ = -1 dBm, I_{bias} = 50 mA

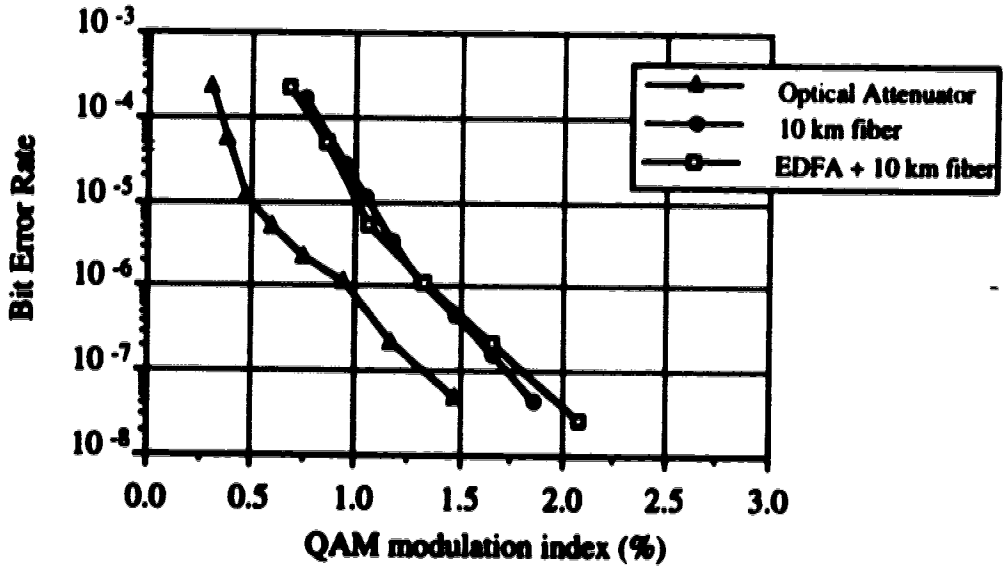

Fig. 6.27(b) $m_{AM\text{-}VSB}$ = 5%, G_{EDFA} = 10 dB, P_{tx} = 5dBm, $P_{received}$ = -1 dBm, I_{bias} = 50 mA

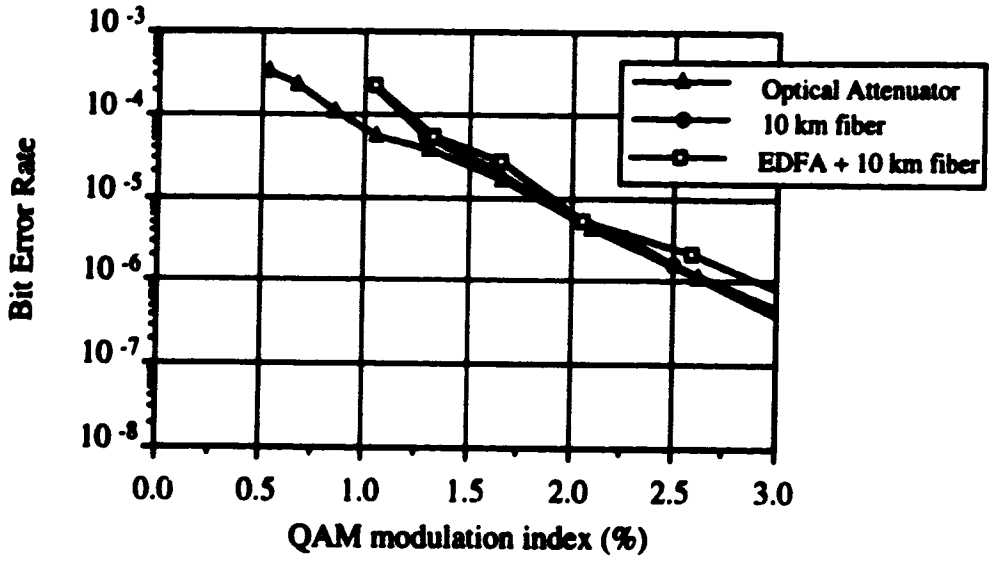

Fig. 6.27(c) $m_{AM\text{-}VSB} = 6\%$, $G_{EDFA} = 10$ dB, $P_{tx} = 5$ dBm, $P_{received} = -1$ dBm, $I_{bias} = 50$ mA

For a system of 42 CATV channels at 4% modulation index per channel, distortion due to signal clipping is negligible. Thus, the difference between the BER curves shown in Fig. 6.27(a) is entirely attributed to the combined effect of fiber dispersion and laser diode chirp. It is also observed that the addition of an EDFA to the link does not degrade BER performance, indicating the dominance of distortion caused by fiber dispersion and laser chirp at $m_{AM\text{-}VSB}$ of 4%.

At $m_{AM\text{-}VSB}$ of 5%, more signal clippings occur and cause degradation in BER performance as shown in Fig. 6.27(b). However, there is still a substantial difference between the BER curve for the system with and without 10 km of fiber. This indicates that distortion due to signal clipping is still small and secondary compared to that caused by fiber dispersion and laser chirp. Finally, in Fig. 6.27(c), it is observed that all three BER curves are now the same. At a value of $m_{AM\text{-}VSB}$ of 6%, signal clipping becomes

more severe and induces a significant amount of distortion which exceeds chirp/dispersion-induced distortion as the dominant source of distortion.

6.6 Investigation of Distortion as Interfering Signal

In a SCM system, all the analog and digital signals are first frequency multiplexed together and then used to modulate the intensity of the laser whose threshold clipping is analogous to that of a hard-limiter. Because of the fact that the signals are mixed together at the laser, it is reasonable to believe that BER performance of 64-QAM is degraded not just by the distortion products that interfere with the signal, but also by some unknown effects attributed to the mixing process at the laser. To resolve this issue, an experiment was devised and performed. The experimental set-up for this experiment is shown in Fig. 6.28.

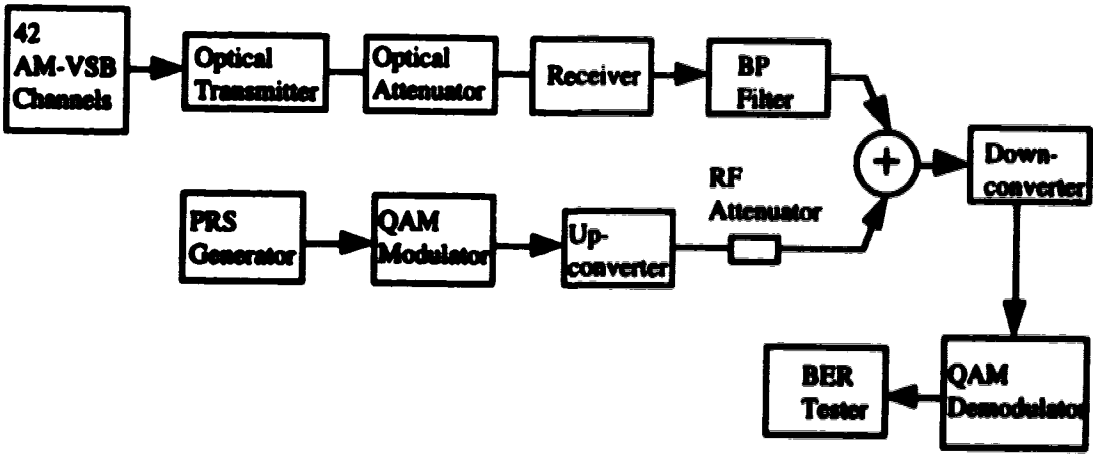

Fig. 6.28 64-QAM signal bypassing the laser

In this experiment, analog carriers are used to generate clipping distortion. The distortion products that fall on the QAM channel allocation are filtered out and added to the QAM signal that bypasses the laser. This QAM signal containing distortion interference is then demodulated and its BER measured Fig. 6.29 shows BER as a

function of SNLD with SNR of 45 dB or better. Also plotted in the same figure are the results obtained for the case where both analog and digital signals are combined to modulate the laser. The experimental operating conditions are the same for both cases.

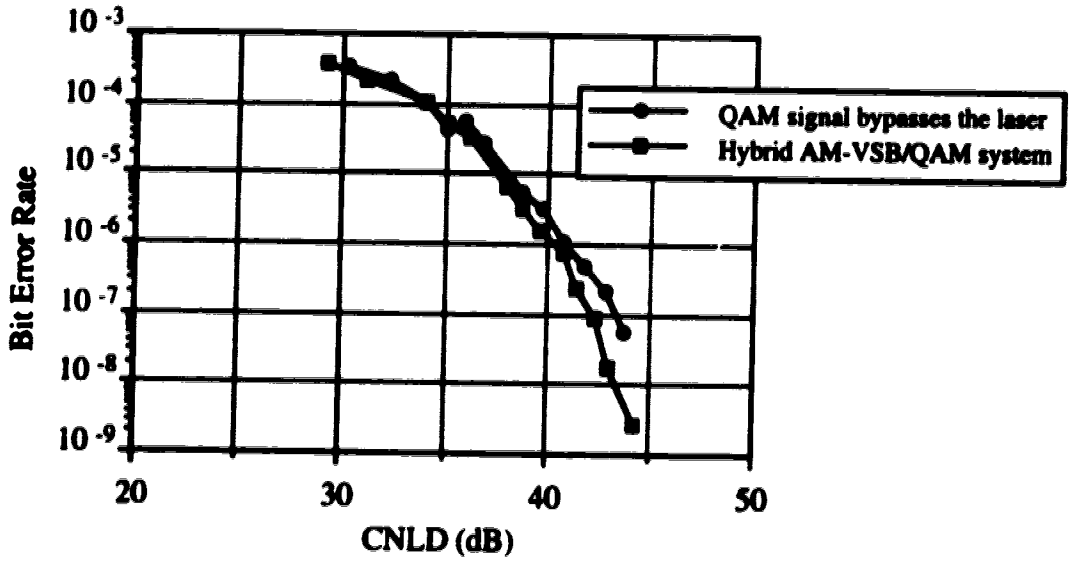

Fig. 6.29 BER performance of 64-QAM signal that bypasses the laser
$m_{AM\text{-}VSB}$ = 6%, $P_{received}$ = -1 dBm, I_{bias} = 50 mA

If it is true that there exist some unknown effects attributable to the mixing process at the laser that degrade BER performance, then we should see an improvement in BER performance for the case where the QAM signal bypasses the laser. However, Fig. 6.29 shows that the two sets of results are the same. The agreement between the two plots proves that there are no other unknown effects and that the observed degradation in BER performance is simply due to interference from the distortion products that fall into the QAM channel.

6.7 Channel Capacity Study for a Hybrid AM-VSB/QAM Optical Transmission System

In this section, a study of channel capacity is presented to demonstrate the feasibility of the simultaneous transmission of AM-VSB and QAM signals over optical fiber. Two important assumptions are made in this study and listed below.

i) The effect of digital signals on analog CATV carriers is negligible. This is generally true if the power of the QAM signals is a small portion of the AM-VSB/QAM composite signal power.

ii) The resonant frequency of the laser biased at 50 mA is far away from the highest frequency component of the composite signal. Under this condition, RIN is relatively constant across the signal spectrum and resonance distortion is negligible.

The performance of a hybrid AM-VSB/QAM optical fiber transmission system depends on the frequency allocations of both the QAM and AM-VSB channels. The frequency allocation of the AM-VSB channels determines the distribution of distortion products over the transmission band, thereby affecting the CSO and CTB performance of the analog signals and BER performance of the digital signals. In addition, the impact of distortion on the QAM signal varies from one QAM channel to another, depending on the frequency allocation of that channel with respect to that of the AM-VSB carriers. Therefore, in order to accurately evaluate the channel capacity of a hybrid AM-VSB/QAM optical fiber transmission system, one would have to account for the impact of distortion on each QAM channel and more importantly, the effects of the variations in the frequency allocation on the system performance. Though this approach would lead to a precise and reliable study of the channel capacity, it is very complex to work with.

In this study, the evaluation of the channel capacity is based on the experimental results obtained from a configuration that has one QAM channel at 417 MHz and 42 AM-VSB carriers from 55.25 MHz to 349.25 MHz. In essence, we only know the effect of

the distortion products induced by a particular set of AM-VSB carriers on one QAM channel. Therefore, this study does not provide a precise prediction, but rather an approximation of the channel capacity. In addition, this study is only valid for the configuration that has the QAM channel cluster allocated at the upper-frequency end of the transmission band.

As mentioned in Section 2.4, the noise and distortion standards for the present coaxial CATV distribution systems require CNR of 44 dB, and CSO and CTB of -52 dBc or better. In this project, the following performance requirements will be used for fiber trunking/feeder distribution systems: CNR = 50 dB, CSO and CTB = -55 ~ -60 dBc. For the digital signals, BER of 10^{-5} before FEC is required in order to obtain at least 10^{-9} after error correction.

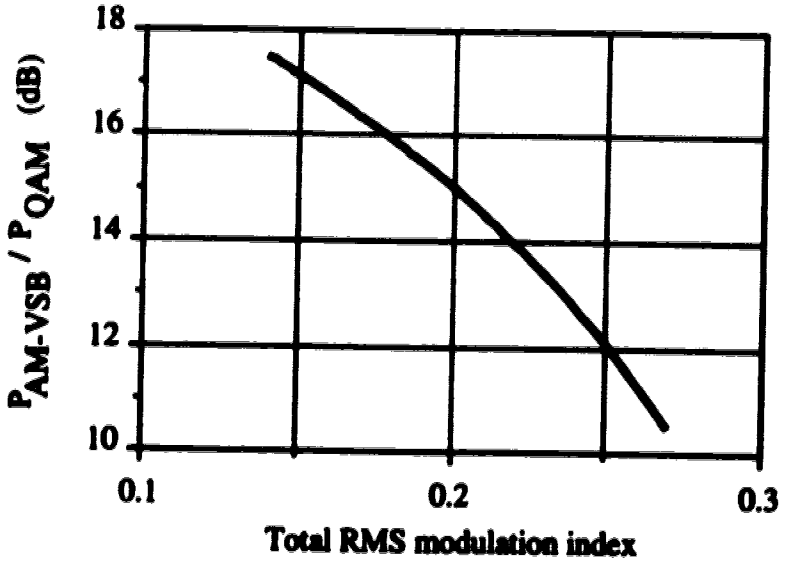

Fig. 6.30 $P_{AM\text{-}VSB}/P_{QAM}$ as a function of μ

For this study, we consider a practical system with 10 km of optical fiber link. The transmitted and received optical power are 6 dBm and -1 dBm respectively, giving a system power margin of 7 dB. The first step taken in this channel capacity study is to determine the total rms modulation index level (μ) at which CSO and CTB performance

of analog carriers meet the required specifications. From Fig. 6.6 and 6.7, for CSO and CTB values of -58 dBc and -65 dBc, the corresponding μ is approximately 0.23. Next, for a desired CNR, one can determine the AM-VSB modulation index per channel. For example, mAM-VSB of 4% corresponds to CNR of 52 dB. With all the necessary parameters for analog signals known, the next step is to determine the relative difference in dB between AM-VSB carrier power and QAM signal power. Based on experimental results reported in Section 6.5, a relation between $P_{AM\text{-}VSB}/P_{QAM}$ and total rms modulation index is found and plotted in Fig. 6.30. At $\mu = 0.23$, $P_{AM\text{-}VSB}/P_{QAM}$ is about 13 dB which corresponds to a ratio of $m_{AM/VSB}/m_{QAM}$ of 4.57. Finally, a relation between the number of analog channels and of digital channels is given by

$$N_{AM-VSB} = \frac{2}{m_{AM-VSB}^{\ 2}} \cdot \left(\mu^2 - \frac{m_{QAM}^{\ 2} \cdot N_{QAM}}{2} \right) \qquad (6.12)$$

where $N_{AM\text{-}VSB}$ is the number of analog channels, and N_{QAM} is the number of QAM channels. A plot of $N_{AM\text{-}VSB}$ as a function of N_{QAM} is shown in Fig. 6.31. In addition, a summary of all the performance parameters is given in Table 6.1.

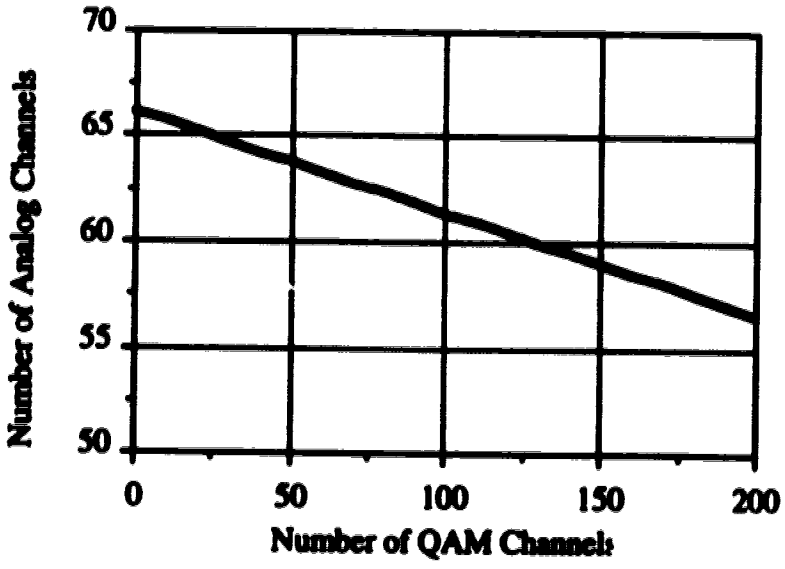

Fig. 6.31 AM-VSB channels versus QAM channels

Table 6.1 Summary of the system operating conditions and performance parameters

- Transmitted Optical Power = 6 dBm
- Received Optical Power = -1 dBm
- System Power Margin = 7 dB
- Total RMS modulation index = 0.23

For Analog Channels

- AM-VSB Modulation Index per channel = 4%
- CNR = 52 dB
- CSO = - 58 dBc
- CTB = - 65 dBc

For Digital Channels

- At power level 13 dB lower than that of AM-VSB
- Bit Error Rate = 10^{-5} before FEC

The focus of the study above is NOT to determine the state-of-the-art channel capacity, or in other words, the maximum number of AM-VSB and QAM channels that can be transmitted. These types of study often provides us with an optimistic number of channel that is in quantity of hundreds and the signal spectrum correspondingly extends into multi-GHz region. In this frequency region, the signal is now affected by other effects such as resonance distortion, increase in RIN, and etc.. that were not accounted for in the study. Therefore, in our view, this type of channel capacity study is unrealistic and hence meaningless.

Of more importance and usefulness to this project is a channel capacity of a sample case that demonstrates the feasibility of a hybrid AM-VSB/QAM optical transmission system, and it is precisely that which was presented in this section. From Fig. 6.31, it is demonstrated that the digital signals are more robust than the AM-VSB

signals with respect to noise and nonlinearity, despite the fact that nonlinear distortion has a significant degradative impact on the BER performance of the digital signals as discussed in Section 6.3.2. It is shown that, with QAM signal power about 13 dB lower than that of AM-VSB carriers, a large number of QAM channels can be augmented to the system with a small sacrifice in the number of analog channels. For example, having one less AM-VSB channel in the system results in an increase of approximately 20 QAM channels , while meeting all the normally accepted transmission specifications for both the analog and digital signals. This lopsided trade-off is a direct consequence of the QAM signals' less stringent requirements on noise and distortion performance than that of AM-VSB signals. In summary, a hybrid AM-VSB/QAM optical transmission system offers many advantages, one of which is that digital signals are more robust than AM-VSB signals with respect to noise and nonlinearity. Therefore, it is a feasible and promising method for video distribution in future CATV.

7. CONCLUSIONS

The purpose of this thesis has been to examine the feasibility of simultaneous transmission of analog and digital video signals over optical fiber, with emphasis on understanding the effects of noise and nonlinear distortion products induced by the carriers of AM-VSB signals on the performance of QAM signals. The results of this comprehensive theoretical and experimental study lead to several important conclusions.

From the qualitative study of the random nature of nonlinear distortion, it was observed that the distortion products in a 10 MHz bandwidth appeared as impulses in the time domain and have a non-Gaussian amplitude distribution. The power and frequency of these impulses determine the severity of QAM signal performance degradation. Thus, it is concluded that a realistic and accurate noise model for a hybrid AM-VSB/QAM optical transmission system should be a mixture of Gaussian and non-Gaussian impulsive noise. On the basis of this conclusion, Middleton's Class A noise model which is a generalized model of Gaussian noise combined with non-Gaussian impulsive noise is an essential component in the theoretical analysis of the performance of a 64-QAM signal in a hybrid transmission system.

The quantitative BER measurements and theoretical results obtained provide important insights on the impact of distortion and noise on the BER performance of 64-QAM signals. The results have consistently demonstrated that distortion due to laser clipping degrades the BER more severely than noise and is the dominant source of degradation in a hybrid transmission system. For example, at SNR of 30 dB, BER of 10^{-8} is obtained for a system where there is no distortion. Whereas, at SNLD of 30 dB , BER of only 10^{-4} is obtained for a system in which the impact of noise on BER performance is negligible (i.e. SNR ~ 40 to 45 dB).

In addition, this work also shows that the assumption that the impulsive index is the same as the probability of clipping is inappropriate because the impact of non-Gaussian impulsive noise on BER is not adequately predicted by the theoretical analysis employing this assumption. On the other hand, the agreement between the experimental results and the theoretical results calculated using the measured impulsive index parameter, A, indicates that our experimental approach in determining the impulsive index is valid and correct. Our measurements of A were made by taking the ratio of the total number of samples containing impulses to the total number of samples.

This work has also indicated that even though the BER of QAM signals is increased by distortion due to laser clipping, the QAM signals are still more robust to noise and distortion than the AM-VSB signals. The results have shown that it is feasible to operate a hybrid system with QAM signal power approximately 10 to 15 dB below that of AM-VSB over a 10 km length of optical fiber, while meeting the normally accepted transmission specifications of CNR, CSO, CTB for analog signals, and BER for digital signals. This low signal power requirement results in an enhanced channel capacity because a large number of QAM channels can be added to the system with only a small sacrifice in the number of analog channels. This advantage of expandability along with that of compatibility with existing CATV systems make the fiber-optic video signal transport scheme employing analog AM-VSB and digital 64-QAM signals a feasible and promising method for video distribution in future CATV.

7.1 Recommendations for Further Research

As a consequence of the work performed in this project, several new research topics have become evident. One of the most obvious and practical avenues for further research is in bidirectional Erbium Doped Fiber Amplified transmission of analog and digital video signals between the host-terminal and subscribers using subcarrier

multiplexing (SCM) techniques. A project in this area would involve a comprehensive study of the effects of added noise, distortion, and Rayleigh backscattered signal due to bidirectional EDFA amplification.

Another research project would be a study focusing on the statistics of the distortion-induced impulses in terms of not only amplitude distribution, but also in terms of time distribution. Knowledge in this area could provide useful insights into the implementation of a system that can minimize the impact of nonlinear distortion on the BER performance of the digital signals. One such system may be an externally modulated system in which the second order distortion can be minimized if the external modulator is biased at the inflection point.

One of the limiting factors in the performance of a lightwave multichannel SCM system is the relative intensity noise (RIN) from the laser diode. This limitation can become critical when a system is required to distribute a large number of channels that occupies a large bandwidth. Therefore, a potential avenue of research may involve the development of a laser that has extremely low RIN at high frequencies. One such laser may be the Erbium Doped Fiber laser.

The channel capacity study conducted in this work is the first order estimation of the channel capacity of a hybrid AM-VSB/QAM optical transmission system. A potential fruitful research project would involve an ultimate channel capacity study that takes into account not only the effect of the analog carriers on the digital signals, but also the effect of the digital signals on the analog carriers, the channel interference, RIN and resonance distortion as the transmission bandwidth is expanded into the GHz range.

REFERENCES

[1] G. R. Boyer, "A Perspective on Fiber in the Loop Systems," *IEEE Lightwave Communications Systems*, vol. 1, no. 3, pp. 6-11, 1990.

[2] J. Terry, "Broadband ISDN Delivery Systems and Technologies," *LEOS Summer Topical Meeting Digest*, ThA4, pp. 38-40, 1992.

[3] D.G. Monteith, "Design of a Digital Fiber Optic CATV Link," *IEEE Transactions on Cable Television*, vol. CATV-3, no. 3, pp. 120-126, July 1978.

[4] Technical staff of Videotron Communications Ltd., Personal correspondence, Oct. 1993.

[5] J. Chiddix, H. Laor, D. Pangrac, L. Williamson, R. Wolfe, "AM Video on Fiber in CATV Systems: Need and Implementation," *IEEE Journal on Selected Areas in Communications*, vol. 8, no. 7, pp. 1229-1239, Sept. 1990.

[6] W. I. Way, "Subcarrier Multiplexed Lightwave System Design Consideration for Subscriber Loop Applications," *Journal of Lightwave Technology*, vol. 7, no. 11, pp. 1806-1818, Nov. 1989.

[7] T. E. Darcie, "Subcarrier Multiplexing for Lightwave Networks and Video Distribution Systems," *IEEE Journal on Selected Areas in Communications*, vol. 8, no. 7, pp. 1240-1246, Sept. 1990.

[8] R. Olshansky, V. A. Lanzisera, "Subcarrier Multiplexed Lightwave Systems for Broadband Distribution,' *Journal of Lightwave Technology*, vol. 7, no. 9, pp. 1329-1341, Sept. 1989.

[9] T. E. Darcie, G. E. Bodeep, "Lightwave Subcarrier CATV Transmission Systems," *IEEE Transaction on Microwave Theory and Techniques*, vol. 38, no. 5, pp. 524-533, May 1990.

[10] B. P. Lathi, "*Modern Digital and Analog Communication Systems*," 2 ed., Holt, Rinehart, and Winston, New York, pp. 260-266, 1983.

[11] L. W. Couch II, "*Digital and Analog Communications Systems,*" 3 ed., Macmillan Publishing Company, New York, pp. 421, 1990.

[12] B. P. Lathi, "*Modern Digital and Analog Communication Systems,*" 2 ed., Holt, Rinehart, and Winston, New York, pp. 542, 1983.

[13] L. W. Couch II, "*Digital and Analog Communications Systems,*" 3 ed., Macmillan Publishing Company, New York, pp. 165, 1990.

[14] Y. Yamamoto, "AM and FM Quantum Noise in Semiconductor Lasers - Part 1: Theoretical Analysis," *IEEE Journal of Quantum Electronics,* vol. QE-19, no. 1, pp. 34-46, Jan. 1983.

[15] K. Petermann, "*Laser Diode Modulation and Noise,*" Kluwer Academic Publishers, Tokyo, pp. 160-163, 1988.

[16] G. Keiser, "*Optical Fiber Communications,*" 2 ed., McGraw-Hill, New York, pp. 366-369, 1991.

[17] W. S. Ciciora, "*An Overview of Cable Television in the United States,*" CableLabs, pp. 14-19, Dec. 1990.

[18] Magnavox CATV Systems, Inc., "*CATV Reference Guide,*" [Unknown], pp. 7.

[19] Paul Langner, Personal Correspondence, Jul. 1993.

[20] G. Keiser, "*Optical Fiber Communications,*" 2 ed., McGraw-Hill, New York, pp. 357-365, 1991.

[21] A. A. M. Saleh, "Fundamental Limit on Number of Channels in Subcarrier-Multiplexed Lightwave CATV System," *Electronics Letters,* vol. 25, no. 17, pp. 776-777, Jun. 1989.

[22] C. J. Chung, I. Jacobs, "Practical TV Channel Capacity of Lightwave Multichannel AM SCM Systems Limited by the Threshold Nonlinearity of Laser Diodes," *IEEE Journal of Lightwave Technology,* vol. 4, no. 3, pp. 289-292, Mar. 1992.

[23] H. Ohtsuka, O. Kagami, S. Komaki, K. kohiyama, M. Kavehrad, "256-QAM Subcarrier Transmission Using Coding and Optical Intensity Modulation in Distribution Networks," *IEEE Photonics Technology Letters*, vol. 3, no. 4, pp. 381-383, Apr. 1991.

[24] M. Kavehrad, E. Savov, "Fiber-Optic Transmission of Microwave 64-QAM Signals," *IEEE Journal on Selected Areas in Communications*, vol. 8, no. 7, pp. 1320-1326, Sept. 1990.

[25] K. Alameh, K. Minasian, "Ultimate Limits of Subcarrier Multiplex Lightwave Transmission," *Electronics Letters*, 1991, vol. 27, no. 14, pp. 1260-1262, Jul. 1991.

[26] J. G. Proakis, "*Digital Communications*," 2 ed., McGraw Hill, New York, pp. 42-44, 1989.

[27] B. P. Lathi, "*Modern Digital and Analog Communication Systems*," 2 ed., Holt, Rinehart, and Winston, New York, pp. 587-590, 1983.

[28] J. Seo, S. Cho, K. Feher, "Impact of Non-Gaussian Impulsive Noise on the Performance of High Level QAM," *IEEE Transactions on Electromagnetic Compatibility*, vol. 31, no. 2, pp. 177-180, May 1989.

[29] E. Lee, D. Messerschmitt, "*Digital Communication*," 1 ed., Kluwer Academic Publishers, Boston, pp. 193-194, 1988.

[30] D. Middleton, "Statistical-Physical Models of Electromagnetic Interference," *IEEE Transactions on Electromagnetic Compatibility*, vol. 19, no. 3, pp. 106-127, Aug. 1977

[31] L. A. Berry, "Understanding Middleton's Canonical Formula for Class A Noise," *IEEE Transactions on Electromagnetic Compatibility*, vol. 23, no. 4, pp. 337-344, Nov. 1981.

[32] A. Spaulding, D. Middleton, "Optimum Reception in an Impulsive Interference Environment-Part I: Coherent Detection," *IEEE Transactions of Communications*, vol. 25, no. 9, pp. 910-923, Sept. 1977.

[33] K. Maeda, H. Nakata, K. Fujito, "Analysis of BER of 16QAM Signal in AM/16QAM Hybrid Optical Transmission System," *Electronics Letters*, vol. 29, no. 7, pp. 640-642, Apr. 1993.

[34] Bob Thomas, Personal Correspondence, Jul. 1993.

[35] Northern Telecom, "*Digital Microwave Radio RD-6B Technical Handbook*," Mar. 1988

[36] L. A. Johnson, "Controlling Temperature of Diode Lasers and Detectors Thermoelectrically," [Unknown].

[37] Ortel Corporation, "Application of Impedance Matched Photodiodes in AM-VSB CATV Links," *Photodiode Module Model 2610C Operator's Manual*," [Unknown].

[38] National Cable Television Association, "*NCTA Recommended Practices for Measurements on Cable Television System*," Nov. 1989.

[39] H. Blauvelt, N. S. Kwong, P. Chen, I. Ury, "Optimum Range for DFB Laser Chirp for Fiber Optic AM Video Transmission," *Journal of Lightwave Technology*, vol. 11, no. 1, pp. 55-59., Jan. 1993.

[40] N. Kanno, K. Ito, "Fiber-Optic Subcarrier Multiplexing Video Transport Employing Multilevel QAM," *IEEE Journal on Selected Areas in Communications*, vol. 8, no. 7, pp. 1312-1319, Sept. 1990.

[41] W. I. Way, "Fiber-Optic Transmissions of Microwave 8-Phase-PSK and 16-ary Quadrature-Amplitude-Modulated Signals at 1.3 μm Wavelength Region", *Journal of Lightwave Technology*, vol. 6, no. 2, pp. 273-280, Feb. 1988.

[42] Q. Shi, "Performance of M-ary QAM in Hybrid AM/QAM Multichannel Lightwave Transmission with and without Coding," *OFC/IOOC '93 Technical Digest*, THL3, pp. 221-223.

[43] R. H. Wentworth, "Performance of Single-Laser Split-Band Analog Video Systems," *OFC/IOOC '93 Technical Digest*, THL4, pp. 223-224.

[44] C. Y. Kuo, "Fundamental Nonlinear Distortion in Analog Link with Fiber Amplifiers," *Journal of Lightwave Technology*, vol. 11, no. 1, pp. 7-15, Jan. 1993.

[45] E. Yoneda, K. Suto, K. Kikushima, and H. Yoshinaga, "All-Fiber Video Distribution (AFVD) Systems using SCM and EDFA techniques," *Journal of Lightwave Technology*, vol. 11, no. 1, pp. 128-137, Jan. 1993.

APPENDIX A

CATV Channel and Frequency Designations

Historical Channel Designation	NCTA Channel Designation	Standard Video Frequency (MHz)
2	2	55.25
3	3	61.25
4	4	67.25
5	5	77.25
6	6	83.25
A	14	121.25
B	15	127.25
C	16	133.25
D	17	139.25
E	18	145.25
F	19	151.25
G	20	157.25
H	21	163.25
I	22	169.25
7	7	175.25
8	8	181.25
9	9	187.25
10	10	193.25
11	11	199.25
12	12	205.25

13	13	211.25
J	23	217.25
K	24	223.25
L	25	229.25
M	26	235.25
N	27	241.25
O	28	247.25
P	29	253.25
Q	30	259.25
R	31	265.25
S	32	271.25
T	33	277.25
U	34	283.25
V	35	289.25
W	36	295.25
AA	37	301.25
BB	38	307.25
CC	39	313.25
DD	40	319.25
EE	41	325.25
FF	42	331.25
GG	43	337.25
HH	44	343.25
II	45	349.25

APPENDIX B

Modulation Index Calibration

Modulation index (m) is defined by

$$m = \frac{\Delta I}{I_{bias} - I_{th}} \qquad \text{(A1)}$$

where ΔI is the peak amplitude of the modulating current, I_{bias} is the bias current, and I_{th} is the threshold current. The parameters, I_{bias} and I_{th}, can be accurately measured for the calculation of m. However, ΔI is more complicated to determine. On the first thought, it seems that ΔI can be determined by measuring the power of optical transmitter's input signal, with an assumption that the signal at the input of the optical transmitter is the same as that at the input of the laser diode. In practice, this assumption is inappropriate because microstrip circuits and electrical connections used in the packaging of the optical transmitter substantially affect the signal before it reaches the laser diode. Therefore, to accurately determine the modulation index, one has to account for the frequency response of the optical transmitter. To achieve this, the following calibration procedure is used.

The objective of this calibration is to determine the input signal power level at which 100 percent modulation index is obtained. This is done by first setting the power of the modulating signal (a single sinusoidal signal) at a fixed level and the bias current far above threshold such that no clipping occurs. Then, the bias current is slowly decreased until the second order harmonic dramatically shoots up indicating the clipping of the signal. At this point, 100 percent modulation index is obtained. The calibration is performed from 50 MHz to 300 MHz in a 50 MHz step for the analog signals, and also at 417 MHz for the QAM signal. In Fig. A1(a) and (b), power of the second order

harmonics is plotted as a function of bias current for input signal frequency of 100 MHz and 250 MHz.

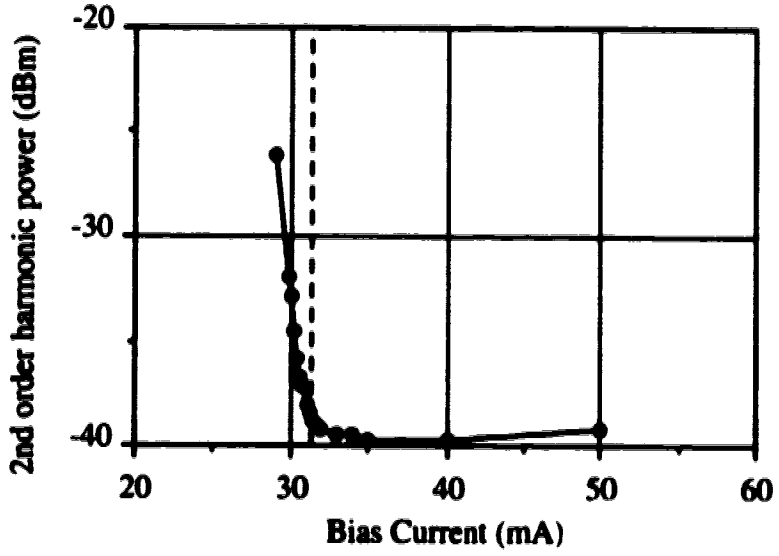

Fig. A1(a) Second order harmonic power as a function of bias current.
f_{sig} = 100 MHz, P_{input} = 6.65 dBm

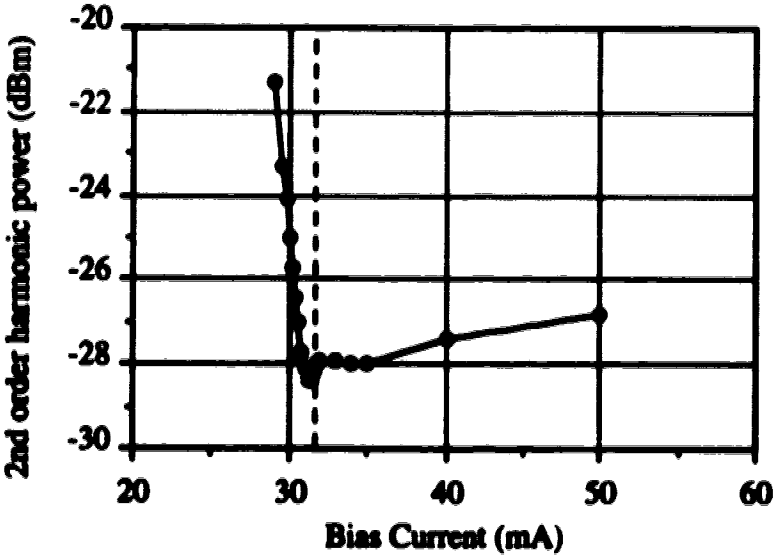

Fig. A1(b) Second order harmonic power as a function of bias current.
f_{sig} = 250 MHz, P_{input} = 7.35 dBm

As shown in Fig. A1(a) and (b), the bias current level at which clipping starts to occur for both cases is about 31 to 32 mA. From these results, one can do a translation to obtain the required input power for 100 percent modulation index at bias current of 50 mA which is the current level used in the experiments. For analog signals whose frequency ranges from 50 MHz to 350 MHz, the average input power level for 100 % modulation index at 50 mA bias current is 14.47 dBm while, for 64-QAM digital signal at 417 MHz, the input power is 10.72 dBm. The difference between the input powers is due to the fact that signal at 417 MHz sees higher gain than that from 50 MHz to 350 MHz as indicated by the frequency response of the optical transmitter shown in Fig. 5.7.

Finally, using the calibration results above, one can determine the modulation index for any input signal level at bias current of 50 mA. For example, using the following equation

$$m = 10^{\frac{P_{input} - 14.47}{20}} = 10^{\frac{-11.55 - 14.47}{20}} = 0.05, \qquad \text{(A2)}$$

the modulation index for input signal power of -11.55 dBm is calculated to be 5%.

In summary, this modulation index calibration technique takes into consideration of the frequency response of the optical transmitter, thus providing an accurate method in determining the modulation index parameter.

APPENDIX C

Computer Program Listings for the Calculations of

- **BER vs. SNR (Program A)**
- **BER vs. Received Optical Power (Program B)**
- **BER vs. QAM Modulation Index (Program C)**
- **BER vs. QAM Modulation Index for AM-VSB Modulation Index per Channel of 5% and 6% (Program D - G)**
- **BER vs. SNR for SNLD of 41 and 44 dB (Program H and I)**
- **BER vs. SNLD (Program J)**

PROGRAM A: QAM Bit Error Rate Vs. SNR

This program calculates the BER of a 64-QAM signal with respect to SNR. This is for the Gaussian noise environment.

BER as a function of the received optical power

$$SNRdB = 22, 23 .. 30$$

$$SNR(SNRdB) = 10^{\left[\frac{SNRdB}{10}\right]}$$

$$BER(SNRdB) = \frac{\left[2\cdot\left[M - \sqrt{M}\right]\right]}{(M\cdot 6)}\cdot\left[1 - erf\left[\left[\frac{\sqrt{(SNR(SNRdB)\cdot 2.328)}}{\left[\sqrt{2}\cdot\left[\sqrt{M} - 1\right]\right]}\right]\right]\right]$$

$$M = 64$$

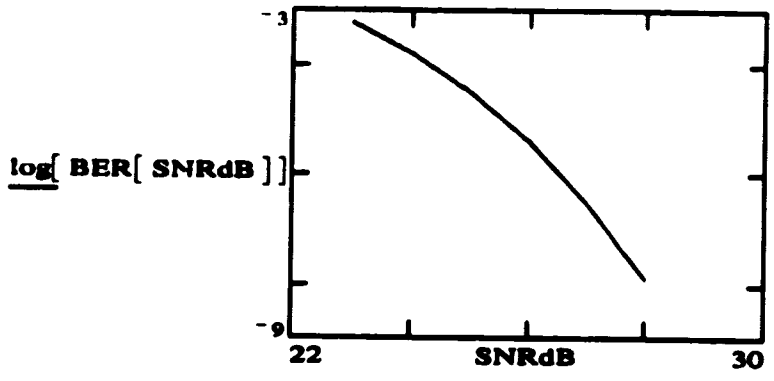

PROGRAM B: QAM Bit Error Rate Vs. Received Optical power

This Program calculates the BER of a 64-QAM signal with respect to the received optical power.

Parameters:

$RINdb := -160\,dB/Hz$ $BW := 5\cdot10^{6}\,Hz$ $R := 0.94$ Responsivity

$mQAM := 0.05546$ Mod Index $q := 1.602\cdot10^{-19}$ $Ith := 7.3\cdot10^{-12}\,A/\sqrt{Hz}$

$GainAmpdB := 18.5dB$ $CurrentGaindB := 7dB$ $NFamp := 6.5dB$

$NFdwncvtr := 22.1dB$

$RIN := 10^{\frac{RINdb}{10}}$ $GainAmp := 10^{\frac{GainAmpdB}{10}}$ $CurrentGain := 10^{\frac{CurrentGaindB}{10}}$

$RIN = 1\cdot10^{-16}$ $GainAmp = 70.795$ $CurrentGain = 5.012$

Calculation of Signal to Noise Ratio (SNR)

Signal Power

$$S(PodBm) := \left[0.5\cdot mQAM^{2}\cdot R^{2}\cdot\left[\left[10^{\frac{PodBm}{10}}\right]\cdot10^{-3}\right]^{2}\right]$$

RIN Noise

$$RINn(PodBm) := RIN\cdot BW\cdot R^{2}\cdot\left[\left[10^{\frac{PodBm}{10}}\right]\cdot10^{-3}\right]^{2}$$

Shot Noise

$$Shn(PodBm) := 2\cdot q\cdot BW\cdot R\cdot\left[\left[10^{\frac{PodBm}{10}}\right]\cdot10^{-3}\right]$$

Amplifier Noise

$$Ampn := \left[7.3\cdot10^{-12}\cdot10^{\frac{NFamp - CurrentGaindB}{20}}\right]^{2}\cdot BW$$

Downconverter Noise

$$Dn := 7.3 \cdot 10^{-12} \cdot 10^{\frac{NFdwncvtr - CurrentGaindB - GainAmpdB}{20}} \cdot BW$$

SNR as function of received optical power

$$SNR(PodBm) := \frac{S(PodBm)}{RINn(PodBm) + Shn(PodBm) + Ampn + Dn}$$

$RINn(-17) = 1.759 \cdot 10^{-19}$ $\quad$ $Shn(-17) = 3.005 \cdot 10^{-17}$

$Ampn = 2.375 \cdot 10^{-16}$ $\quad$ $Dn = 1.218 \cdot 10^{-16}$

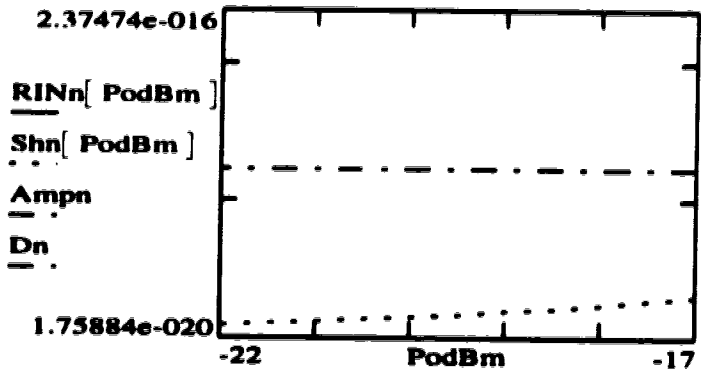

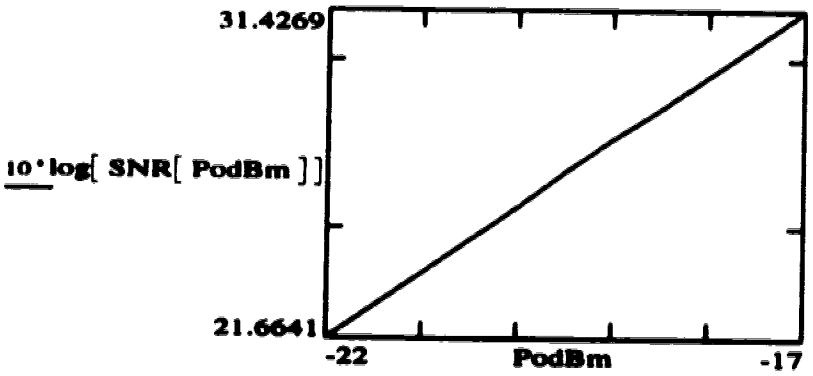

$PodBm \equiv -17, -17.5 .. -22 \qquad M := 64$

BER as a function of the received optical power

$$BER(PodBm) := \frac{\left[2 \cdot \left[M - \sqrt{M}\right]\right]}{(M \cdot 6)} \cdot \left[1 - erf\left[\left[\frac{\sqrt{(SNR(PodBm) \cdot 2.328)}}{\left[\sqrt{2} \cdot \left[\sqrt{M} \quad 1\right]\right.}\right.\right.\right.$$

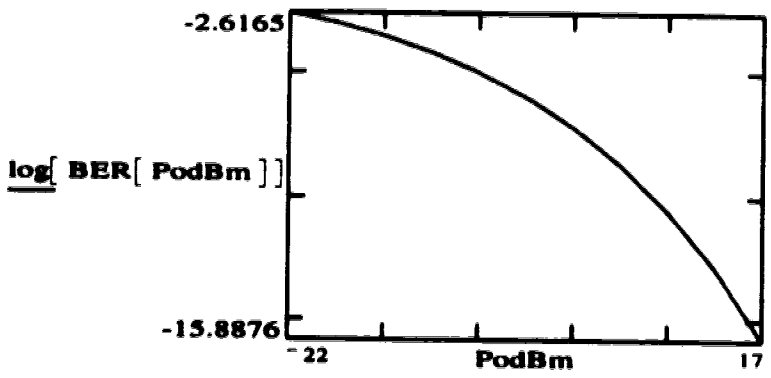

PROGRAM C: QAM Bit Error Rate Vs. QAM signal modulation index

This program calculates the BER of a 64-QAM signal with respect to the QAM signal modulation index.

Parameters:

$RINdb := -160\,dB/Hz$ $BW := 5\cdot10^{6}\,Hz$ $R := 0.94\,Responsivity$

$GainAmpdB := 18.5dB$ $q := 1.602\cdot10^{-19}$ $Ith := 7.3\cdot10^{-12}\,A/sqrt(Hz)$

$CurrentGaindB := 7dB$ $NFamp := 6.5dB$ $NFdwncvtr := 22.1dB$

$$RIN := 10^{\frac{RINdb}{10}} \qquad GainAmp := 10^{\frac{GainAmpdB}{10}} \qquad Po := 10^{\frac{PodBm}{10}}\cdot10^{-3}$$

$RIN = 1\cdot10^{-16}$ $GainAmp = 70.7946$ $Po = 7.9433\cdot10^{-4}$

Calculation of Signal to Noise Ratio (SNR)

Signal Power

$$S(mQAM) := \left[0.5\cdot mQAM^{2}\cdot R^{2}\cdot\left[10^{\frac{PodBm}{10}}\cdot10^{-3}\right]^{2}\right]$$

RIN Noise

$$RINn := RIN\cdot BW\cdot R^{2}\cdot\left[\left[10^{\frac{PodBm}{10}}\cdot10^{-3}\right]^{2}\right]$$

Shot Noise

$$Shn := 2\cdot q\cdot BW\cdot R\cdot\left[\left[10^{\frac{PodBm}{10}}\cdot10^{-3}\right]\right]$$

Amplifier Noise

$$Ampn := \left[7.3\cdot10^{-12}\cdot10^{\frac{NFamp-CurrentGaindB}{20}}\right]^{2}\cdot BW$$

Downconverter Noise

$$Dn = \left[7.3 \cdot 10^{-12} \cdot 10^{\frac{NFdwncvtr - CurrentGaindB - GainAmpdB}{20}} \right]^2 \cdot BW$$

SNR as a function of modulation index

$$SNR(mQAM) = \frac{S(mQAM)}{RINn + Shn + Ampn + Dn}$$

$RINn = 2.7876 \cdot 10^{-16}$ $\quad Shn = 1.1962 \cdot 10^{-15}$

$Ampn = 2.3747 \cdot 10^{-16}$ $\quad Dn = 1.2179 \cdot 10^{-16}$

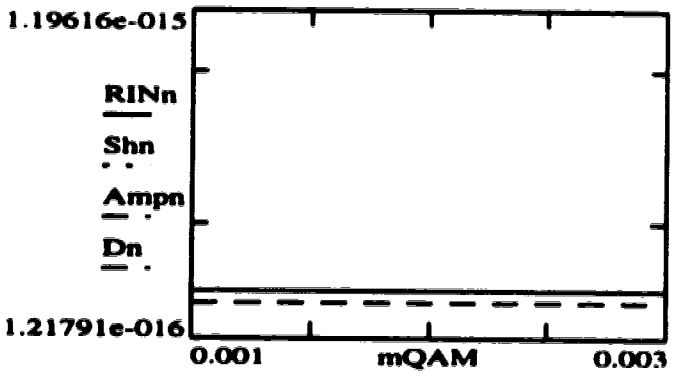

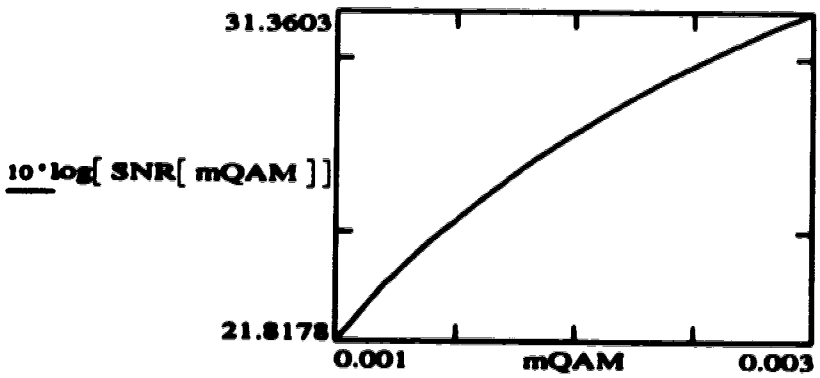

BER as a function of modulation index

$$BER(mQAM) := \left[\frac{2\cdot\left[M-\sqrt{M}\right]}{(M\cdot 6)}\right]\cdot\left[1-\operatorname{erf}\left[\frac{\sqrt{SNR(mQAM)\cdot 2.328}}{\sqrt{2}\cdot\left[\sqrt{M}-1\right]}\right]\right]$$

$M := 64$ $\quad$ $PodBm := -1$ $\quad$ $mQAM := 0.001, 0.0012 .. 0.003$

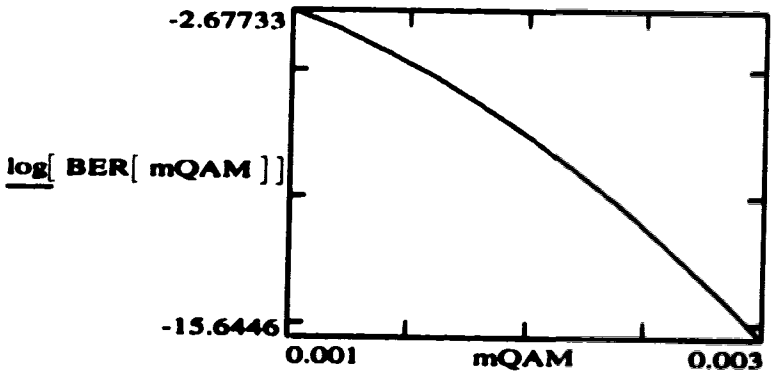

PROGRAM D: QAM Bit Error Rate Vs. QAM signal modulation index for AM-VSB modulation index per channel of 5% (hybrid AM-VSB/QAM system)

This program calculates the BER of a 64-QAM signal with respect to the QAM modulation index. This is to predict the performance of a 64-QAM signal in a hybrid AM-VSB/QAM system. (Gaussian combined with non-Gaussian impulsive noise environment.)

Parameters:

$RINdb := -160\,dB/Hz$ $BW := 5\cdot10^{6}\,Hz$ $R := 0.94$ Responsivity

$q := 1.602\cdot10^{-19}$ $Ith := 7.3\cdot10^{-12}\,A/sqrt(Hz)$

$GainAmpdB := 18.5dB$ $CurrentGaindB := 7\,dB$ $NFamp := 6.5dB$

$NFdwncvtr := 22.1dB$

$RIN := 10^{\frac{RINdb}{10}}$ $GainAmp := 10^{\frac{GainAmpdB}{10}}$ $Po := 10^{\frac{PodBm}{10}}\cdot10^{-3}$

$RIN = 1\cdot10^{-16}$ $GainAmp = 70.795$ $Po = 7.943\cdot10^{-4}$

Calculation of Signal to Noise Ratio (SNR)

Signal Power

$$S(mQAM) := \left[0.5\cdot mQAM^{2}\cdot R^{2}\cdot\left[\left[10^{\frac{PodBm}{10}}\right]\cdot10^{-3}\right]^{2}\right]$$

RIN Noise

$$RINn := RIN\cdot BW\cdot R^{2}\cdot\left[\left[10^{\frac{PodBm}{10}}\right]\cdot10^{-3}\right]^{2}$$

Shot Noise

$$Shn := 2\cdot q\cdot BW\cdot R\cdot\left[\left[10^{\frac{PodBm}{10}}\right]\cdot10^{-3}\right]$$

Amplifier Noise

$$Ampn := \left[7.3\cdot10^{-12}\cdot10^{\frac{NFamp-CurrentGaindB}{20}}\right]^{2}\cdot BW$$

Downconverter Noise

$$Dn := \left[7.3 \cdot 10^{12} \cdot 10^{\frac{NFdwncvtr - CurrentGaindB - GainAmpdB}{20}} \right]^2 \cdot BW$$

$RINn = 2.788 \cdot 10^{16}$ $\quad$ $Shn = 1.196 \cdot 10^{-15}$

$Ampn = 2.375 \cdot 10^{-16}$ $\quad$ $Dn = 1.218 \cdot 10^{-16}$

$Noisepower := RINn + Shn + Ampn + Dn$

$Noisepower = 1.834 \cdot 10^{-15}$

NONLINEAR DISTORTION POWER:

(NLDpower is obtained from
Mathematica Program F: Calculation of Nonlinear Distortion)

$NLDpower := 1.64 \cdot 10^{-16}$

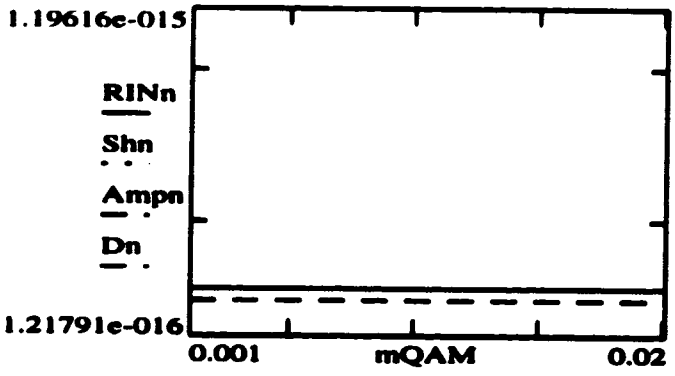

$$SNR(mQAM) := \frac{S(mQAM)}{Noisepower + NLDpower}$$

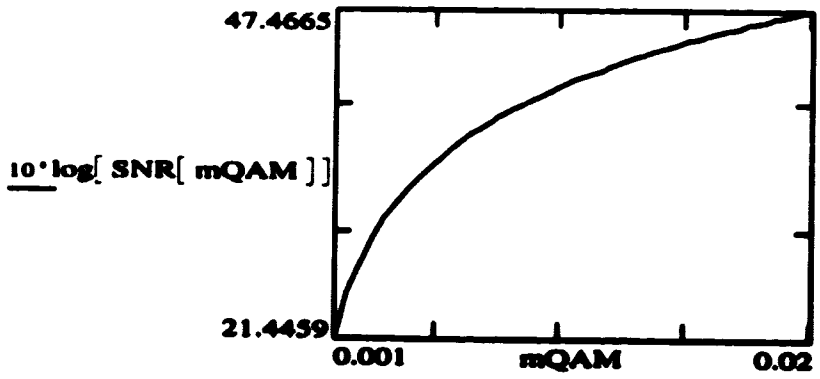

$$G = \frac{\text{Noisepower}}{\text{NLDpower}}$$

$$BER(mQAM) = \frac{2}{6}\cdot\frac{M-\sqrt{M}}{M}\cdot\exp(-1\cdot A)\cdot\sum_{j}\left[\frac{A^{j}}{j!}\cdot\left|1-\operatorname{erf}\left(\frac{\sqrt{((SNR(mQAM))\cdot 2.328)}}{\sqrt{2}\cdot\sqrt{M}-1}\cdot\sqrt{\frac{j}{A}+G}\right)\right|\right]$$

$j \equiv 0, 1 .. 20$ $\quad M \equiv 64$ $\quad A \equiv 0.0012$

$G = 11.184$ $\quad PodBm \equiv -1$ $\quad mQAM \equiv 0.001, 0.0015 .. 0.02$

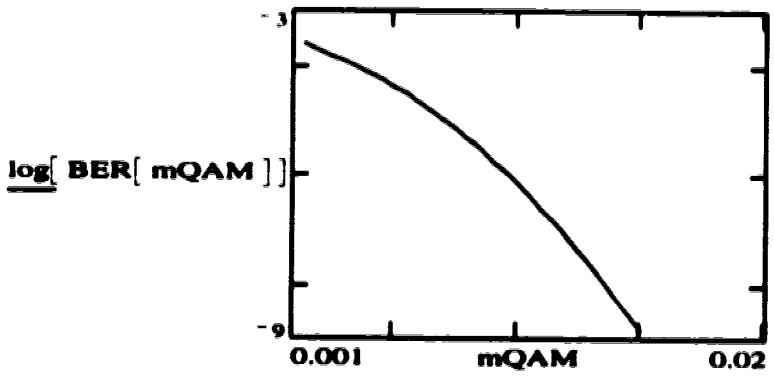

PROGRAM E: QAM Bit Error Rate Vs. QAM signal modulation index for AM-VSB modulation index per channel of 6 % (hybrid AM-VSB/QAM system)

This program calculates the BER of a 64-QAM signal with respect to QAM signal modulation index. This is to predict the performance of a 64-QAM signal in a hybrid AM-VSB/QAM system. (Gaussian combined with non-Gaussian impulsive noise environment.)

Parameters:

$RINdb := 160\,dB/Hz$ $BW := 5\cdot10^{6}\,Hz$ $R := 0.94$ Responsivity

$q := 1.602\cdot10^{-19}$ $Ith := 7.3\cdot10^{-12}A/sqrt(Hz)$

$GainAmpdB := 18.5dB$ $CurrentGaindB := 7\,dB$ $NFamp := 6.5dB$

$NFdwncvtr := 22.1dB$

$RIN := 10^{\frac{RINdb}{10}}$ $GainAmp := 10^{\frac{GainAmpdB}{10}}$ $Po := 10^{\frac{PodBm}{10}}\cdot10^{-3}$

$RIN = 1\cdot10^{-16}$ $GainAmp = 70.795$ $Po = 7.943\cdot10^{-4}$

Calculation of Signal to Noise Ratio (CNR)

Signal Power

$$S(mQAM) := \left[0.5\cdot mQAM^{2}\cdot R^{2}\cdot\left[\left[10^{\frac{PodBm}{10}}\right]\cdot10^{-3}\right]^{2}\right]$$

RIN Noise

$$RINn := RIN\cdot BW\cdot R^{2}\cdot\left[\left[10^{\frac{PodBm}{10}}\right]\cdot10^{-3}\right]^{2}$$

Shot Noise

$$Shn := 2\cdot q\cdot BW\cdot R\cdot\left[\left[10^{\frac{PodBm}{10}}\right]\cdot10^{-3}\right]$$

Amplifier Noise

$$Ampn := \left[7.3\cdot10^{-12}\cdot10^{\frac{NFamp-CurrentGaindB}{20}}\right]^{2}\cdot BW$$

Downconverter Noise

$$Dn := \left[7.3 \cdot 10^{-12} \cdot 10^{\frac{NFdwncvtr \cdot CurrentGaindB \quad GainAmpdB}{20}} \right]^2 \cdot BW$$

$RINn = 2.788 \cdot 10^{-16}$ $\quad Shn = 1.196 \cdot 10^{-15}$

$Ampn = 2.375 \cdot 10^{-16}$ $\quad Dn = 1.218 \cdot 10^{-16}$

$Noisepower = RINn + Shn + Ampn + Dn$

$Noisepower = 1.834 \cdot 10^{-15}$

NONLINEAR DISTORTION POWER:

(NLD power is obtained from
Mathematica Program G: Calculation of Nonlinear Distortion)

$NLDpower = 5.5 \cdot 10^{-15}$

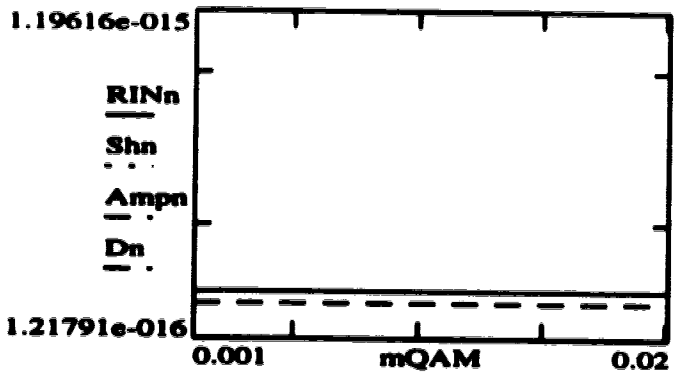

$$SNR(mQAM) = \frac{S(mQAM)}{Noisepower + NLDpower}$$

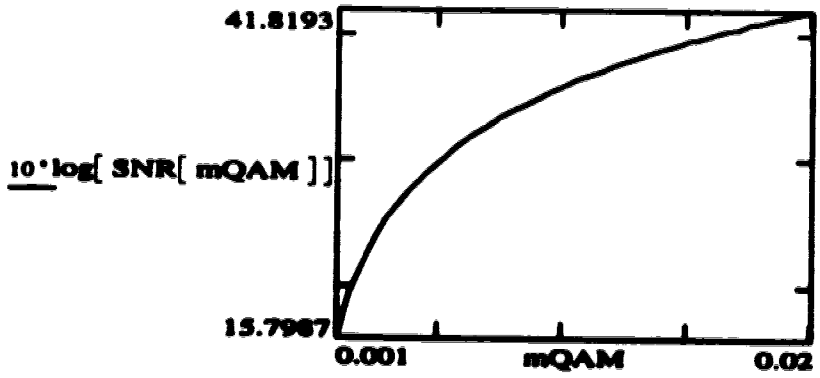

$$G \quad \frac{\text{Noisepower}}{\text{NLDpower}}$$

$$BER(mQAM) := \frac{2}{6}\cdot\frac{M-\sqrt{M}}{M}\cdot\exp(-1\cdot A)\cdot\sum_{j}\left[\frac{A^{j}}{j!}\cdot\left[1-\operatorname{erf}\left[\frac{\sqrt{((SNR(mQAM))\cdot 2.328)}}{\sqrt{2}\cdot\left[\sqrt{M}-1\right]\cdot\sqrt{\frac{\frac{j}{A}+G}{1+G}}}\right]\right]\right]$$

$j := 0, 1 .. 20$ $\quad M := 64$ $\quad A := 0.022$

$G = 0.333$ $\quad PodBm := -1$ $\quad mQAM := 0.001, 0.0015 .. 0.02$

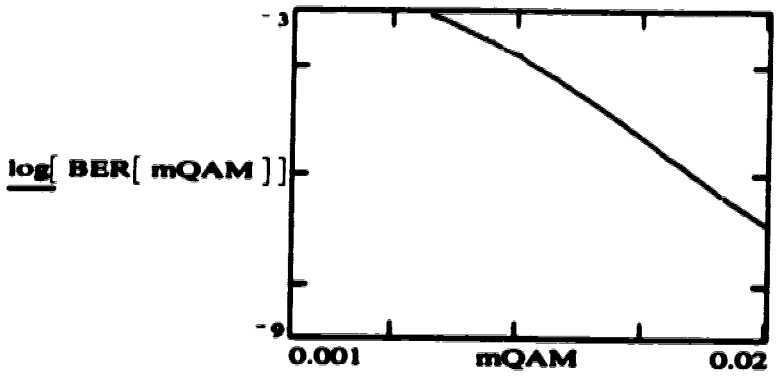

PROGRAM F: Calculation of nonlinear distortion power

This program calculates the nonlinear distortion power induced by laser clipping, using the equations from the paper written by Alameh et al [24].

```
(*CALCULATION OF NLD POWER SPECTRAL DENSITY AT F=417 MHZ*)

(*Constants*)
(*The values of the constants are the same as that used in the experiments*)

NN=42;              (*Number of channels*)
B=5*10^6;           (*Channel Bandwidth*)
fo=199.25*10^6;     (*Frequency of the center channel*)
fp=417*10^6;        (*Frequency of the channel under test*)
mu=0.238;           (*Total rms modulation index, ~ 5% mod. index per channel*)
Po= -1              (*Received optical power in dBm*)
Resp= 0.94          (*Responsivity*)


(*Calculation of sigma (variance)*)

sigma:=mu*Resp*(10^(Po/10))*0.001


(*Calculation of g[k]*)

g[k_]:=Sum[Binomial[k-2,j]*(I/((2^0.5)*mu))^j*Integrate[Exp[-u^2]*u^(k-2-j),{u,-
10,10}],{j,0,k}];


(*Calculation of hk*)

hh[k_]:=((1/(2*Pi))*(I^((k-2)))*((2^0.5/sigma)^(k-1))*(Exp[-
1/(2*mu^2)])*g[k])^2*1/k!*(sigma^(2*k));


(*Calculation of power spectral density by taking the Fourier")
(*Transform of the autocorrelation function.*)

Shape[y_,k_]:= (((Sin[Pi*y])/(Pi*y))^k)*(Cos[2fo/NN/B*y]^k)*Cos[2*fp/NN/B*y];

(*Summing the infinite series (100 terms)*)
```

```
store={};
total=0

For[x=2,x<100,x=x+1,
temp=hh[x]*(NIntegrate[Shape[t,x],{t,o,5}])*2/Pi/NN/B;total=total+temp;
store=Append[store,temp];
;]
```

To obtain the NLD power within a channel, perform the following calculation:

NLDpower = total*(2B), where B is the channel bandwidth.

PROGRAM G: Calculation of nonlinear distortion power

This program calculates the nonlinear distortion power induced by laser clipping, using the equations from the paper written by Alameh et al [24].

```
(*CALCULATION OF NLD POWER SPECTRAL DENSITY AT F=417 MHZ*)

(*Constants*)
(*The values of the constants are the same as that used in the experiments*)

NN=42;          (*Number of channels*)
B=5*10^6;       (*Channel Bandwidth*)
fo=199.25*10^6; (*Frequency of the center channel*)
fp=417*10^6;    (*Frequency of the channel under test*)
mu=0.284;       (*Total rms modulation index, ~ 6% mod. index per channel*)
Po= -1          (*Received optical power in dBm*)
Resp= 0.94      (*Responsivity*)


(*Calculation of sigma (variance)*)

sigma:=mu*Resp*(10^(Po/10))*0.001


(*Calculation of g[k]*)

g[k_]:=Sum[Binomial[k-2,j]*(I/((2^0.5)*mu))^j*Integrate[Exp[-u^2]*u^(k-2-j),{u,-
10,10}],{j,0,k}];


(*Calculation of hk*)

hh[k_]:=((1/(2*Pi))*(I^((k-2)))*((2^0.5/sigma)^(k-1))*(Exp[-
1/(2*mu^2)])*g[k])^2*1/k!*(sigma^(2*k));


(*Calculation of power spectral density by taking the Fourier")
(*Transform of the autocorrelation function.*)

Shape[y_,k_]:= (((Sin[Pi*y])/(Pi*y))^k)*(Cos[2fo/NN/B*y]^k)*Cos[2*fp/NN/B*y];

(*Summing the infinite series (100 terms)*)
```

```
store={};
total=0

For[x=2,x<100,x=x+1,
temp=hh[x]*(NIntegrate[Shape[t,x],{t,o,5}])*2/Pi/NN/B;total=total+temp;
store=Append[store,temp];
;]
```

To obtain the NLD power within a channel, perform the following calculation:

NLDpower = total*(2B), where B is the channel bandwidth.

PROGRAM H: Bit Error Rate vs. SNR, at SNLD = 41 dB

This program calculates the BER of a 64-QAM signal with respect to SNR at SNLD = 41 dB. This is for a hybrid AM-VSB/QAM transmission system.

Signal to Noise (Gaussian) Ratio

$$SNR(SNRdB) := 10^{\frac{SNRdB}{10}}$$

Signal to NLD (non-Gaussian impulsive noise) Ratio

$$SNLD := 10^{\frac{SNLDdB}{10}}$$

$$G(SNRdB) := \frac{SNLD}{SNR(SNRdB)}$$

Signal to Total Noise Ratio

$$SNRtotal(SNRdB) := \frac{1}{\frac{1}{SNR(SNRdB)} + \frac{1}{SNLD}}$$

BER as a function of SNR at SNLD = 41 dB

$$BER(SNRdB) := \frac{M - \sqrt{M}}{M \cdot 3} \cdot \exp(-1 \cdot A) \cdot \sum_j \left[\frac{A^j}{j!} \cdot \left[1 - \operatorname{erf}\left[\frac{\sqrt{SNRtotal(SNRdB) \cdot 2.328}}{\sqrt{2} \cdot \left[\sqrt{M} - 1 \right] \cdot \sqrt{\frac{\frac{j}{A} + G(SNRdB)}{1 + G(SNRdB)}}} \right] \right] \right]$$

$j := 0, 1 .. 10 \qquad A := 0.022 \qquad M := 64 \qquad SNRdB := 20, 21 .. 45 \qquad SNLDdB := 41$

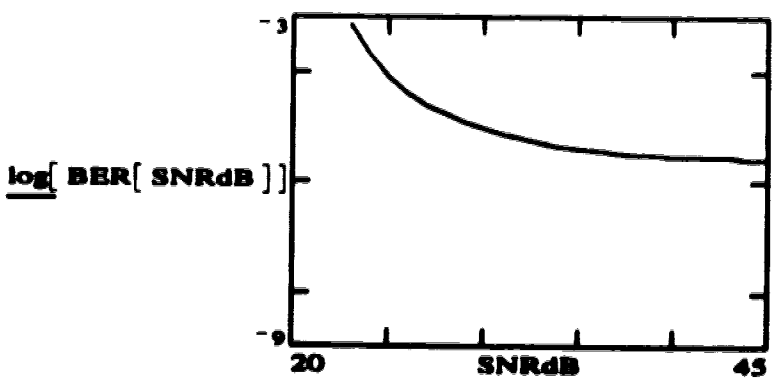

PROGRAM I: Bit Error Rate vs. SNR, at SNLD = 44 dB

This program calculates the BER of a 64-QAM signal with respect to SNR at SNLD = 44 dB. This is for a hybrid AM-VSB/QAM transmission system.

Signal to Noise (Gaussian) Ratio

$$SNR(SNRdB) := 10^{\frac{SNRdB}{10}}$$

Signal to NLD (non-Gaussian impulsive noise) Ratio

$$SNLD := 10^{\frac{SNLDdB}{10}}$$

$$G(SNRdB) := \frac{SNLD}{SNR(SNRdB)}$$

Signal to Total Noise Ratio

$$SNRtotal(SNRdB) := \frac{1}{\frac{1}{SNR(SNRdB)} + \frac{1}{SNLD}}$$

BER as a function of SNR at SNLD = 44 dB

$$BER(SNRdB) := \frac{M - \sqrt{M}}{M \cdot 3} \cdot \exp(-1 \cdot A) \cdot \sum_j \left[\frac{A^j}{j!} \cdot \left[1 - \operatorname{erf}\left[\frac{\sqrt{SNRtotal(SNRdB) \cdot 2.328}}{\sqrt{2} \cdot \left[\sqrt{M} - 1 \right] \cdot \sqrt{\frac{j}{A} + G(SNRdB)}} \right] \right] \right]$$

$j := 0, 1 .. 10 \qquad A := 0.022 \qquad M := 64 \qquad SNRdB := 20, 21 .. 45 \qquad SNLDdB := 44$

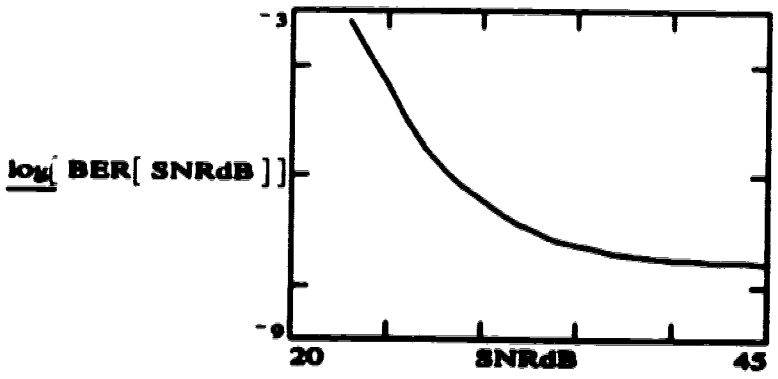

PROGRAM J: BER vs. SNLD

This program calculates the BER of a 64-QAM signal with respect to SNLD (Signal to Nonlinear Distortion Ratio). The SNR is 45 dB. At this SNR value, noise has negligible effect on the BER performance of a 64-QAM signal.

Signal to Noise (Gaussian Noise) Ratio

$SNRdB \equiv 45$

$$SNR = 10^{\frac{SNRdB}{10}}$$

Signal to Nonlinear Distortion (non-Gaussian impulsive) Ratio

$$SNLD(SNLDdB) = 10^{\frac{SNLDdB}{10}}$$

$$G(SNLDdB) = \frac{SNLD(SNLDdB)}{SNR}$$

Signal to Total Noise (Gaussian + non-Gaussian) Ratio

$$SNRtotal(SNLDdB) = \frac{1}{\left[\frac{1}{SNR}\right] + \frac{1}{SNLD(SNLDdB)}}$$

BER as a function of SNLD

$$BER(SNLDdB) = \frac{M - \sqrt{M}}{M \cdot 3} \cdot \exp(-1 \cdot A) \cdot \sum_j \left[\frac{A^j}{j!} \cdot \left[1 - \operatorname{erf}\left[\frac{\sqrt{SNRtotal(SNLDdB) \cdot 2.328}}{\sqrt{2} \cdot \left[\sqrt{M} - 1\right] \cdot \sqrt{\frac{\frac{j}{A} + G(SNLDdB)}{1 + G(SNLDdB)}}} \right] \right] \right]$$

$j \equiv 0, 1 .. 10$ $\quad A \equiv 0.022$ $\quad M \equiv 64$ $\quad SNLDdB \equiv 30, 31 .. 45$